# CHANNEL ENGINEERING OF HYDROXIDE ION EXCHANGE POLYMERS FOR ELECTROCHEMICAL DEVICES

A Dissertation
Presented to
The Academic Faculty

by

Garrett Huang

In Partial Fulfillment
of the Requirements for the Degree
Doctor of Philosophy in the
School of Chemical and Biomolecular Engineering

Georgia Institute of Technology
December 2020

# CHANNEL ENGINEERING OF HYDROXIDE ION EXCHANGE POLYMERS FOR ELECTROCHEMICAL DEVICES

Approved by:


Dr. Paul A. Kohl, Advisor
School of Chemical and Biomolecular Engineering
*Georgia Institute of Technology*

Dr. Hailong Chen
George W. Woodruff School of Mechanical Engineering
*Georgia Institute of Technology*

Dr. Thomas F. Fuller
School of Chemical and Biomolecular Engineering
*Georgia Institute of Technology*

Dr. Marta Hatzell
George W. Woodruff School of Mechanical Engineering
*Georgia Institute of Technology*

Dr. Nian Liu
School of Chemical and Biomolecular Engineering
*Georgia Institute of Technology*


Date Approved: December 1, 2020

For the betterment of the environment

# ACKNOWLEDGEMENTS

I would like to express my deep and sincere appreciation to my advisor, Prof. Paul A. Kohl, who gave me an opportunity to study a topic I am truly passionate about. You have been a role model and I am grateful that you always pushed me to be the best scientist and engineer I can be. I would also like to thank my thesis committee members for sharing their constructive feedback and support in my research. I would also like to express my gratitude to all of my external collaborators from the University of South Carolina, Rensselaer Polytechnical Institute, Nel Hydrogen, Pajarito Powder, Xergy, and the National Renewable Energy Laboratory.

My Ph.D. experience would not have been complete without my wonderful graduate student and post-doctoral colleagues from the Kohl Research Group. I am immensely grateful to have met you all and to have made life-long friendships. I would also like to thank all of the undergraduate students who I have had the honor to mentor over the years for their invaluable contribution to this thesis. Celebrating our achievements, ranting about our frustrations and growing wiser together will always be some of my fondest memories from Georgia Tech.

I am incredibly thankful to all those who inspired me to go on this journey. Completing my doctorate degree has been a lifelong dream and was a genuinely transformative experience. Last but not least, I would like to give a special thanks to my family (and anyone else I call my “family”—you know who you are!) for their unconditional love and motivation. I hope that I have made you all proud.

# TABLE OF CONTENTS

# LIST OF TABLES

# LIST OF FIGURES

# LIST OF SYMBOLS AND ABBREVIATIONS

| | |
|---|---|
| ACI | anion conductive ionomer |
| AEL | alkaline electrolyzer |
| AEM | anion exchange membrane |
| AEMEL | anion exchange membrane electrolyzer |
| AEMFC | anion exchange membrane fuel cell |
| ASR | area specific resistance |
| BBNB | bromobutyl norbornene |
| BCP | block copolymer |
| BPNB | bromopropyl norbornene |
| BTMA | benzyl trimethylammonium |
| BuNB | butyl norbornene |
| CL | catalyst layer |
| CPE | constant phase element |
| Đ | polydispersity index |
| DI | deionized water |

| | |
|---|---|
| DMA | dynamic mechanical analysis |
| DSC | differential scanning calorimetry |
| EIS | electrochemical impedance spectroscopy |
| ETFE | ethylene tetrafluoroethylene |
| FCEV | fuel cell electric vehicle |
| FT-IR | Fourier-transform infrared spectroscopy |
| G’ | storage modulus |
| GDE | gas diffusion electrode |
| GDL | gas diffusion layer |
| GPC | gel permeation chromatography |
| HER | hydrogen evolution reaction |
| HFR | high frequency resistance |
| HOR | hydrogen oxidation reaction |
| HPLC | high-performance liquid chromatography |
| IEC | ion exchange capacity |
| IPA | isopropyl alcohol |
| LTE | low-temperature electrolysis |

| | |
|---|---|
| MEA | membrane electrode assembly |
| $M_n$ | number average molecular weight |
| $M_w/M_n$ | polydispersity index |
| $N_{bound}$ | number of non-freezable water molecules |
| $N_{free}$ | number of freezable water molecules |
| NMR | nuclear magnetic resonance |
| OER | oxygen evolution reaction |
| ORR | oxygen reduction reaction |
| PDI | polydispersity index |
| PEM | proton exchange membrane |
| PEMEL | proton exchange membrane electrolyzer |
| PEMFC | proton exchange membrane fuel cell |
| PNB | poly(norbornene) |
| PTFE | poly(tetrafluoroethylene) |
| $q$ | wave vector |
| QA | quaternary ammonium |
| RH | relative humidity |

| | |
|---|---|
| SAXS | small angle X-ray scattering |
| TEM | transmission electron microscopy |
| TFT | α,α,α-trifluorotoluene |
| $T_g$ | glass transition temperature |
| TGA | thermogravimetric analysis |
| THF | tetrahydrofuran |
| TMA | trimethylamine |
| TMHDA | N,N,N′,N′-tetramethyl-1,6-hexanediamine |
| UHP | ultra-high purity |
| WU | water uptake |
| λ | hydration number |
| σ | ionic conductivity |
| 2θ | scattering angle |

# SUMMARY

Anion exchange membrane (AEM) fuel cells and electrolyzers are of interest because they have potential advantages over their acidic counterparts for the production and storage of renewable energy. Alkaline conditions are attractive because of the facile electrochemical reaction kinetics at high pH for oxygen reduction and water oxidation. Device operation at high pH allows for the use of non-precious metal catalysts, simpler design for the balance of plant, and reduced fuel crossover. However, it is imperative that the AEMs are thin, have long-term alkaline stability, and high hydroxide ion conductivity. There have been issues in the past with AEMs showing low ionic conductivity, poor stability at high pH, and high water uptake (leading to dimensional change); however, these issues have all been systematically addressed in this work.

A series of stable, non-hydrolysable, hydroxide-conducting tetrablock copolymers containing an all-hydrocarbon backbone were synthesized by Dr. Mrinmay Mandal (Georgia Tech) for the purposes of this work. The synthesis methods are outlined in Appendix A. To characterize the polymers, the tetrablock polymers were cast into membranes with an ion-exchange capacity (IEC) between 1.55 and 2.60 milliequivalents per gram (meq/g). Excellent hydroxide conductivity (>120 mS/cm at 80 °C) was obtained at an ion-exchange capacity of 1.88 meq/g. The results show that hydroxide mobility was aided by phase segregation within the tetrablock copolymer. The number of bound and unbound water molecules per ion pair was measured and correlated with conductivity. The presence of excess unbound water led to flooding of the ion conductive channels and low hydroxide ion conductivity. The optimal anion conductivity was found with about 6.7

unbound and 11.9 bound water molecules per ion pair. The ion conducting polymers were stable in 1 M NaOH solution at 80 °C, showing essentially no loss in ion conductivity for 1200 h. Thermogravimetric analysis showed that the membrane backbone was stable up to 400 °C, consistent with previous poly(norbornene)-based materials. The peak power density of a $H_2/O_2$, hydroxide conducting fuel cell containing one of these membranes was 542.57 mW/cm$^2$ at 0.43 V and current density of 1.26 A/cm$^2$ at 60 °C.

To enable the use of very high IEC (>3 meq/g) polymers with high hydroxide conductivity, light cross-linking of the polymers was performed using *N*,*N*,*N*′,*N*′-tetramethyl-1,6-hexanediamine (TMHDA). The addition of the cross-linker was found to be adequate for providing critical control over unwanted water uptake and providing additional film rigidity. Without light cross-linking, the unwanted water uptake would cause swelling and softening of the membrane. The cross-linked membranes also showed no significant drop in ionic conductivity over 1,000 h of aging in 1 M NaOH at 80 °C and record high ionic conductivity for a chemically stable AEM. The number of bound and free water molecules per ion pair is correlated with the ion mobility within the materials.

Composite membranes composed of poly(norbornenes) tetrablock copolymers with pendant quaternary ammonium head-groups and a proprietary polymer reinforcement were prepared for use in AEM fuel cells. It was found that the reinforced membranes were more suitable for use in alkaline hydrogen/oxygen fuel cells due to their thinness. The reinforcement layer and light cross-linking provided additional mechanical stability and hydrophobicity which allowed very high ion exchange capacity polymers to be used without penalty of excessive water uptake and swelling. The optimum membrane and fuel cell operating conditions were able to achieve a peak power density of 3.4 W/cm$^2$ using

hydrogen and oxygen. The performance increase was greater than expected from minimizing ohmic losses because mechanical deformations within the membrane due to excess water uptake can disrupt full cell operation. Cells were also run for over 500 h under load with no change in the membrane resistance and minimal loss of operating voltage.

High water transport and thinness are critical aspects of the membrane in extending the power and current density of AEM fuel cells to new record values. Very high hydroxide conductivity was achieved through reinforced and cross-linked norbornene-based tetrablock copolymers with an ion-exchange capacity of 3.88 meq/g. A $H_2/O_2$ alkaline polymer electrolyte fuel cell was assembled and was able to achieve a record peak power density of 3.5 W/cm$^2$ with a maximum current density of 9.7 A/cm$^2$ at 0.15 V at 80 °C. The effects of membrane thickness were explored to show the influence of anode to cathode water transport on the achievable current density and peak power. Finally, the detrimental effects of electrolyte carbonation by ambient $CO_2$ were reduced using very high conductivity AEMs.

The recent advances in AEMs and catalysts have made alkaline devices increasingly competitive with PEM-based technology. However, less attention has been paid to the anion conductive ionomers (ACI) used in the fabrication of electrodes for AEM devices and in particular, AEM electrolyzers. A series of poly(norbornene)-based ionomers were synthesized, characterized and used to fabricate oxygen evolving anodes for low-temperature AEM water electrolysis. The IEC of the ionomers (0 to 4.73 meq/g) was adjusted by controlling the ratio of ion conducting to non-ion conducting norbornene monomers in the ACI tetrablock copolymers. Low conductivity ionomers were shown to yield the best-performing oxygen evolution electrodes, in the absence of ACI polymer

cross-linking because they do not experience excessive water swelling. Light cross-linking within the anode ACI was used as a means to independently lower WU of the ionomer without compromising ionic conductivity. This control over water swelling allows higher ionic conductivity within the ACI to be used in water-fed electrolyzer applications. Other methods of water management were compared including the use of hydrophobic additives and adjustment of the ionomer concentration in the electrode. It was shown that the cell performance greatly benefits from a highly conductive ionomer in the oxygen evolution reaction electrode if the WU is managed. In addition, a series of poly(norbornene)-based ACIs were characterized and used to fabricate hydrogen evolving electrodes for AEM electrolyzers. Unlike the oxygen evolving electrode, higher water uptake was preferred in the hydrogen evolving electrode. Light cross-linking of the cathode ionomer was used to fine-tune the WU and ionomer swelling to achieve optimum cell performance. These results demonstrate the importance of managing water content for the reactions at each electrode in an AEM electrolyzer and suggest the use of asymmetric ionomers to achieve optimal cell performance.

# CHAPTER 1. INTRODUCTION

## 1.1 Anion exchange membrane fuel cells and electrolyzers

Energy conversion devices containing solid polymer electrolytes (e.g., fuel cells and electrolyzers) are seen as promising options for producing and storing clean, renewable energy because of their high thermodynamic efficiency and solid-state design.[1-4] Specifically, fuel cells are used to convert hydrogen directly into electricity and electrolyzers are used to split water into hydrogen and oxygen. These types of devices are scalable and can be used for transportation, remote and distributed power, and large-scale facilities for electricity and hydrogen production.[5, 6]

Polymer electrolyte-based fuel cells and electrolyzers are both typically composed of two electrodes, an anode and a cathode, that are electronically separated by an ionically conductive polymer membrane. Solid polyelectrolyte membranes simplify the fabrication of electrodes with a three-phase boundary because liquid/gas pressures do not have to be balanced like in liquid electrolyte devices. Polymer electrolyte membranes are divided into two broad categories based on the dominant charge carrying ion: proton exchange membranes (PEMs) and anion exchange membranes (AEMs). Most of the fuel cells and electrolyzers today are based on PEMs which are operated in highly acidic conditions. In a PEM fuel cell (Figure 1.1, left), hydrogen fuel supplied at the anode is oxidized into protons which move through the membrane separator to the cathode. The electrons from this half reaction are sent through an external circuit to do useful work before reentering the cell on the cathode side. Oxygen, typically from air, is supplied at the cathode which recombines with the protons and electrons and is reduced to from water. In a PEM

electrolyzer (Figure 1.2, left), the direction of the oxidation-reduction reactions is reversed. Water is oxidized at the positively charged anode to form oxygen, protons, and electrons. The protons move through the separator while the electrons travel through an external circuit to the negatively charged cathode. A power supply (ideally from a renewable source such as wind or solar) provides voltage control for the electronic circuit. The electrons and protons then recombine at the cathode to form hydrogen gas.

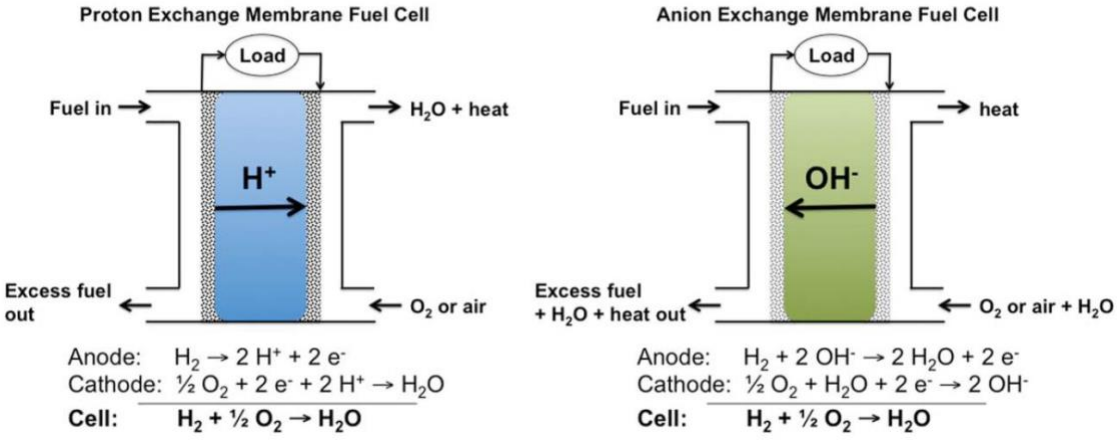


**Figure 1.1 – Comparison of PEM and AEM fuel cells and their associated half-reactions.[7]**

AEM devices work very similarly to PEM devices, with the main difference being the negatively charged hydroxide ion as the charge carrier species. The overall chemical reactions at the electrodes in AEM-based fuel cells and electrolyzers are identical to those in their PEM counterparts. In an AEM fuel cell (Figure 1.1, right), water and oxygen are reduced at the cathode to form hydroxide ions that are transported through the separator to the anode. Hydrogen supplied at the anode reacts with the hydroxide ions to form water and electrons. The electrons from this half reaction are sent through an external circuit to do useful work before reentering the cell on the cathode side. In an AEM electrolyzer (Figure 1.2, right), an external power supply is used to reduce water at the cathode to form

hydrogen and hydroxide ions. The hydroxide ions move through the separator to the anode where they recombine to form oxygen and water. It is often advantageous to supply water to only the oxygen evolving electrode in order to keep the hydrogen evolving electrode dry. For an AEM electrolyzer, water must first diffuse through a separator to the cathode side before it can react to form hydrogen.

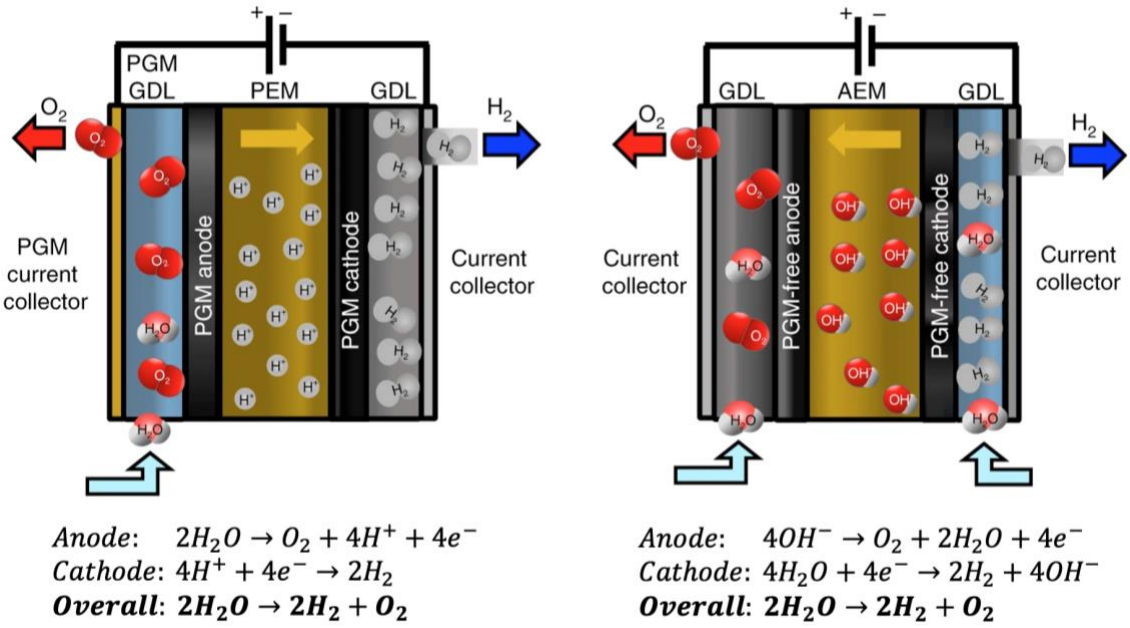


$$Anode: \quad 2H_2O \rightarrow O_2 + 4H^+ + 4e^-$$
$$Cathode: \quad 4H^+ + 4e^- \rightarrow 2H_2$$
$$\boldsymbol{Overall: \quad 2H_2O \rightarrow 2H_2 + O_2}$$

$$Anode: \quad 4OH^- \rightarrow O_2 + 2H_2O + 4e^-$$
$$Cathode: \quad 4H_2O + 4e^- \rightarrow 2H_2 + 4OH^-$$
$$\boldsymbol{Overall: \quad 2H_2O \rightarrow 2H_2 + O_2}$$

**Figure 1.2 – Comparison of PEM and AEM electrolyzers and their associated half-reactions.[8]**

There are already several examples commercialized fuel cell electric vehicles (FCEV) from major automobile manufacturers such as Toyota, Honda and Hyundai based on PEM membranes. Yet, widespread adoption of PEM devices has still been stagnant due to lack of hydrogen infrastructure and significant costs associated with the platinum-based electrocatalysts and perfluorosulfonic acid (PFSA) membranes.[9] Despite recent developments in catalyst optimization that have significantly reduced the amount required, platinum is necessary as the electrocatalyst because it is one of the only materials that can

overcome the sluggish oxygen reduction reaction kinetics in low pH conditions.[10] Nafion (DuPont) also remains as the preferred proton conductor due to its high conductivity and excellent thermal and mechanical properties even though it is expensive and difficult to manufacture.[11]

AEM-based devices, on the other hand, have the potential to lower the cost of ownership compared to PEM-based devices. Operation of fuel cells and electrolyzers at high pH allows the use of non-precious metal catalysts, especially for the oxygen reduction and evolution reactions, and reduced fuel crossover compared to proton-exchange membranes devices.[2, 7, 12-20] Also, a variety of low-cost and safe monomers can be used to synthesize hydrocarbon-based hydroxide ion conducting polymers that are stable in alkaline conditions, compared to the perfluorinated polymers like Nafion needed for PEM-based electrochemical devices.[2, 21] This is because PFSAs are expensive and present significant hazards due to monomer reactivity. The majority of research and development has been focused primarily on PEM-based devices in recent decades.[9] As such, early AEMs have suffered from low ionic conductivity, poor stability at high pH, and high water uptake (leading to dimensional change). However, these issues have all been systematically addressed in this work.[1, 22-32]

### 1.2 Rational design of anion exchange membranes

For realistic deployment of AEMs as a PEM alternative, the critical metrics for AEMs are (i) high anion (e.g., hydroxide) conductivity, (ii) long-term alkaline stability at the AEM fuel cell operating temperature, (iii) control over excessive water uptake and (iv) robust mechanical properties for withstanding in-use pressure differences and avoiding polymer creep under compression, which can disrupt ion transport within the electrodes

and membrane.[2, 33, 34] The following sub-chapters outline the strategies employed in this work to simultaneously achieve all these properties using a single, low-cost material. To date, the composite poly(norbornene)-based AEMs developed in this work have demonstrated the highest performance ever reported in an alkaline fuel cell system.[35, 36] This notable progress has shown that certain structural moieties can be used to address pervious AEM deficiencies and truly rival Nafion in PEM systems.

### *1.2.1 Phase segregated ion conduction channels*

High hydroxide conductivity is critical in membranes for fuel cells and electrolyzers. Hydroxide conductivity is a function of the ion mobility and ion exchange capacity (IEC). The IEC of the AEM is often kept to a modest value in an effort to avoid high water uptake which can result in swelling of the membrane and low ion mobility. The mobility can be improved by the formation of efficient (i.e., ordered, interconnected, continuous and appropriately sized) ion conducting channels and preventing excess water uptake within the membrane.[18]

The high conductivity of Nafion is often attributed to the formation of nanochannels created through nanophase segregation of a hydrophobic polymer backbone and hydrophilic ion conducting side groups.[18] Block copolymer (BCP) architecture, where ionic groups are concentrated in segments along a polymer backbone, is effective in constructing continuous ionic domains to improve the proton mobility.[37] Attempts have been made to create alternative proton conducting materials with Nafion-like morphology using hydrophilic−hydrophobic multiblock copolymers based on comb-shaped poly(arylene ether sulfone) copolymers with highly sulfonated side chains.[38] Similar

attempts have also been made to apply these design principles in creating Nafion-like morphology in hydroxide conducting materials. In anion conductive poly(arylene ether)s, it was shown that the multiblock copolymer versions of these materials had higher hydroxide conductivity over their corresponding random copolymers.[39] This underlines the importance of an ordered polymer structure in both proton and hydroxide conducting materials.

Understanding the relationships between polymer structure and morphology is critical for improving ionic conductivity. The use of multiblock copolymers can improve the hydroxide mobility compared to random copolymers due to the high degree of phase segregation in block copolymers leading to efficient ion-channel formation.[18, 40-44] There have been several reports of AEMs with hydroxide conductivity of over 100 mS/cm (60 °C to 80 °C) and chemical stability (80 °C in 1 M NaOH) has been achieved by a number of researchers.[23, 32, 34, 45-48] More recent reports of AEMs have shown conductivity above 200 mS/cm (at 80 °C) using phase segregated BCP schemes.[36, 45, 49, 50] It is important to note that not all BCP morphologies lead to high conductivity because the channels must also be interconnected for efficient ion conduction.[51]

### *1.2.2 Alkaline stability*

The long-term stability of AEMs largely depends on the chemical nature of the polymer backbone, position of the cation within the polymer architecture and chemical nature of the fixed cation. In the past, polymers based on poly(arylene ether sulfone)s[52-54] and poly(arylene ether ketone)s[55, 56] were investigated as AEMs. It has been experimentally shown that polar moieties, such as ether, ketone or ester linkages, within the polymer or

side-groups, are susceptible to nucleophilic attack of the C−O bonds in the polymer backbone at high pH which limits the long-term use.[22, 34, 57-60] Figure 1.3 shows an example of backbone cleavage occurring in the ether linkage of BTMA substituted aryl group of poly(aryl ether).

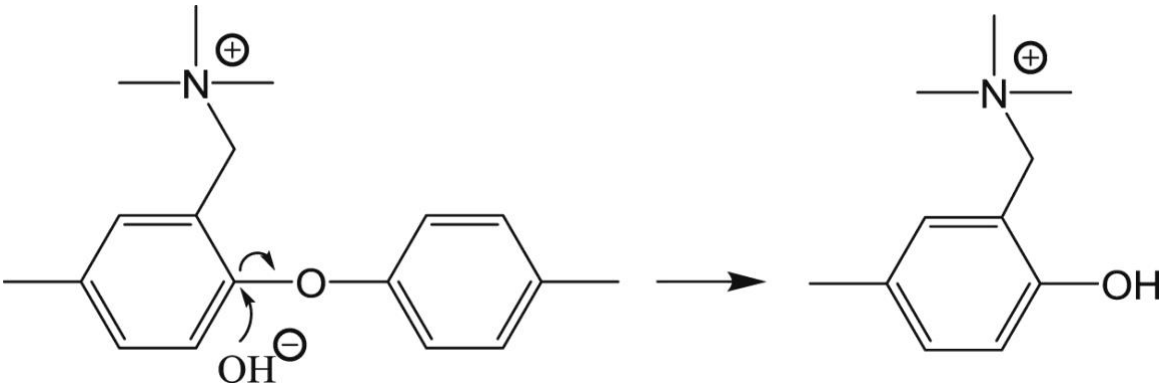


**Figure 1.3 – Aryl-ether cleavage occurring in the ether linkage with benzyl trimethyl ammonium substituted aryl group of poly(aryl ether).[58]**

In addition to the polymer backbones, nucleophilic attack of the fixed cation headgroups also results in degradation. The mechanisms for degradation of quaternary ammonium headgroups are illustrated in Figure 1.4 and include β-hydrogen Hofmann elimination, direct nucleophilic substitution ($S_N2$) and elimination via ylide formation.[60-62] Hibbs et al. found that a hexamethylene spacer between the trimethylammonium (TMA) cation and the polymer backbone results in better stability than the benzyltrimethylammonium (BTMA) cation in 4 M KOH at 80 °C.[63] Later, Mohanty et al. reported that a quaternary ammonium headgroup tethered to the backbone by a long alkyl chain had the best alkaline stability by comparing the stability of small molecules.[22] A cation attached to a long alkyl chain increases the barrier for the Hofmann elimination reaction and minimizes the risk of degradation.[64]

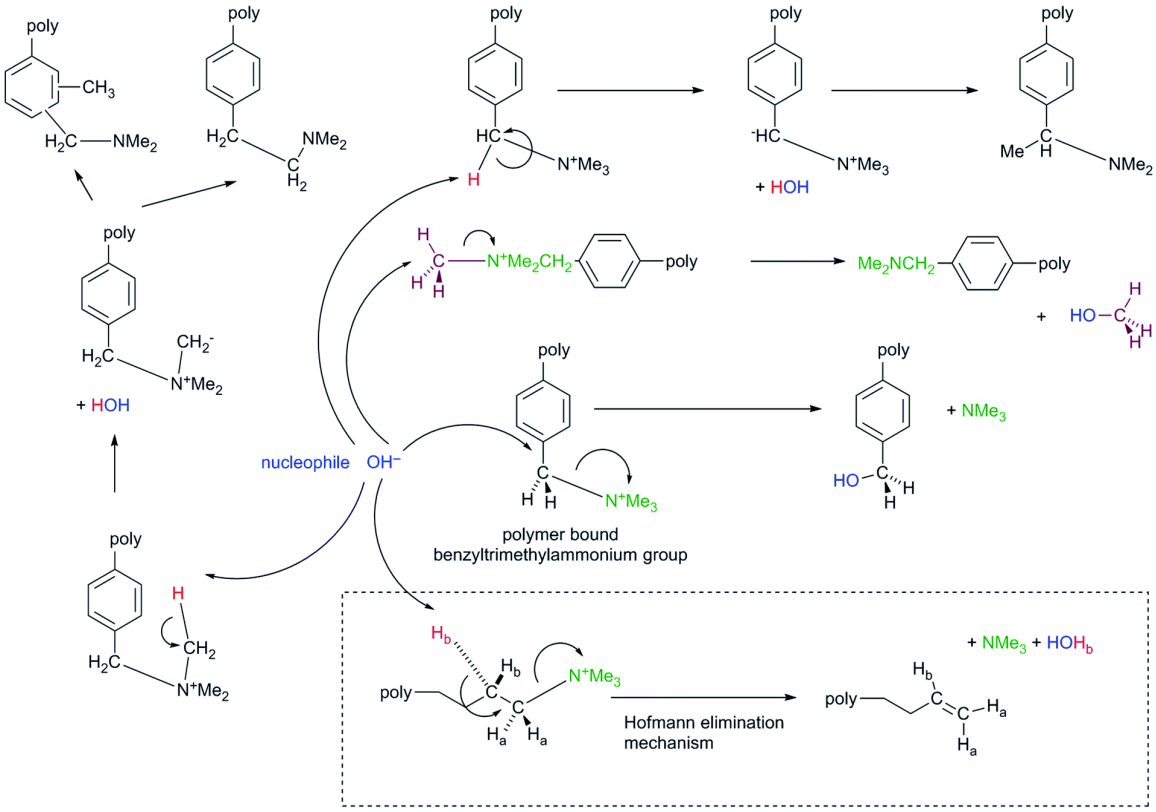


**Figure 1.4 – Common degradation pathways involving $OH^-$ nucleophiles with benzyltrimethylammonium cationic groups. The dashed box shows the Hofmann Elimination degradation mechanism that can occur with alkyl-bound QA groups.[2]**

These degradation mechanisms are easily resolved by modifying the polymer structure of the AEM. Backbone degradation issues are mitigated by the use of a polymer with an all-hydrocarbon backbone which is impervious to aryl-ether cleavage by completely eliminating sulfone, ketone and ether linkages.[32] Positioning the cation head groups at the ends of pendant alkyl tethers, typically 4 to 6 carbons long, has also been found to be an effective strategy for mitigating polymer degradation.[64, 65] Quaternary ammonium head groups, especially the trimethyl ammonium cation, has been found to have an excellent balance of conductivity and stability, although other conducting groups show merit as well.[31, 47, 63] In addition, the alkyl tether can isolate the cation head-group from the electron withdrawing inductive effect of aromatic groups in the tether or polymer

backbone (if aromatic groups are present). Hence, stable AEMs under realistic operating conditions (e.g., 80 °C and 1 M KOH) can be synthesized by combining the advantages of an all-hydrocarbon backbone with an adequate glass transition temperature with tethered cations on long alkyl chains.[66-68]

### *1.2.3 Water management and swelling*

AEM fuel cells are known to be sensitive to the relative humidity of the fuel and oxidant streams, as well as the water uptake in the AEM and ionomer. Proper water management in the membrane and electrodes is critical for achieving high power density.[69] Water is needed in the membrane to form the ionic hydration shell for the mobile hydroxide ion and stationary cation. However, excessive water uptake can lead to swelling of the ion conduction channels resulting in lower ionic conductivity (i.e., lower ion mobility) and softening of the membrane.[18] Thus, it is necessary to optimize the ion conducting channel size so that the amount of free, unbound (unproductive) water is minimized.

The AEM plays a key role in balancing the water content and distribution during device operation.[69, 70] Efficient ion channels are needed in the AEM to achieve high conductivity because the number of ions cannot be independently increased (i.e., higher ion exchange capacity) because of the penalty due to excessive water uptake.[32] Water is electrochemically generated at the anode during the hydrogen oxidation reaction (HOR) and is consumed at the cathode by the oxygen reduction reaction (ORR) in an AEM fuel cell. In an electrolyzer, water is consumed at the hydrogen evolution reaction (HER) electrode and generated at (OER) electrode. It has been shown that a significant majority of the reacting water at the AEMFC cathode is provided by back-diffusion of water

produced at the AEMFC anode.[71] This suggests that high AEM water permeability is beneficial in AEMFCs. However, excessive AEM water uptake can flood the ion conducting channels within the polymer and lead to higher internal stresses and expansion which causes the membrane to soften and experience mechanical failure.[43, 72] Thus, high water permeability without high water solubility appears to be a critical feature for AEMFCs.

Bulk water uptake alone does not precisely describe the issue with membrane swelling. Water molecules in the membrane can be divided into two types: (i) bound or productive waters of hydration that aid in creating a solvation shell around the tethered cationic and mobile anionic species and are necessary for ion conduction and (ii) unbound or free water molecules that populate the ion channels. Excessive unbound water leads to low hydroxide mobility and membrane distortion.[45] Hence, it is necessary to balance the amount of free and bound water inside the membranes to yield the maximum hydroxide mobility and water transport.[32, 45, 46] This is typically controlled by limiting the ion exchange capacity to relatively low values (i.e., <1.5 meq/g).[23, 31, 48] More recently, cross-linking has been shown to be an effective way to reduce water uptake and swelling.[35] Unfortunately, AEMs with high cross-linking density can become too rigid, leading to poor ion mobility, mechanical properties and water diffusivity (i.e., high water solubility without high diffusivity).[73-75] However, the work in this thesis shows that a light amount of cross-linking has been found to be an effective strategy in polymers with high IEC (>3 meq/g) to balance the high conductivity and water uptake (WU) without sacrificing IEC.[45, 46] In addition, thinner membranes can enable rapid water transport without high water uptake,

and enable high current density AEMFCs. Conveniently, light cross-linking also helps in the production of thin membranes with good mechanical properties.

### *1.2.4 Dimensionally stable reinforced composite membranes*

Dimensional stability allows the efficient transport of anions throughout the entire membrane electrode assembly. Thin membranes are desired to minimize ohmic losses in the AEM however they are inherently more fragile and difficult to handle and integrate into an electrochemical device. A thin reinforcement layer made of a chemically inert polymer such as poly(tetrafluoroethylene) (PTFE) can be used to form composite membranes to mitigate mechanical swelling and promote scalable manufacturing.[25, 76-78] Swelling in the z-direction is to be expected, but swelling in the x-y direction will be a function of (i) the substrate material employed for compositing process and (ii) the ability to crosslink the polymer in-situ within the pores of the substrate material so that it essentially follows the behavior of the substrate material as it operates in a cell environment. If the substrate is strong and the material is properly crosslinked, then swelling in the x and y directions will be minimized.

### *1.2.5 Carbon dioxide mitigation*

The conductivity, pH, and mechanical properties of the AEM are all affected by the presence of carbon dioxide in air because it readily reacts with hydroxide ions to form bicarbonate and subsequently carbonate ions within the membrane. Exposure to even small amounts of $CO_2$ (5-50 ppm) during any part of the manufacturing, assembly, and operation of AEM devices could severely impact operating voltage in AEMFCs. The dominating mechanism for voltage loss is accumulation of carbonate anions in the anode, which results

in two performance-robbing mechanisms: (i) a Nernstian thermodynamic shift in the anode potential from a decrease in the anode pH with carbonates; and (ii) an increase in charge transfer resistance due to a lack of availability of reacting $OH^-$ anions.[79]

Steps can be taken mitigate the negative effects of $CO_2$ at the air-cathode in AEMFCs such as the removal of the $CO_2$ from air before it is used. Conductivity tests are often performed with only hydroxide conductive ions. Fuel cell measurements are often made with $CO_2$-free air to avoid the complications of carbonate formation.[80] This is not a practical solution when operating a fuel cell with ambient air as PEM fuel cells typically are, and the balance of plant penalties for including a $CO_2$ scrubber would lower the overall efficiency of the system.

The lower ion mobility for bicarbonate and carbonate compared to hydroxide results in higher ohmic losses within the anion conducting membrane and the possible accumulation of $CO_2$ in the hydrogen at the anode.[81] The adverse effects of membrane carbonation could be minimized by using AEMs with very high ionic conductivity so that the decrease in mobility upon carbonation can be mitigated. The only means to remove the carbon dioxide is to vent unused hydrogen (a very undesirable process) or let the carbon dioxide diffuse back across the membrane, which converts hydroxide to carbonate. Thus, under steady-state conditions, carbonate conductivity will dominate. Cell decarbonation during operation through the so-called "self-purging" mechanism can occur more rapidly. Bench scale fuel cell tests using fresh feed hydrogen avoid facing this critical issue of carbon dioxide build-up and carbonate conduction. Hence, it is imperative that the IEC and ion mobility be as high as possible for efficient carbonate conduction as well as hydroxide conduction.[45, 71, 79]

## 1.3 Anion conductive ionomers in electrochemical devices

Fuel cells and electrolyzers electrodes are often fabricated by spraying a slurry of catalyst, ion conducting polymer (i.e., ionomer) and solvent onto a gas diffusion layer (GDL). This slurry is sometimes referred to as a catalyst ink and when dried forms the catalyst layer on the surface of the GDL. The sprayed electrode is then pressed onto the ion conducting membrane to form a membrane electrode assembly (MEA).

The anion conductive ionomer (ACI) serves two primary purposes: (i) facilitate hydroxide conduction between the catalyst and bulk electrolyte and (ii) bind the catalyst to the porous transport layer and membrane. High ion exchange capacity (IEC) ACIs are desired, however, high IEC can cause excessive water uptake (WU) and detrimental ACI swelling. Proper water management is a key factor in obtaining maximum performance in AEM-based devices. Because ionomers and membranes serve different functions in the cell, the materials used for these functions should be different and optimized for each purpose.[82] For example, the membrane should have low oxygen permeability and high mechanical strength while the ionomer for the air-cathode should have high oxygen permeability. Free-standing mechanical strength is not an issue for the ionomer. Some properties, such as ion conductivity and chemical stability, are common to both.

# CHAPTER 2. EXPERIMENTAL METHODS

The purpose of this chapter is to illustrate the common experimental methods used for characterizing the physical properties of the vinyl addition poly(norbornene) anion conductive polymers after synthesis as well as the methods for AEM fuel cell and electrolyzer testing. Nuclear magnetic resonance (NMR), Fourier transform infrared (FT-IR) spectroscopy, gel permeation chromatography (GPC) and thermogravimetric analysis (TGA) measurements and analysis were conducted by Dr. Mrinmay Mandal (Georgia Tech). Assistance with small angle X-ray scattering at Brookhaven National Laboratory was provided by Dr. Jong Yeob Jeon (RPI). Assistance with transmission electron spectroscopy (TEM) was provide by Hong Yi (Emory).

## 2.1 Characterization

### *2.1.1 Chemical structure and ion exchange capacity (IEC)*

The chemical structures of the polymer samples were analyzed by one-dimensional $^{1}$H NMR using Bruker Avance 400 MHz NMR instrument using $CDCl_3$ as the solvent. The absence of olefinic protons in the $^{1}$H NMR spectra of the polymer produced shows that the polymerization reaction proceeded through the vinyl addition pathway, eliminating the occurrence of ring-opening metathesis polymerization (ROMP). A representative spectrum is shown in Figure 2.1. The polymerization time for the individual monomers for the different monomer-to-initiator feed ratios ($[M]_0/[Pd]$) was optimized in order to avoid branching side-reactions.[83] Incomplete conversion of the polymer into monomer would

also create problems in synthesizing the block copolymer via the sequential addition of different monomers.[84]

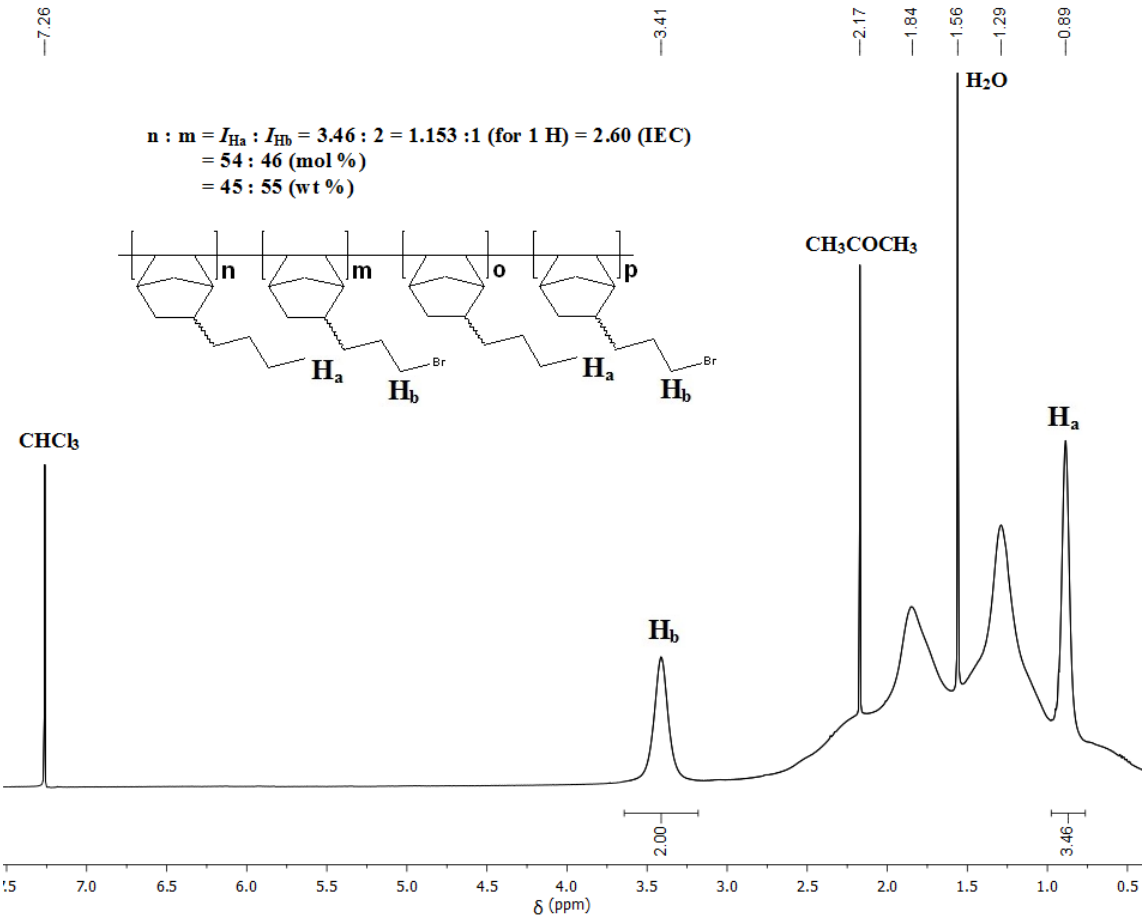


**Figure 2.1 – Representative $^1$H NMR spectrum of tetrablock GT46 in $CDCl_3$ showing only polymerization through the vinyl addition pathway.**

The IEC was evaluated via $^1$H NMR analysis by integration of the terminal methyl protons ($H_a$) of the hydrophobic (not halogenated) block which resonate at 0.89 ppm and the methylene protons ($H_b$) adjacent to the bromine atom of the halogenated block which appear at 3.42 ppm. $^1$H NMR is a more accurate means of determining IEC because of the quantitative nature of solution NMR. The integration ratio of $H_a$ and $H_b$ was used to calculate the IEC (Figure 2.1). This value was used to calculate the molar ratio between

the hydrophobic and halogenated blocks by recognition of the fact that the hydrophobic block has three methyl protons and the halogenated block has two methylene protons.

The membrane IEC was also verified by titration.[85] The titration involved converting the counter anion to chloride, followed by titration of the chloride in the membrane. The membrane in $Br^-$ form was first immersed in 0.1 M NaCl solution for 24 h to exchange the bromide ions for chloride ions. Next, the membrane in chloride form was thoroughly washed with DI water and dried under vacuum for 24 h to obtain the dry weight. The dried membrane was immersed in a fixed volume of 0.5 M aqueous $NaNO_3$ solution for 24 h. The $Cl^-$ ions released from the membrane were titrated with 0.05 M $AgNO_3$ using $K_2CrO_4$ (10 wt. %) as the indicator. The IEC was calculated using Equation 3.

$$IEC = \frac{C_{AgNO_3} \times V_{AgNO_3}}{M_d} \tag{3}$$

In Eq. 3, $V_{AgNO_3}$ (mL) is the volume of $AgNO_3$ solution, $C_{AgNO_3}$ (0.05 $mol \cdot L^{-1}$) is the concentration of $AgNO_3$ solution, and $M_d$ (g) is the weight of the dried membrane sample.

It was found that IEC measurements obtained via $^1H$ NMR (pre-aminated samples) and titration (post-aminated samples) were the same (within experimental error).[32] For example, the IEC of GT33 (Table 3.1), was found by titration and NMR and results were 1.90 meq/g and 1.92 meq/g, respectively.[32] The fact that they match shows that each bromoalkyl group was quantitatively converted into a quaternary ammonium head-group.[32, 86] That is, each available bromoalkyl group available was reacted with trimethyl

amine. $^{1}$H NMR was found to be the more dependable method and is the preferred technique for measuring IEC in this thesis.

In order to confirm that the brominated head-groups were fully quaternized, the films were analysed by FT-IR. A representative analysis performed on a cross-linked membrane is shown in Figure 2.2 for the polymer in precursor form, after cross-linking, and after cross-linking and quaternization. The disappearance of the alkyl bromide peak at 646 $cm^{-1}$ and the appearance of quaternary ammonium peaks at 908 $cm^{-1}$, 968 $cm^{-1}$, and 1481 $cm^{-1}$ show complete quaternization, within the sensitivity of the FT-IR, Figure 2.2. In addition, the successful incorporation of TMHDA after cross-linking was also indicated by the appearance of a new quaternary ammonium peak at 1481 cm-1 in the IR spectra, Figure 2.2.

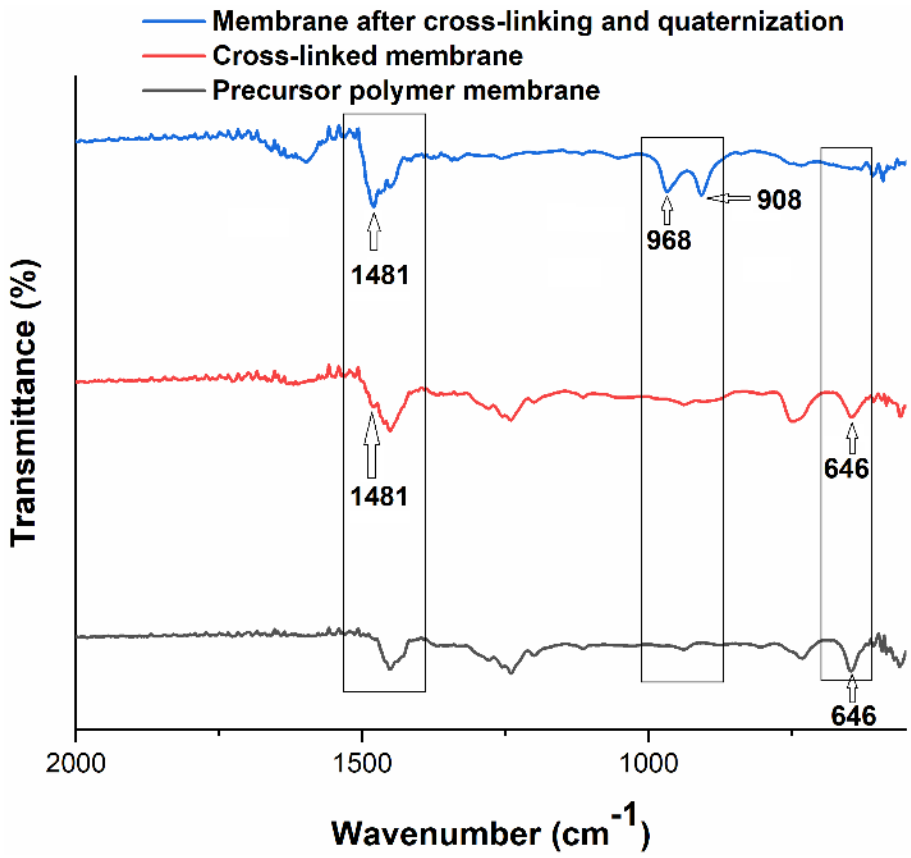


**Figure 2.2 – Representative FT-IR spectra of the GT82 film in precursor polymer form, after cross-linking, and after cross-linking and quaternization.**

*2.1.2 Number average molecular weight ($M_n$) and polydispersity index ($Đ$)*

The number average molecular weight ($M_n$) and polydispersity index ($M_w/M_n$) of the polymer samples were determined by GPC (Shimadzu) equipped with an LC-20 AD HPLC pump and a refractive index detector (RID-20 A, 120 V). Measurements were performed in THF with the eluent flow rate of 1.0 mL/min at 30 °C with a polystyrene standard. A representative GPC trace of tetrablock copolymer is shown in Figure 2.3 to demonstrate the sequential growth of each block in the formation of the tetrablock copolymer.

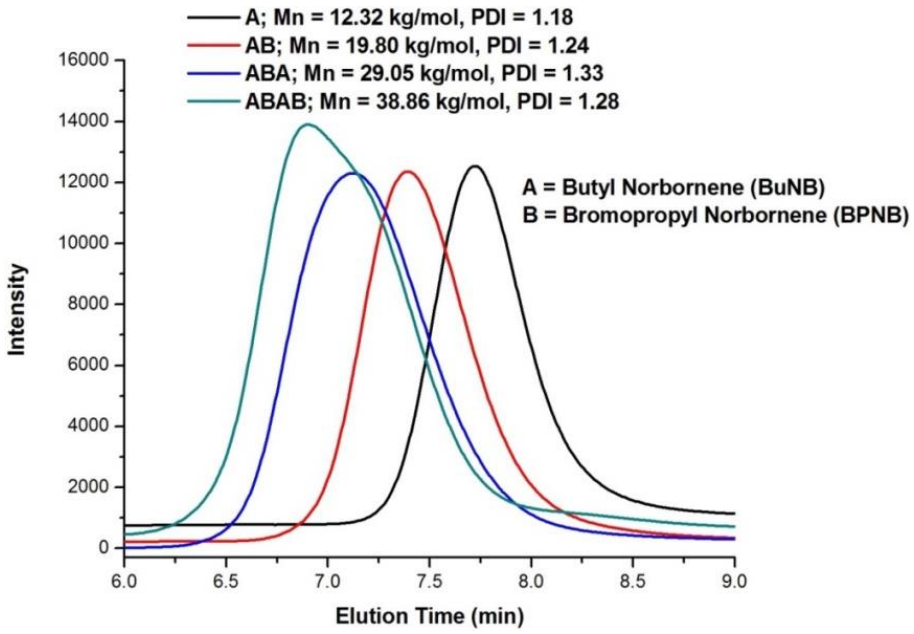


**Figure 2.3 – Representative GPC trace of GT33 showing the sequential growth of each block during the formation of tetrablock copolymer.**

### *2.1.3 Morphological characterization*

SAXS was used to analyze the morphology of AEMs. Hydrated membranes in bromide form were tested in air using either a Malvern Panalytical Empyrean XRD instrument with a Pixel 3D detector or the NSLS-II beamline at the Center for Functional Nanomaterials (Brookhaven National Laboratory, Upton, NY). The wave vector ($q$) was calculated using Equation 1, where 2θ is the scattering angle.

$$q = \frac{4\pi}{l \sin 2\theta} \tag{1}$$

The characteristic separation length, or inter-domain spacing (d) (i.e., the Bragg spacing) was calculated using Equation 2.

$$d = \frac{2\pi}{q} \quad (2)$$

Transmission electron microscopy (TEM) was also used to analyze the morphology of membranes. TEM was performed with a JEOL JEM-1400 Transmission Electron Microscope. Dry membranes with a bromide counter ion were stained by fuming with osmium tetroxide at room temperature prior to TEM examination. The stained membranes were embedded within an epoxy resin, sectioned into ca. 50 nm thick samples with a Leica UC6rt Ultramicrotome, and placed on a copper grid for observation.

### *2.1.4 Ionic conductivity (σ) and alkaline stability*

The hydroxide conductivity of the membranes was measured using a four-point, in-plane probe and electrochemical impedance spectrometry (1 Hz to 1 MHz) with a PAR 2273 potentiostat. All samples were tested in HPLC-grade water under a nitrogen purge to minimize the detrimental effects of $CO_2$. The samples were allowed to equilibrate for 30 min prior to each measurement. The in-plane ionic conductivity was calculated using Equation 4.

$$\sigma = \frac{L}{WTR} \quad (4)$$

In Eq. 4, $\sigma$ is the ionic conductivity in S/cm, L is the length between sensing electrodes in cm, W and T are the width and thickness of the membrane in cm, respectively, and R is the resistance measured in Ohms. The $CO_3^{2-}$ conductivity was measured in a similar manner after storing the films (initially in hydroxide form) in saturated aqueous $K_2CO_3$ for 24 h.

The long-term (>1000 h) alkaline stability testing was performed by immersing the membrane in 1 M NaOH solution at 80 °C in a Teflon-lined Parr reactor. Prior to each measurement, the membranes were taken out of solution and thoroughly washed with DI water. After each measurement, the membranes were stored in the reactors with a freshly prepared NaOH solution. The change in ionic conductivity was used to evaluate the long-term alkaline stability. During measurement, each data point was measured in triplicate and the average value was reported (deviation in the measurement of each data point was <0.5%). The deviation in the measurements of each data point was <1%. In addition, the alkaline stability was further analyzed by characterizing the chemical structure of the same samples using a Nicolet 6700 FT-IR spectrometer. FT-IR was used rather than NMR due to the insolubility of the membrane samples after quaternization and ion-exchange.

### *2.1.5 Water uptake (WU), hydration number (λ) and swelling*

The water uptake of the membranes was calculated using Equation 5. In Eq. 5, $M_d$ is the dry mass of the membrane and $M_w$ is the wet mass of the membrane after removing excess surface water. The membranes were in hydroxide form and measured at room temperature.

$$WU\ (\%) = \frac{M_w - M_d}{M_d} \times 100 \tag{5}$$

The hydration number (λ) or the number of water molecules per ionic group was calculated using Equation 6 from the previously measured WU and IEC.

$$\lambda = \frac{1000 \times WU\%}{IEC \times 18} \quad (6)$$

The percent swelling was calculated by Equation 7, where $V_d$ is dry volume of the membrane and $V_w$ is the volume of the fully hydrated membrane after removing excess surface water.

$$Swelling\ (\%) = \frac{V_w - V_d}{V_d} \times 100 \quad (7)$$

### *2.1.6 Number of freezable ($N_{free}$) and non-freezable ($N_{bound}$) water molecules*

The number of freezable water ($N_{free}$) and bound water (or non-freezable water) ($N_{bound}$) were determined by differential scanning calorimetry (DSC). DSC measurements were carried out on a Discovery DSC with autosampler (TA Instruments). In the DSC thermogram, free water freezes just below 0 °C. Using the hydration number, the number of free water $N_{free}$ can be obtained by subtracting the number of bound waters. The membrane samples were fully hydrated by soaking in deionized water for one week. After the water on the membrane surface was dabbed off, a 5 to 10 mg sample was quickly sealed in an aluminum pan. The sample was cooled to -50 °C and then heated to 30 °C at a rate of 5 °C/min under $N_2$ (20 mL/min). The quantity of freezable and non-freezable water was determined by Equations 8 to 10.[87-89]

$$N_{free} = \frac{M_{free}}{M_{tot}} \times \lambda \quad (8)$$

$M_{free}$ is the mass of freezable water and $M_{tot}$ is the total mass of water absorbed in the membrane. The weight fraction of freezable water was calculated using Equation 9.

$$\frac{M_{free}}{M_{tot}} = \frac{H_f / H_{ice}}{(M_W - M_d)/M_w} \tag{9}$$

$H_f$ is the enthalpy obtained by the integration of the DSC freezing peak and $H_{ice}$ is enthalpy of fusion for water, corrected for the subzero freezing point according to Equation 10.

$$H_{ice} = H_{ice}^{o} - \Delta C_p \Delta T_f \tag{10}$$

$\Delta C_p$ is the difference between the specific heat capacity of liquid water and ice. $\Delta T_f$ is the freezing point depression. A representative DSC trace is shown in Figure 2.4.

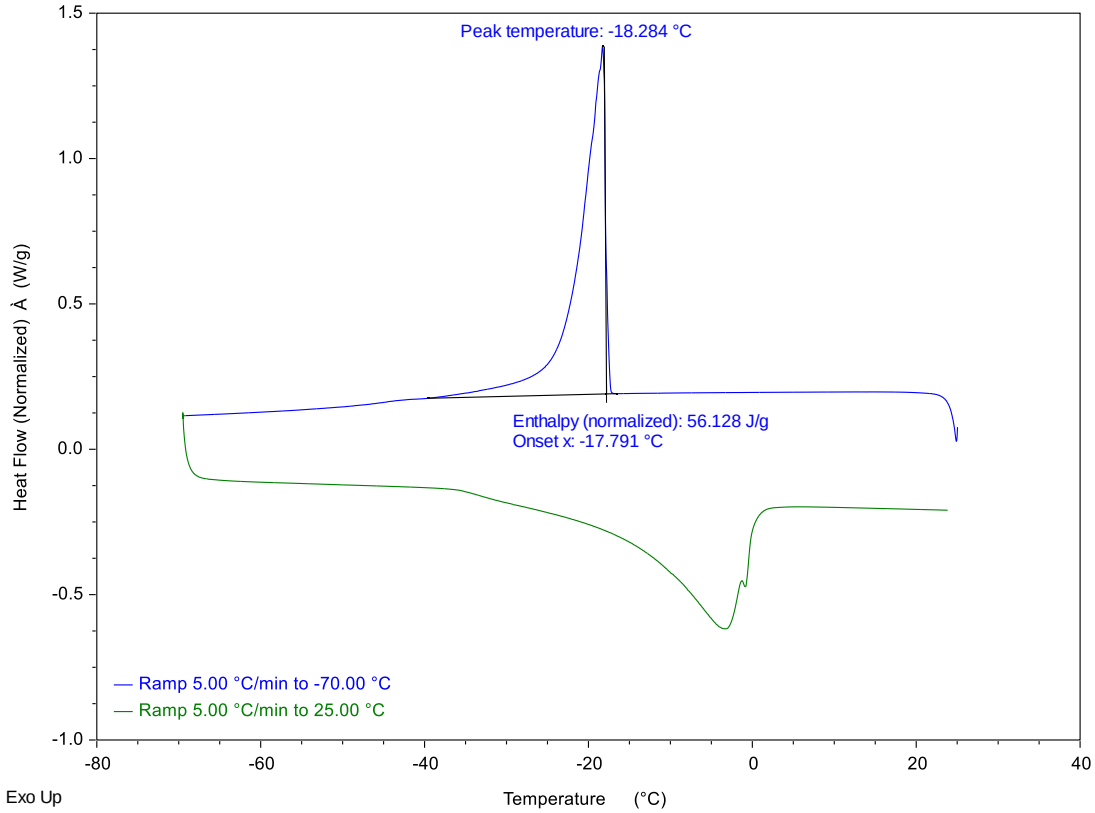


**Figure 2.4 – Representative DSC trace with enthalpy integration from GT66-5.**

### *2.1.7 Thermal stability and glass transition temperature ($T_g$)*

The thermal stability of the membranes was investigated by thermogravimetric analysis (TGA) on a TA Instruments Q50 analyzer. The temperature was ramped at 10 °C/min up to 800 °C in a nitrogen atmosphere. Figure 2.5 shows several representative TGA traces for poly(norbornene) AEMs with varying IEC. Four degradation stages were observed. The first stage of decomposition, below 100 °C, was due to water loss from the membrane. The second stage around 250 °C was due to the decomposition of the quaternary ammonium group. The third stage from 300 °C to 400 °C resulted from the degradation of the alkyl side chains in the polymer. The fourth stage, above 400 °C, was due to the decomposition of polymer backbone.[23, 84] These results suggest that the

membranes were sufficiently stable at the operating conditions for low temperature AEM fuel cells or electrolyzers, which typically operate below 80 °C.

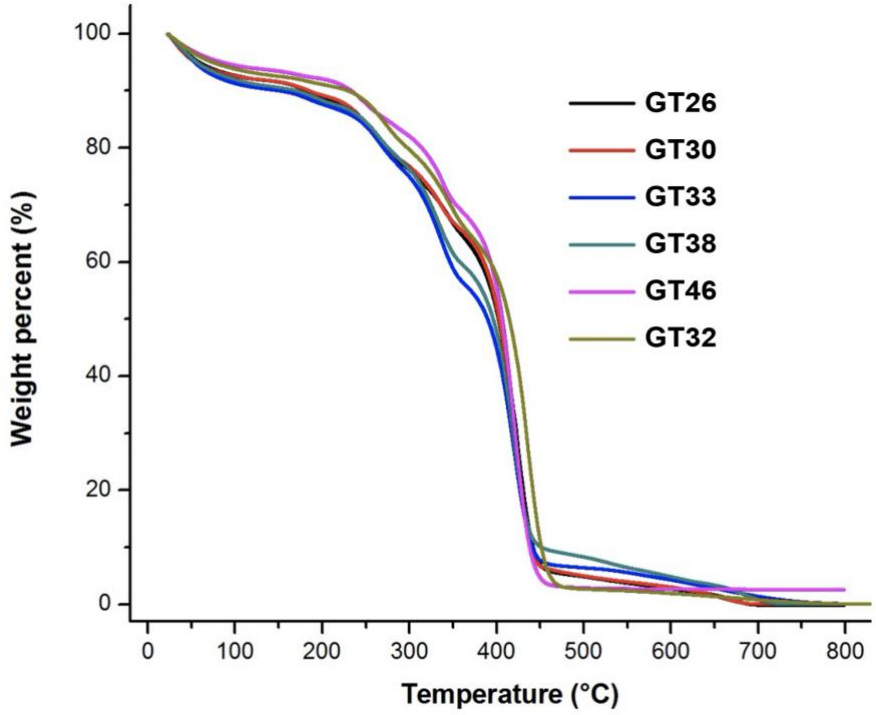


**Figure 2.5 – Representative TGA traces of the poly(norbornene) AEMs under nitrogen atmosphere.**

Vinyl addition poly(norbornene) copolymers are known to have high $T_g$ (250 °C to 400 °C).[90-93] The addition of flexible alkyl side-chains tends to lower the $T_g$ of the polymer. DSC experiments were performed on the tetrablock copolymers used in this study. The AEM samples were heated from 25 °C to 400 °C. However, a $T_g$ was not detected below the decomposition temperature of the polymer (<300 °C). The quaternary ammonium head-groups are known to break-down at or below 250 °C.[32] The $T_g$ of the polymer in other forms (e.g., non-quaternized form) is of no interest because forming the ionic head-groups and absorbing water will affect the $T_g$ of the final polymer.

### *2.1.8 Mechanical properties*

The storage modulus (G') of the reinforced composite membranes was measured by dynamic mechanical analysis (DMA) using a TA Instruments Q800 under a 1 Hz single-frequency strain mode in air at 30 °C. A fully hydrated, rectangular sample was loaded into the DMA with tension clamps after removing surface water. Experiential parameters for the DMA were set to 0.1 % strain and a preload force of 0.01 N with a force track of 125%.

## 2.2 Alkaline exchange membrane fuel cell (AEMFC) testing

### *2.2.1 Electrode fabrication and membrane electrode assembly (MEA)*

AEM gas diffusion electrodes (GDE) used for preliminary evaluations of MEAs containing unreinforced membranes were fabricated by spraying a catalyst and ionomer slurry directly onto a carbon paper gas diffusion layer (GDL). Both the anode and cathode electrodes used Pt on Vulcan carbon as the electrocatalyst and were identical in composition. A lower molecular weight (20.5 kg/mol) version of the poly(BuNB-*b*-BPNB-*b*-BuNB-*b*-BPNB) tetrablock copolymer anion-conductive ionomer powder was first synthesized using the same method as the membranes discussed earlier. Low molecular weight ionomer material was previously found to be advantageous for use as a polymeric binder in fuel cell and electrolyzer electrode fabrication.[42] The dry ionomer powder and 50% platinum on Vulcan XC-72 (carbon) catalyst was ground together with a mortar and pestle in 1.5 mL of isopropyl alcohol (IPA) for 10 minutes to produce finer particles. An additional 2 mL of IPA was added and the mixture and ground for another 5 minutes to achieve the proper slurry viscosity for spraying. The catalyst and ionomer slurry was further sonicated in a water bath at room temperature for 30 min to ensure even dispersion.

The homogenized catalyst and ionomer slurry was sprayed onto 1% water-proofed Toray TGPH-060 carbon paper and dried for 24 h at room temperature. The platinum loading was approximately 2.1 mg/cm$^2$ and an ionomer/carbon ratio of 40% was used. The high metal loading was chosen intentionally to minimize any kinetic losses caused by the non-optimized catalyst.

Prior to MEA testing, the electrodes and membranes were soaked in 1 M NaOH for 1 h (replacing the solution every 20 mins) in a nitrogen atmosphere to convert the membrane and ionomer to hydroxide form. The MEA was placed into Fuel Cell Technologies (Albuquerque, NM) hardware between single-pass serpentine graphite plates with 6 mil PTFE gaskets. The MEAs were tested in a Scribner 850e Fuel Cell Test Station at a cell temperature of 60 °C. Humidified $H_2$ and $O_2$ gas feeds were supplied at the anode and cathode, respectively, at 0.5 L/min. The dew points of the anode and cathode streams were adjusted throughout the course of testing in order to optimize the water balance within the AEMFC.

### *2.2.2 USC and NREL electrode fabrication method*

Highly optimized gas diffusion electrodes were used for evaluating MEAs built with reinforced composite membranes through collaborations with the University of South Carolina (USC) and the National Renewable Energy Laboratory (NREL). Gas diffusion electrodes (GDEs) were prepared by hand spraying the catalyst layer onto a gas diffusion layer (GDL, Toray TGP-H-060 with 5% or 20% PTFE wetproofing) using a similar method described in Omasta et al.[70] ETFE-[poly(ethylene-co-tetrafluoroethylene)]-based radiation grafted anion conductive ionomer (ACI) was provided by Varcoe and Poynton et al.[94] The

ETFE ACI solid ionomer was finely ground with a mortar and pestle and then mixed with platinum on Vulcan carbon (Pt/C, Alfa Aesar HiSPEC 4000) to form the cathode catalyst ink mixture (20 wt% ionomer). Then, a small amount of DI water (1 ml) was added to the solid mixture and the mixture was ground for additional 10 minutes to avoid aggregated particles and then transferred to a vial. 2-propanol was added (a total of 9 ml) to the mortar to rinse the residual powder and then transferred to the mixture. The 2-propanol was added in 2 to 3 steps to ensure that the majority of the ink mixture was collected. The final ground ink mixture was sonicated with a sonic probe for 20 seconds followed by an additional 20 minutes of sonication in an ice bath before it was hand sprayed onto the GDL to produce one 25 $cm^2$ GDE. This process was repeated for the anode catalyst ink mixture using PtRu on Vulcan carbon catalyst with 8% PTFE (20 wt% ionomer). The platinum and platinum ruthenium metal loading of these GDEs were determined by X-ray fluorescence (XRF) or by weighing the mass of the loaded GDE and subtracting the weight of the GDL. 5 $cm^2$ GDEs were cut from the larger Pt/C and PtRu/C 25 $cm^2$ GDEs and combined with an oversized 5 $cm^2$ composite PNB AEM to assemble the MEAs.

The anode and cathode GDEs and membrane were ion exchanged in 1 M KOH solution for a total of 60 minutes (refreshing the base solution every 20 minutes) prior to cell assembly. The membrane was sandwiched between two GDEs and pressed together and secured in 5 $cm^2$ Fuel Cell Technologies hardware between two graphite single pass serpentine flow-fields and PTFE gaskets. The torque applied to the cell was 40 in-lb with a compression ratio of 25%.

### *2.2.3 Single-cell AEMFC testing*

AEMFCs with 5 $cm^2$ active area were assembled by placing the anode and cathode GDEs on opposite sides of the AEM in Fuel Cell Technologies fuel cell hardware with a single channel serpentine flow field. Fuel cell experiments were controlled using a Scribner 850e fuel cell test station. At cell start-up, $N_2$ at 100% relative humidity was flowed through the anode and cathode until a cell temperature of 60 °C was reached. Then, the $N_2$ feeds were switched to ultra-high purity (UHP) $H_2$ and $O_2$ and a constant voltage of 0.5V was applied to allow the cell to break-in. After a stable current density was established, the dew points of the anode and cathode reacting gases were optimized. The cell temperature was gradually increased to 80 °C in 5 °C increments, with the anode/cathode dew points being simultaneously optimized with the cell temperature to avoid membrane dry out. After the cell temperature reached 80 °C, the degree of back-pressurization was also set. After the cell equilibrated at the desired conditions, a polarization curve was collected by slowly sweeping the voltage from open circuit to 0.1 V at 10 mV/s scan rate. Cell performance was also investigated with $CO_2$-free air fed to the cathode. In this case, after the $H_2/O_2$ cell testing, the cathode gas was switched to air and the system was allowed to equilibrate at the same reacting gas dew points and back pressurization for 10 min. Then, the reacting gas dew points and back pressurization were again optimized using the same procedure as above before the polarization curve was collected.

Constant current density stability tests were performed for ca. 100 hours at 600 $mA/cm^2$. These cells were broken-in using the same procedure described above. UHP $H_2$ was fed to the anode and $CO_2$-free air was fed to the cathode in lieu of UHP $O_2$. The dew points of the reacting gases were adjusted periodically during durability testing to ensure

adequate membrane hydration. The cell high frequency resistance was also monitored (at a frequency of 7 kHz) by the fuel cell test station throughout the test.

### *2.2.4 Electrochemical impedance spectroscopy (EIS)*

High frequency resistance (HFR) was analyzed by electrochemical impedance spectroscopy (EIS) using a Metrohm Autolab potentiostat/galvanostat with booster at a constant current of 600 $mA/cm^2$ prior to cell polarization measurements. Cell temperature was either 60 °C or 80 °C with $H_2$ and $O_2$ or $CO_2$-free air flowed at the anode and cathode, respectively. Area specific resistance (ASR) of the membranes was calculated using the HFR. The hydrogen crossover rate was measured by from a linear voltage sweep from 0 to 0.5 V while $H_2$ and $N_2$ flowed at the anode and cathode, respectively. The cell temperature was set to 60 °C with anode and cathode dew points set to 50 °C.

## 2.3 Alkaline exchange membrane electrolysis (AEMEL) testing

### *2.3.1 Membrane electrode assembly (MEA) fabrication*

Anodes and cathodes were fabricated using the catalyst-coated substrate (CCS) method by using an airbrush to spray catalyst ink directly onto the porous transport layer (PTL). The dry ACI powder was first dry ground into finer particles using a mortar and pestle. The amount of ACI is specified in the experiments described in the Chapters 6-7. A small amount of DI water (1mL) was used to wet the dry ACI powder and allowed to hydrate for 20 to 30 min before use. The hydrated ionomer was wet ground for 10 min using a mortar and pestle. 200 mg of platinum on carbon black (Pt/C, Nel Hydrogen), 30 wt% platinum ruthenium alloy on ECS-3701 (PtRu, Pajarito Powder) or 30 wt% platinum

nickel alloy on ECS-3701 (PtNi, Pajarito Powder) was added to the ACI and mixed together with the mortar and pestle to form the cathode catalyst ink mixture. 5 mL of isopropyl alcohol (IPA) was added to the solid mixture and ground for an additional 10 min to break up aggregated clumps. The mixture was then transferred to a vial and another 9 mL of IPA was added to the mortar to rinse the residual catalyst slurry. This was combined with the rest of the mixture. IPA was added in 2 or 3 steps to ensure that the majority of the catalyst ink was collected. The final ink mixture was sonicated for at least 60 min in an ice bath before it was hand sprayed with an airbrush onto the PTL (Toray TGP-H-090 with 5% wetproofing) to produce a 16 $cm^2$ electrode.

The same fabrication method was used for the anode using iridium oxide ($IrO_2$, Nel Hydrogen) or lead ruthenate ($PbRuO_x$, Pajarito Powder) to form the catalyst ink mixture (25 wt% ionomer) and sprayed on a platinized titanium PTL (Nel Hydrogen). The target catalyst loading of the cathode and anode electrodes was 2 $mg/cm^2$. Smaller electrodes (4 $cm^2$) were cut from the larger 16 $cm^2$ anode and cathode electrodes and combined with an oversized 5 $cm^2$ poly(norbornene) AEM to assemble the MEAs.

The AEM, OER and HER electrodes were ion exchanged individually in 1.5 M NaOH solution for a total of 60 min (refreshing the base solution every 20 minutes) prior to cell assembly. A nitrogen cover gas was applied during the entire ion exchange. The AEM was placed between the two electrodes and pressed together in 5 $cm^2$ Fuel Cell Technologies hardware between two 316 stainless steel single-pass serpentine flow-fields and 10 mil Tefzel gaskets. The torque applied to the cell hardware was 25 in-lb.

### *2.3.2 Single-cell AEMEL testing*

The MEA was tested in a custom-built electrolysis test station and operated at a cell temperature of 50 °C. Potassium carbonate in DI water (1 or 3 wt%) was supplied at 0.2 L/min to the anode side only. The cathode side was left open to the atmosphere. The cell was allowed to equilibrate at the desired temperature for 1 hr before testing. A linear polarization sweep was performed prior to break-in of the cell. Cell break-in was performed by first applying 125 $mA/cm^2$ of current until the cell voltage no longer changed. The current density was then increased and allowed reach steady state in steps of 250 $mA/cm^2$ until the desired operating current density was reached. Additional polarization curves were taken periodically throughout the course of the operational test.

### *2.3.3 Electrochemical impedance spectroscopy (EIS)*

The high frequency resistance (HFR) and low frequency resistance (LFR) were measured via electrochemical impedance spectroscopy (EIS) using a PARSTAT 2263 potentiostat after the cell break-in period. Measurements were conducted at 0 V with a frequency range from 10 mHz to 1 kHz. Area specific resistance (ASR) and charge transfer resistance were calculated from the EIS data.

# CHAPTER 3. PROPERTIES OF POLY(NORBORNENE) ANION CONDUCTIVE POLYMERS

The purpose of this chapter is to summarize the physical properties of the materials used as anion exchange membranes and anion conductive ionomers in this thesis. These polymers were synthesized by Dr. Mrinmay Mandal (Georgia Tech) following the methods outlined in Appendix A and cast into freestanding films for characterization.

## 3.1 Background

Stable, non-hydrolysable, hydroxide-conducting polymers are of interest for high-pH electrochemical devices such as fuel cells and low-temperature electrolyzers. Guided by the rational design principles outlined in Chapter 1, poly(norbornene) was chosen as a platform because of its compact monomer size, all-hydrocarbon backbone, high thermal stability and inexpensive precursor (dicyclopentadiene). In this chapter, a facile synthetic strategy was used to prepare a series of anion conducting tetrablock copolymers with long quaternary ammonium head-group tethers based on vinyl addition polymerization of norbornenes. This strategy was found to produce highly conductive membranes and ionomers with high head-group tether density (ion exchange capacity), alkaline and thermal stability, strong mechanical properties and scalable manufacturing.

Poly(norbornene)s can be polymerized through two different synthetic routes that produce materials with glass-transition temperatures ($T_g$) relevant to fuel cells and electrolyzers, Figure 3.1. In this work, the properties of vinyl addition polymerization of norbornenes were explored. The properties of ring-opening metathesis polymerization

(ROMP) of norbornenes are disclosed in a separate publication.[46] The methods of synthesis and resulting properties of the ROMP and vinyl addition polymer are different. Especially notable between these two materials is the glass transition temperature ($T_g$). Vinyl addition polymerized norbornenes have a high glass transition temperature.[90-93] Vinyl addition PNB has high $T_g$, very good thermal stability, and excellent mechanical properties. Vinyl additional poly(norbornene) has a $T_g$ of 390 °C and poly(hexylnorbornene) has a $T_g$ of 265 °C. A variety of norbornene copolymers were shown to have a $T_g$ between 340 °C and 355 °C,[90] 203 °C and 331 °C,[91] 293 °C and 360 °C,[92] and over 380 °C for poly(methylnorbornene).[93] By contrast, many ROMP norbornenes have been reported to have $T_g$ below 150 °C.[95-97] While ROMP norbornene was not used in this work, there is interest in ion conducting polymers with different properties for ion conducting adhesion layers between the electrode and membrane.

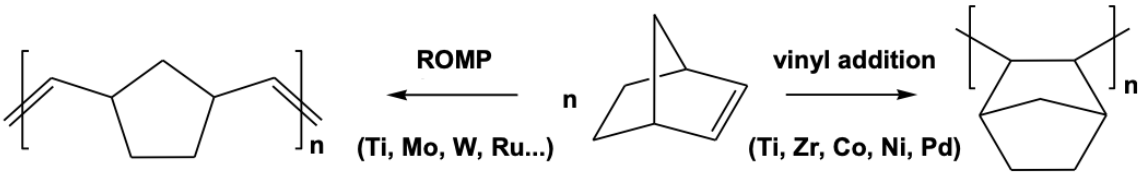


**Figure 3.1 – Vinyl addition and ring-opening metathesis polymerization of norbornene.**

In this work, it was shown that the vinyl addition polymerization route could produce AEMs and ionomers with high hydroxide conductivity and excellent alkaline and thermal stability. For these materials to be useful in electrochemical devices (e.g., fuel cells, electrolyzers), the ion conducting polymers should have the highest possible ion conductivity. A multiblock structure of these polymers consisting of ion conducting "hydrophilic" blocks and structural "hydrophobic" blocks was designed to allow for the

formation of continuous nanophase segregated ion conduction channels and improve the ion mobility and conductivity, as shown in earlier examples.[23, 31, 48] For anion conducting polymers, there is a compromise between the polydispersity of the blocks, overall molecular weight of the polymer and product yield. Tetrablock copolymer was chosen for this work because it has a sufficiently high molecular weight and good yield. Butyl norbornene (BuNB) and bromopropyl norbornene (BPNB) were used as the hydrophobic and hydrophilic monomers, respectively. The post-polymerized materials were treated with trimethylamine (TMA) to convert the bromoalkyl sites to anion conducting quaternary ammonium head-groups. The bromide counter ions were exchanged with hydroxide ions before being used. The compact size of the norbornene monomer allows for high ion exchange capacity (IEC) because the tethered quaternary ammonium head groups can be concentrated along the chemically stable all-hydrocarbon backbone. High IEC can be useful for increasing ionic conductivity, but it can also lead to excessive water uptake and swelling if not properly managed. It was found that light cross-linking of post-polymerized norbornene extended the usable IEC range to very high values (>3 meq/g) without unwanted water uptake or swelling. Figure 3.2 shows the tetrablock copolymers used in this work cross-linked via the hydrophilic groups using N,N,N′,N′-tetramethyl-1,6-hexanediamine (TMHDA) as the cross-linking agent. This configuration preserved the number of ion conductive head groups and spacing from the polymer backbone while improving the mechanical properties and increasing the molecular weight.

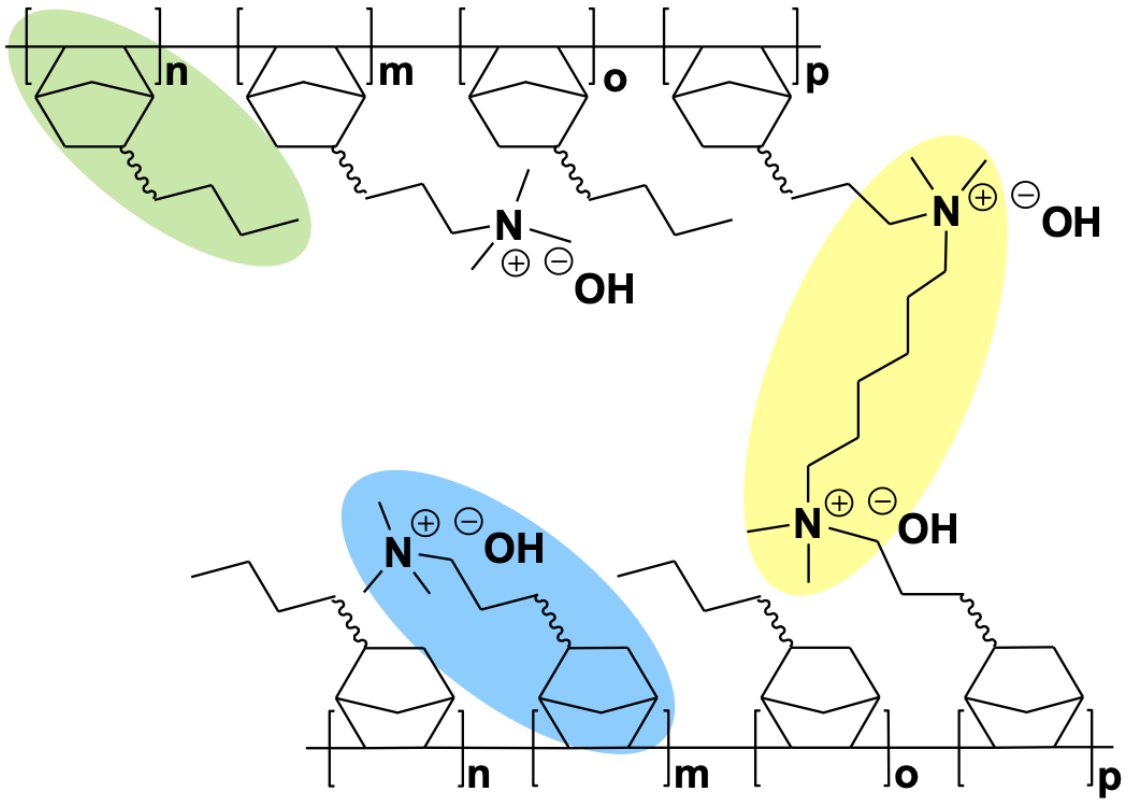


**Figure 3.2 – Vinyl addition poly(norbornene) tetrablock copolymers cross-linked with TMHDA (yellow). Hydrophobic blocks (green) and hydrophilic blocks (blue) are highlighted.**

In the following sections of this chapter, the molecular weight, polydispersity, IEC, ionic conductivity, alkaline stability, water uptake, swelling, and morphology for the non-cross-linked and cross-linked poly(norbornene) tetrablock copolymers are described. Later, the properties of composite AEMs composed of the cross-linked polymers and a proprietary polymer reinforcement layer are also described. The IEC was controlled by varying the length of the hydrophobic and hydrophilic blocks and related to the ionic conductivity. The block sizes were changed by adjusting the monomer-to-initiator feed ratio in toluene during polymerization. The ion mobility was quantified by the ratio of the ionic conductivity to the IEC ($\sigma$/IEC) in units of g S/cm eq. The alkaline stability was

characterized by aging the polymers in 1 M NaOH at 80 °C and measuring the loss in ionic conductivity vs. time. The distribution of water in the membranes, in terms of the number of bound and unbound water molecules per ion pair, was measured and correlated with ionic conductivity. The nanophase segregated morphology was examined to determine the size, shape and continuity of the ion conduction channels. In Chapters 4-7, the polymers were evaluated in AEM fuel cells and electrolyzers. The results were used to help elucidate the relationship between the polymer structure and physical properties with device performance.

Throughout this thesis, the poly(norbornene) tetrablock copolymers are denoted as GTXX, where XX is the mol% of bromoalkyl norbornene monomer (resulting in the quaternary ammonium head group) in the block copolymer. Larger XX values result in a higher IEC and WU. Cross-linked versions of these polymers are denoted as GTXX-Y, where Y represents the mol% of cross-linker relative to the available cationic sites. Larger Y values result in lower WU. A non-ionic homopolymer with no ionic conductivity (GT0) and a fully ionic homopolymer (GT100) were also used in this work.

## 3.2 Vinyl addition poly(norbornene) anion conducting polymers

### *3.2.1 Physical properties and ion exchange capacity*

The properties of the vinyl addition poly(norbornene) tetrablock copolymers used in this thesis are listed in Table 3.1. The number average molecular weight ($M_n$) of the synthesized polymers ranged from 38 to 116 kDa with polydispersity of 1.11 to 1.88. This range of molecular weights was previously found to be effective for highly conductive anion conducting polymers.[23, 31, 42, 45, 48, 98] The IEC value was determined by $^1$H NMR

spectroscopy scaled linearly with the hydrophilic monomer content and found to range from 0 to 4.88 meq/g. There was a general trend between molecular weight and membrane performance for similar IEC polymers which will be discussed in greater detail in the Section 3.2.2. For example, GT32 and GT38 have a similar IEC, however, the conductivity of GT32 is 22% higher than GT38 at 80 °C due to its higher molecular weight. The physical presence of more ion conducting head groups and chain entanglement within longer polymers may be responsible for improved performance.

The hydroxide conductivity, ion mobility ($\sigma$/IEC), alkaline stability, water uptake (WU), hydration number ($\lambda$), free and bound waters ($N_{free}$, $N_{bound}$), inter-domain spacing (d) and morphology are discussed in detail in the following subsections. Conductivity and water uptake were not measured for GT0 due to the absence of ion conduction. The conductivity of high IEC polymers (e.g., GT69, GT72, GT74, GT75, GT82, GT100) could not be measured as-is because the materials were soft and delicate when hydrated and could not be handled. These materials were used primarily as the anion conductive ionomer (ACI) for electrolyzer anodes and cathodes in Chapters 6 and 7.

**Table 3.1 – Properties of poly(norbornene) tetrablock copolymers in hydroxide form.**

| Block copolymer | $M_n$ [a] (kg/mol) | Đ | IEC [b] (meq/g) | $OH^-$ Conductivity (mS/cm) [c] | | $\sigma$/IEC [d] | Water Uptake (%) [e] | Hydration number ($\lambda$) | $N_{free}$ | $N_{bound}$ | *d*-spacing (nm) [f] |
|---|---|---|---|---|---|---|---|---|---|---|---|
| | | | | 25°C | 80°C | | | | | | |
| GT0 | 84.45 | 1.11 | 0 | ND | ND | ND | ND | ND | ND | ND | ND |
| GT11 | 84.73 | 1.62 | 0.69 | 0.47 | 0.79 | 1.14 | 3.7 | 2.98 | ND | ND | ND |
| GT18 | 36.53 | 1.38 | 1.13 | 5.8 | 11.6 | 10.3 | 15 | 7.37 | ND | ND | ND |
| GT25 | 68.6 | 1.88 | 1.49 | 27.5 | 60.4 | 40.5 | 24 | 8.95 | ND | ND | ND |

| | | | | | | | | | | | |
|---|---|---|---|---|---|---|---|---|---|---|---|
| GT26 | 39.58 | 1.42 | 1.55 | 23.4 | 61.3 | 39.5 | 26.2 | 9.41 | 0.91 | 8.50 | ND |
| GT30 | 37.97 | 1.29 | 1.77 | 27.0 | 67.4 | 38.1 | 59.6 | 18.71 | 5.42 | 13.29 | 37.2 |
| GT32 | 114.9 | 1.42 | 1.88 | 62.0 | 122.7 | 65.2 | 63.0 | 18.62 | 6.74 | 11.88 | ND |
| GT33 | 38.86 | 1.28 | 1.92 | 32.2 | 71.8 | 37.4 | 68.8 | 19.91 | 7.81 | 12.10 | 44.2 |
| GT38 | 50.77 | 1.54 | 2.21 | 50.9 | 101.9 | 46.1 | 71.0 | 17.85 | 7.61 | 10.24 | 49.9 |
| GT46 | 45.33 | 1.55 | 2.60 | 44.9 | 80.0 | 30.8 | 133.6 | 28.55 | 10.65 | 17.90 | 86.4 |
| GT64 | 50.96 | 2.02 | 3.37 | ND | ND | ND | >1000 | ND | ND | ND | ND |
| GT66 | 29.15 | 1.42 | 3.46 | ND | ND | ND | >1000 | ND | ND | ND | ND |
| GT69 | 116.4 | 1.56 | 3.45 | ND | ND | ND | >1000 | ND | ND | ND | ND |
| GT72 | 68.2 | 1.17 | 3.53 | ND | ND | ND | >1000 | ND | ND | ND | ND |
| GT74 | 40.35 | 1.26 | 3.63 | ND | ND | ND | >1000 | ND | ND | ND | ND |
| GT75 | 73.8 | 1.51 | 3.70 | ND | ND | ND | >1000 | ND | ND | ND | ND |
| GT78 | 103.6 | 1.30 | 3.73 | ND | ND | ND | >1000 | ND | ND | ND | ND |
| GT82 | 57.7 | 1.41 | 3.95 | ND | ND | ND | >1000 | ND | ND | ND | ND |
| GT100 | 23.31 | 1.42 | 4.88 | ND | ND | ND | >1000 | ND | ND | ND | ND |

[a] Measured in bromopropyl form by gel permeation chromatography at RT in THF relative to polystyrene standards. [b] IEC (Ion Exchange Capacity) was calculated via $^1$H NMR results in bromopropyl form. [c] $OH^-$ conductivity was measured by four-probe conductivity cell. [d] Ionic conductivity at 80 °C/IEC. [e] Water uptake was measured at room temperature. [f] Inter-domain spacing measured using small angle X-ray scattering (SAXS) in bromide form; GTXX (GT = Georgia Tech; XX = molar ratio of halogenated block) GT18, GT32, GT38, and GT100 were synthesized using BPNB as the halogenated block and the others used BBNB. Standard deviation for WU was ± 3%. ND = not determined.

### *3.2.2 Hydroxide conductivity, ion mobility and alkaline stability*

High hydroxide conductivity (σ) is desired in membranes used in electrochemical devices.[27] The ionic conductivity of the polymer samples generally increased with IEC. Among the samples measured, GT32 had the highest hydroxide conductivity and mobility ($\sigma$/IEC = 65.2), despite having a more modest IEC compared to the others (Table 3.1). Conversely, the hydroxide mobility in GT46, for example, was among the lowest the membranes even though the IEC was the higher than GT32 (Table 3.1). A possible explanation for the outliers (e.g., GT33, GT38 and GT46) is that the higher molecular

weight of GT32 contributed to greater chain entanglement which enables better ion mobility through more efficient ion conduction channel formation. The effect of molecular weight is particularly clear when comparing the GT32 to the GT33 and GT38 (Table 3.1). The number of blocks is the same and the IEC values are close (ca., 1.88 to 2.21). However, the σ/IEC is almost double for GT32 due to its longer block length.

Figure 3.3 shows that the hydroxide conductivity of a representative selection of samples from Table 3.1 increased with temperature from 25 °C to 80 °C and followed an Arrhenius relationship. In general, the hydroxide conductivity of all samples approximately doubled when the temperature was increased from 25 °C to 80 °C. The hydroxide transport activation energy ($E_a$) was calculated from the of slope ln$\sigma$ vs. 1000/T in Figure 3.4 and was found to be 9.33 to 15.28 kJ $mol^{-1}$. These $E_a$ values were close to that of proton exchange membranes such as Nafion-117 (12.75 kJ $mol^{-1}$).[99]

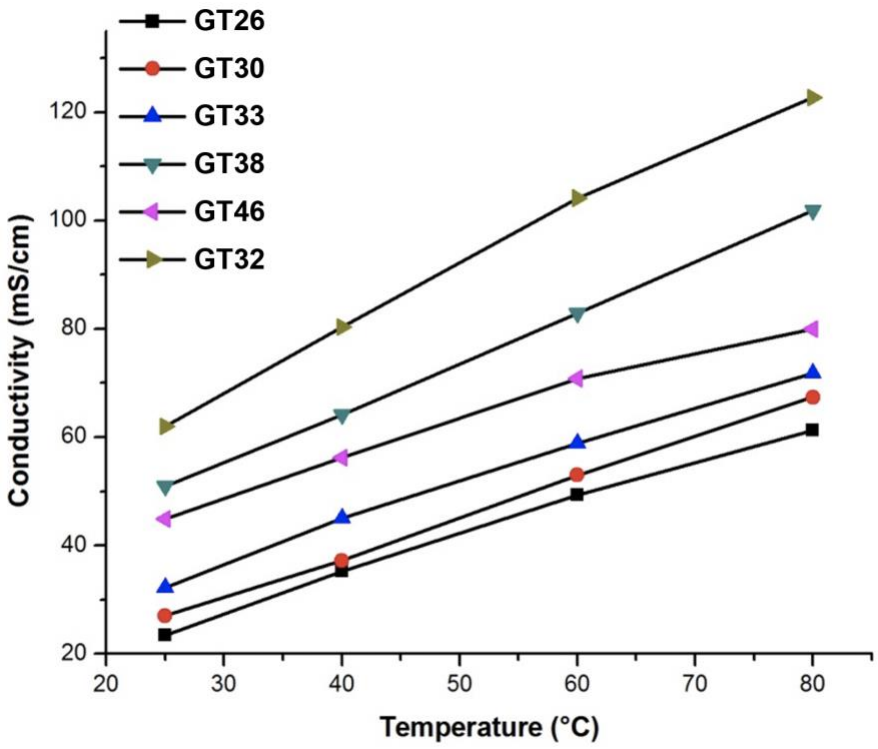


**Figure 3.3 – Ionic conductivity of poly(norbornene) AEMs at different temperatures.**

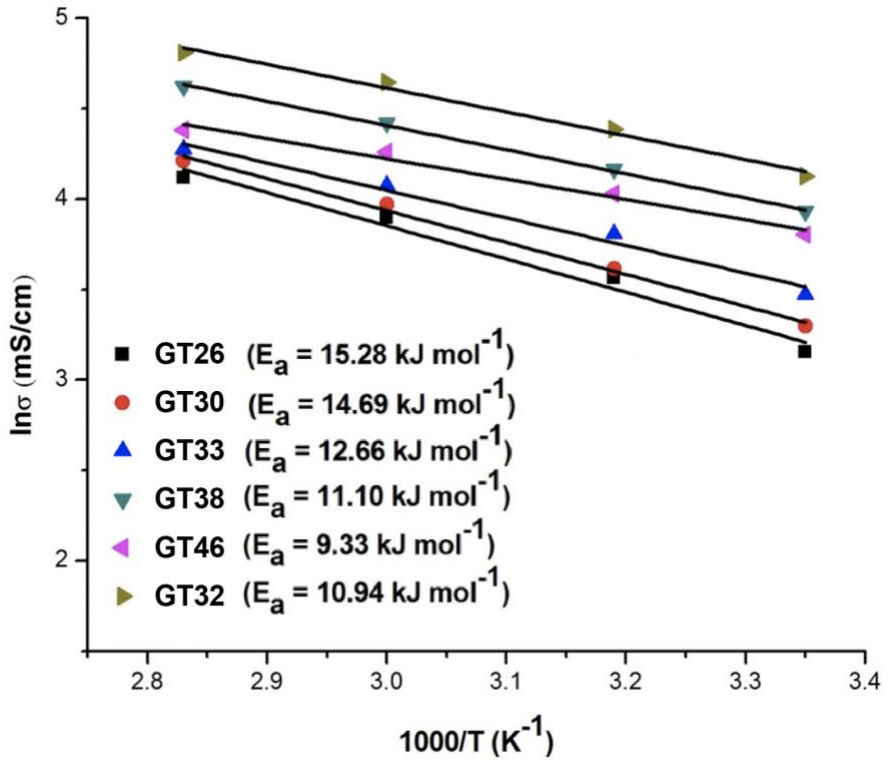


**Figure 3.4 – Arrhenius plot of ln(σ) vs. inverse temperature for poly(norbornene) AEMs.**

Membrane durability is essential for long operational life in electrochemical devices. Figure 3.5 shows the alkaline stability assessment of a representative selection of samples from Table 3.1. The membranes were soaked in 1 M NaOH solution at 80 °C and the loss of ionic conductivity was measured vs. time for 1200 h. Each data point was measured in triplicate and there was <0.5% deviation in the individual measurements. No detectable (<1 %) loss was observed in the ionic conductivity over 1200 h. Hence, it can be concluded that the non-hydrolysable polymer backbone with cations tethered via long side chains displays adequate alkaline stability compared to hydrolysable polymer

backbones (e.g., polysulfone, polyketone, polyethers) and the benzyl attachment of cations to the polymer chains.[53, 63, 75, 100]

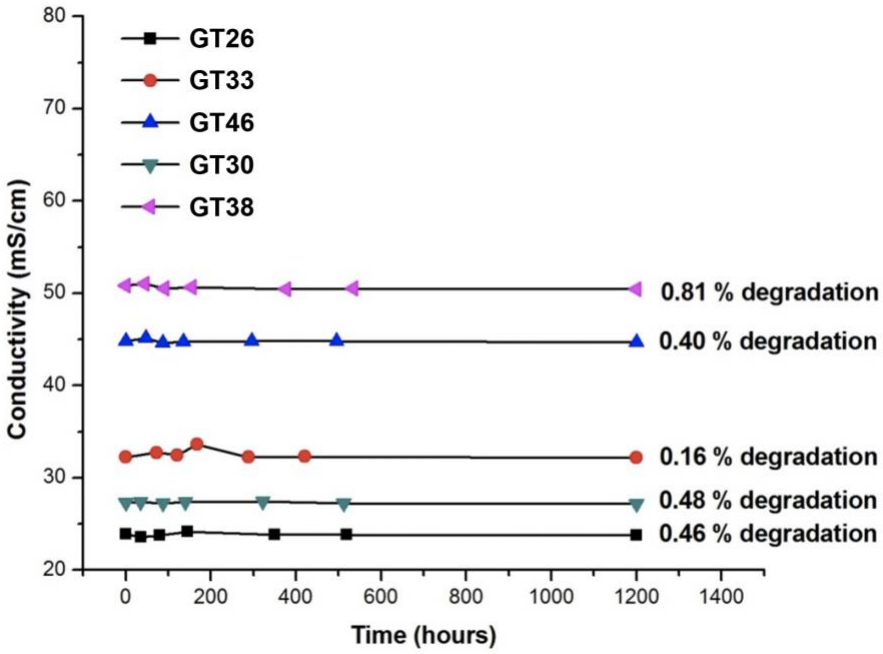


**Figure 3.5 – The alkaline stability of poly(norbornene) AEMs at 1 M NaOH solution at 80 °C.**

### *3.2.3 Water uptake, hydration number, free and bound water molecules*

Water uptake is a key parameter in determining the conductivity and mechanical stability of the AEMs. An adequate amount of water is necessary for ion hydration and conduction. However, excess water in the form of free water can lead to swelling and poor performance of the membrane electrode assembly (MEA) due to membrane softening and channel flooding. Hence, an optimum amount of bound water in the membrane is required to form the ion solvent shell.[23, 31, 48] As shown in Table 3.1, the water uptake of the membranes increased linearly with increasing IEC. Molecular weight of the polymer did not have significant effect on the WU. Polymer samples with high IEC (e.g., GT69, GT72,

GT74, GT75, GT82 and GT100) had excessive water uptake which was estimated to be greater than 1000%.

The hydration number ($\lambda$) is the number of water molecules per ionic head-groups. The high hydration number of GT46 was the result of the presence of unproductive water. Differential scanning calorimetry was used to differentiate the waters of hydration and measure the number of freezable water molecules ($N_{free}$) and bound, non-freezable water molecules ($N_{bound}$) in the membrane. The results of several representative samples are shown in Table 3.1. In the case of GT32, the amount of $N_{free}$ and $N_{bound}$ in the membrane was 6.7 and 11.9, respectively. This was close to the optimum number of bound waters (9 to 10 per ionic pair), as previously reported.[31] Consequently, this membrane also showed the highest conductivity, 122.7 mS/cm at 80 °C. The presence of higher free (10.6) and bound (17.9) water for GT46 resulted in a decrease in the conductivity, 80 mS/cm at 80 °C, although the IEC (2.60 vs. 1.88) was higher than GT32. This can be attributed to the formation of overly large ion conducting channels flooded with unproductive water. The lower free water content (0.9) for GT26 was not sufficient to support effective ion transport. Hence, the conductivity was lower (61.3 mS/cm at 80 °C). In case of GT33, even though the free water (7.8) was acceptable, the higher bound water (12.1) resulted in lower conductivity due to the larger number of waters of hydration. The lower free water (5.4) and higher bound water (13.3) for GT30 was the reason for lower ionic conductivity in the membrane.

### *3.2.4 Morphology*

SAXS and TEM were used to investigate the phase segregated microstructure of the poly(norbornene) membranes synthesized for this work. The inter-domain spacing (*d*), or the average separation length between inhomogeneities in the membranes, was determined from the Bragg spacing of the primary scattering peak in the SAXS spectra, as shown in Figure 3.6. The inter-domain spacing of several representative samples are listed in Table 3.1. The domain size range was 37.2 to 86.4 nm, which directly correlated with water uptake. More specifically, it can be seen that the number of unbound waters tracks with the domain size. This shows that the unproductive, free-water can populate ion channels when they are larger than the optimum size.[18] For example, GT46 showed a very high water uptake, 133.6%, and a *d*-spacing, 86.4 nm. By comparison, these values are about twice as large as the ones for GT33, which had a water uptake of 68.8% and a *d*-spacing of 44.2 nm.

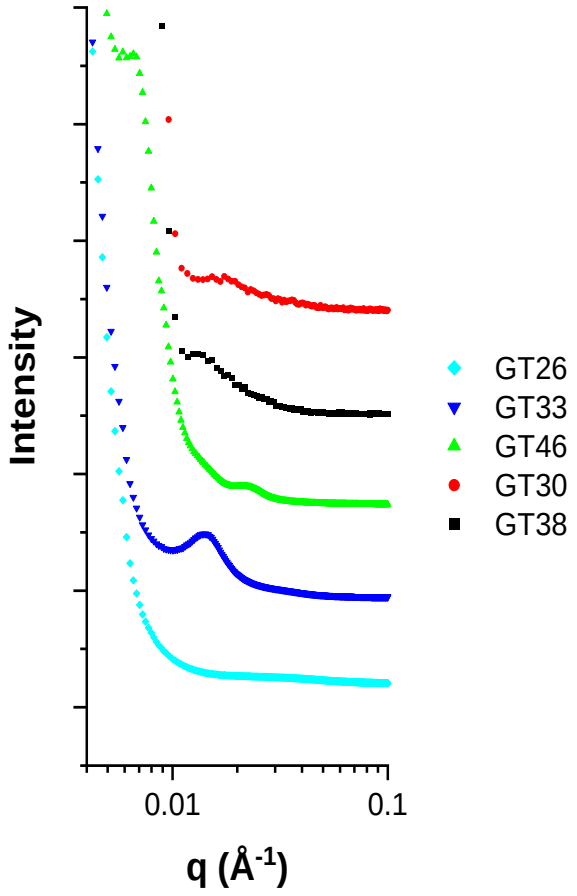


**Figure 3.6 – SAXS spectra of hydrated tetrablock copolymer poly(norbornene) membranes in bromide form.**

TEM analysis was performed on several representative samples from Table 3.1. TEM was done in bromide form rather than in hydroxide form to avoid inadvertent degradation of the membranes due to concentrated hydroxide in dry membranes. Figure 3.7 shows TEM micrographs for five membranes with varying IEC. The dark regions correspond to the hydrophilic domains with bromide counter ions and the bright regions correspond to hydrophobic domains. Membranes with higher IEC also contain more dark regions in the TEM micrographs. It was observed that the size of the hydrophilic phase appeared to increase with the IEC of the membranes. This is consistent with the increasing inter-domain spacing observed previously using SAXS. The ion channels also appear to

lose their definition and structure as the channel size became larger. It should be noted that trends observed using TEM in the dry state would likely be more pronounced if the membranes could be observed hydrated with water as in the SAXS measurements.

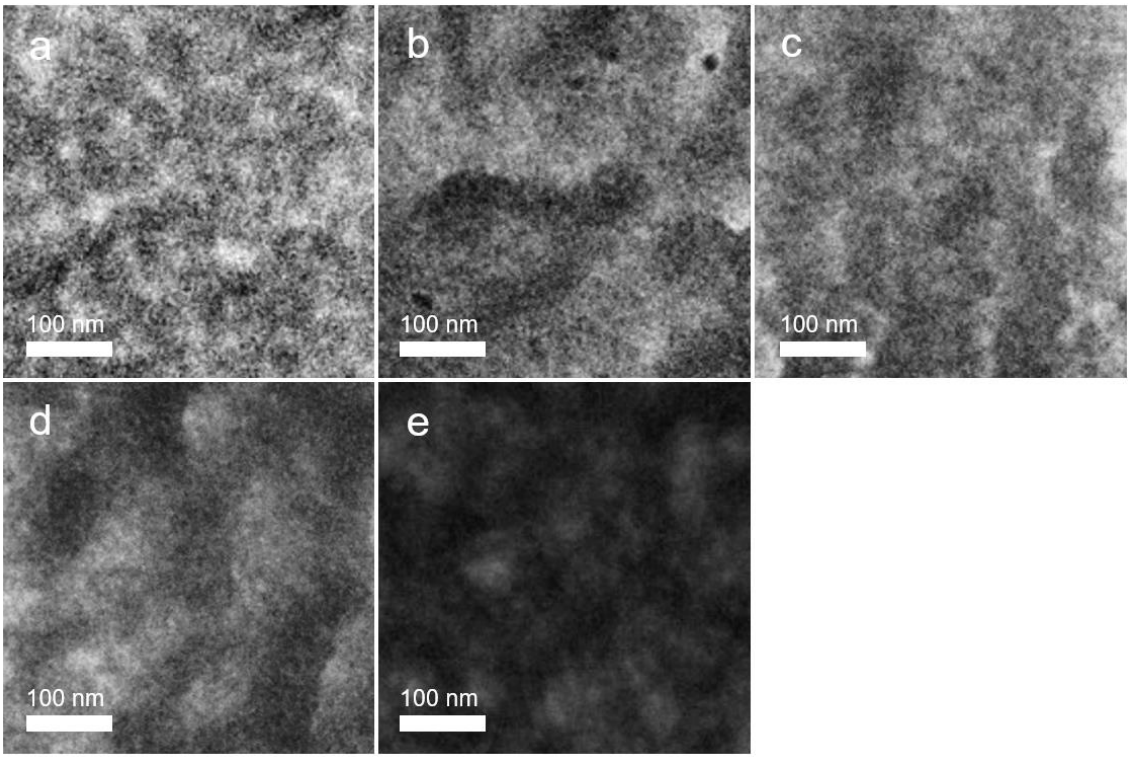


**Figure 3.7 – TEM micrographs of a) GT26, b) GT30, c) GT33, d) GT38, e) GT46 in bromide form.**

## 3.3 Cross-linked poly(norbornene) anion conducting polymers

### *3.3.1 Physical properties and ion exchange capacity*

High IEC is desired to increase the conductivity of ion conducting polymers. However, the membranes become mechanically unstable due to excessive water uptake as discussed in the previous section. Light cross-linking of post-polymerized norbornene was

used to extend the usable IEC range to very high values (>3 meq/g) without unwanted water uptake or swelling. Several high IEC polymers from Table 3.1 (e.g., GT64, GT66, GT72, GT74, GT78, GT82) were selected to be precursors for cross-linked membrane and ionomer studies. A cross-linking agent, TMHDA, was added to the at different concentrations (1-50 mol%) with respect to the total moles of the halogenated monomer in the tetrablock polymer. The properties of the cross-linked vinyl addition poly(norbornene) tetrablock copolymers used in this thesis are listed in Table 3.2

The number average molecular weight and polydispersity of the could not be measured using GPC after cross-linking because the polymers were no longer soluble. It is assumed that the cross-linked polymer samples have significantly higher molecular weight than their non-cross-linked counterparts. The IEC of the cross-linked polymers was calculated from the IEC of the precursor polymer measured previously using NMR and the mass of the cross-linker added. These IEC values were also verified by titration and were found to be nearly identical. In all samples, the IEC decreased linearly with the addition of the cross-linker shown in Table 3.2. The change in IEC after cross-linking was minimal and decreased by 0-9%. Like the non-cross-linked polymers, there was a general trend between precursor polymer molecular weight and performance of similar IEC polymers. For example, the precursor to GT75-5 ionomer has twice the molecular weight of the precursor to GT74-5 ionomer and its conductivity at 80 °C is 26% higher than GT74-5 even though their IEC values are nearly identical. Again, the physical presence of more ion conducting head groups and chain entanglement within longer polymer chains may be responsible for improved performance which will be discussed in more in the Section 3.3.2.

The hydroxide conductivity, ion mobility ($\sigma$/IEC), alkaline stability, water uptake (WU), hydration number ($\lambda$), free and bound waters ($N_{free}$, $N_{bound}$) and inter-domain spacing ($d$) are discussed in detail in the following subsections. These materials were used to make reinforced composite membranes used fuel cells and electrolyzers in Chapters 4-7 as well as the anion conductive ionomer (ACI) for electrolyzer anodes and cathodes in Chapter 6 and 7.

**Table 3.2– Properties of cross-linked poly(norbornene) tetrablock copolymers in hydroxide form.**

| Block copolymer | XL (mol. %) [a] | $OH^-$ Conductivity (mS/cm) | | IEC (meq/g) [b] | IEC (meq/g) [c] | $\sigma$/IEC [d] | WU (%) | Hydration num. ($\lambda$) | $N_{free}$ | $N_{bound}$ | $d$-spacing (nm) |
|---|---|---|---|---|---|---|---|---|---|---|---|
| | | 25°C | 80°C | | | | | | | | |
| GT64-5 | 5 | 84 | 181 | 3.34 | 3.3 | 54.2 | 90 | 15.0 | 3.18 | 11.8 | ND |
| GT64-10 | 10 | 74 | 162 | 3.31 | 3.24 | 48.9 | 61 | 10.2 | 0.13 | 10.1 | ND |
| GT64-15 | 15 | 62 | 142 | 3.28 | 3.26 | 43.3 | 52 | 8.81 | 0.05 | 8.76 | ND |
| GT64-20 | 20 | 52 | 119 | 3.25 | 3.16 | 36.7 | 43 | 7.35 | 0.09 | 7.26 | ND |
| GT66-4 | 4 | 86.8 | 184 | 3.43 | ND | 53.5 | 73.7 | 11.9 | 6.20 | 5.73 | 49.0 |
| GT66-5 | 5 | 95.2 | 198 | 3.43 | ND | 57.8 | 69.1 | 11.2 | 5.21 | 6.00 | 48.9* |
| GT66-7 | 7 | 81.2 | 175 | 3.41 | ND | 51.4 | 66.2 | 10.8 | 4.22 | 6.56 | 48.6 |
| GT66-10 | 10 | 74.8 | 167 | 3.39 | ND | 49.3 | 52.9 | 8.67 | 2.31 | 6.35 | 51.8 |
| GT66-20 | 20 | 45.9 | 111 | 3.33 | ND | 33.3 | 50.8 | 8.47 | 0.96 | 7.52 | 51.8 |
| GT66-50 | 50 | 29.0 | 74.0 | 3.15 | ND | 23.5 | 42.0 | 7.39 | 0.00 | 7.40 | 49.7 |
| GT69-5 | 5 | 89 | 178 | 3.38 | ND | 52.7 | 115 | 18.90 | ND | ND | ND |
| GT72-1 | 1 | ND | ND | 3.53 | ND | ND | 502 | 79.01 | ND | ND | ND |
| GT72-3 | 3 | ND | ND | 3.52 | ND | ND | 198 | 31.25 | ND | ND | ND |
| GT72-5 | 5 | 83 | 175 | 3.50 | ND | 50.0 | 96 | 15.24 | ND | ND | ND |
| GT72-10 | 10 | 69 | 153 | 3.47 | ND | 44.1 | 78 | 12.49 | ND | ND | ND |
| GT72-15 | 15 | 57 | 131 | 3.44 | ND | 38.1 | 66 | 10.66 | ND | ND | ND |
| GT74-3 | 3 | ND | ND | 3.58 | ND | ND | 219 | 33.99 | ND | ND | ND |
| GT74-5 | 5 | 80 | 160 | 3.56 | ND | 44.9 | 103 | 16.07 | ND | ND | ND |
| GT75-5 | 5 | 99 | 201 | 3.63 | ND | 55.4 | 119 | 18.21 | ND | ND | ND |

| | | | | | | | | | | | |
|---|---|---|---|---|---|---|---|---|---|---|---|
| GT78-5 | 5 | 96 | 162 | 3.70 | 3.61 | 43.8 | 163 | 24.5 | 12.7 | 11.0 | ND |
| GT78-15 | 15 | 65 | 138 | 3.62 | 3.52 | 38.1 | 65 | 9.98 | 1.71 | 8.26 | ND |
| GT82-5 | 5 | 109 | 212 | 3.84 | 3.76 | 55.2 | 122 | 17.6 | 7.59 | 10.1 | ND |
| GT82-10 | 10 | 90 | 193 | 3.80 | 3.71 | 50.8 | 87 | 12.7 | 1.04 | 11.7 | ND |
| GT82-15 | 15 | 67 | 147 | 3.76 | 3.70 | 39.1 | 67 | 9.90 | 1.41 | 8.49 | ND |
| GT82-20 | 20 | 55 | 128 | 3.72 | 3.69 | 34.4 | 61 | 9.11 | 0.00 | 9.11 | ND |
| GT100-15 | 15 | 66 | 148 | 4.73 | ND | 31.3 | 89 | 10.45 | ND | ND | ND |

[a] Cross-linker concentration. [b] IEC was determined by $^1$H NMR [c] IEC was determined by titration. [d] Ionic conductivity at 80 °C/IEC. [e] Water uptake was measured at room temperature. XL = cross-linked, PNB = poly(norbornene); [*] d-spacing was estimated via linear interpolation. GTXX-Y (GT = Georgia Tech; XX = molar ratio of halogenated block; Y = cross-linker concentration). Standard deviation for WU was ± 3%. ND = not determined.

### *3.3.2 Hydroxide conductivity, ion mobility and alkaline stability*

High hydroxide conductivity is needed for membranes used in electrochemical devices. The addition of an adequate amount of cross-linking agent enables the use of higher IEC materials (>3 meq/g) without mechanical instability. Like the non-cross-linked versions of these polymers, the ionic conductivity tracked with the IEC of the polymer. For example, GT82-5 had a higher conductivity than GT64-5 (212 vs. 181 mS/cm at 80 °C) due to its higher IEC (3.84 vs. 3.34 meq/g). Figure 3.8 shows the effect of cross-linker concentration on ionic conductivity for a representative polymer series (GT66). In general, it was observed that highest ionic conductivity for any polymer series was measured at 5 mol% cross-linker concentration. In all polymers, the ionic conductivity decreased with higher cross-linker concentration. The ionic conductivity also decreased when there was not enough cross-linking (<5 mol%). The trend can be seen in the slightly lower conductivity of the 4% cross-linker sample in Figure 3.8. In some cases of samples with very high IEC (e.g., GT72 and GT74), mechanically stable films could not even be made

for conductivity measurements with cross-linker concentrations <5%. This shows that only a light amount of cross-linking is needed to enable full use of high IEC materials.

The hydroxide mobility ($\sigma$/IEC) gives insight into the cause of lower hydroxide conductivity with higher cross-linker concentrations. Since the IEC value of each membrane in a series is approximately the same (the only mass change is due to the added cross-linker), the hydroxide mobility tracks with conductivity. The data in Table 3.2 shows that the highest mobility values were in samples with 5 mol% cross-linker whereas, samples with high amounts of cross-linker (≥15 mol%) displayed the lowest mobility. This shows that a high degree of cross-linking limits mechanical deformation in the membranes and inhibits ion mobility.[101]

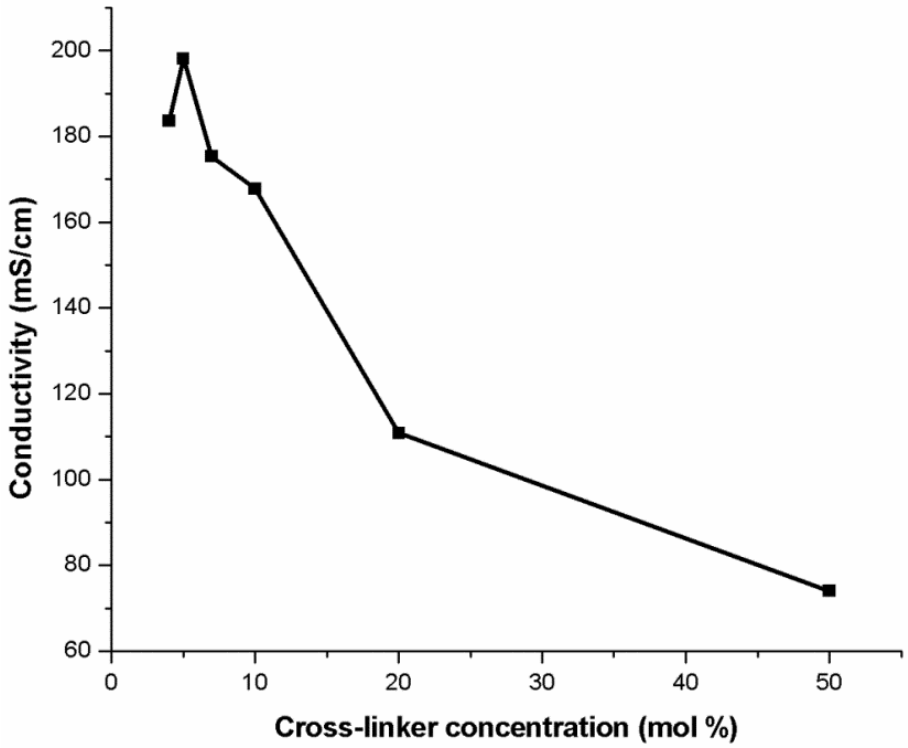


**Figure 3.8 – The variation of hydroxide ion conductivity with cross-linker concentration in GT66.**

As expected, the hydroxide conductivity was found to increase linearly with temperature as shown for two representative cross-linked polymer series (GT64 and GT82) in Figure 3.9. Like the non-cross-linked versions of these polymers, conductivity approximately doubled when temperature was increased from 25 °C and 80 °C. The slope of ln(σ) vs. 1/T was used to calculate an effective activation energy ($E_a$) using the Arrhenius Equation, Figure 3.10. The calculated activation energy, 10.8 to 13.6 kJ/mol, is also comparable to previously reported AEM materials and Nafion-117.[99, 102, 103]

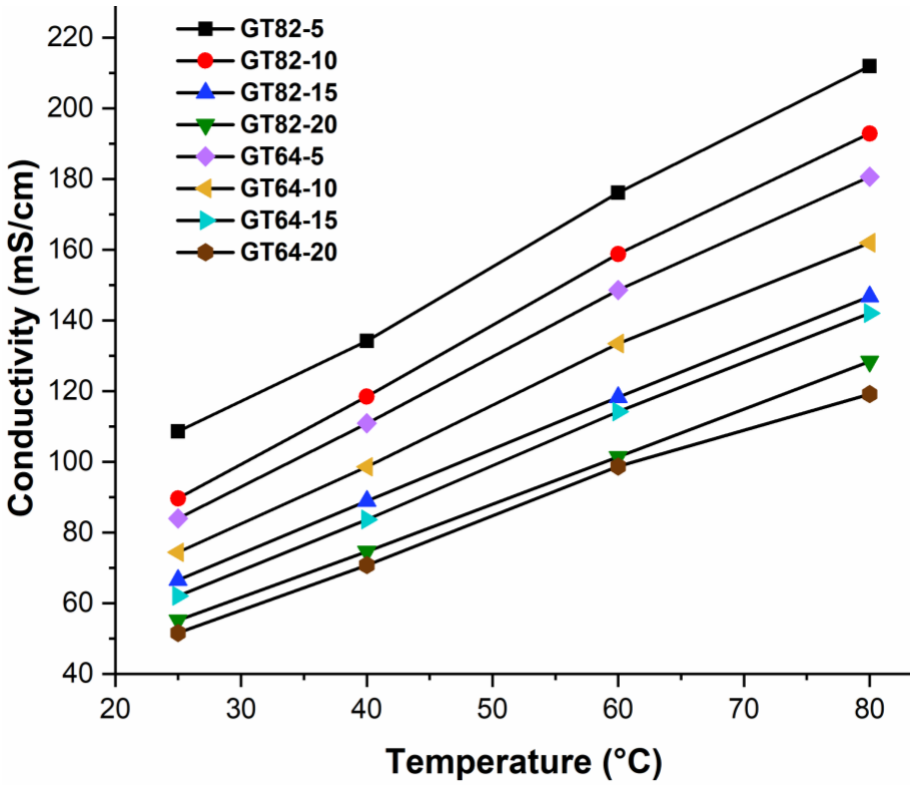


**Figure 3.9 – Plot of ionic conductivity of cross-linked AEMs at different temperatures.**

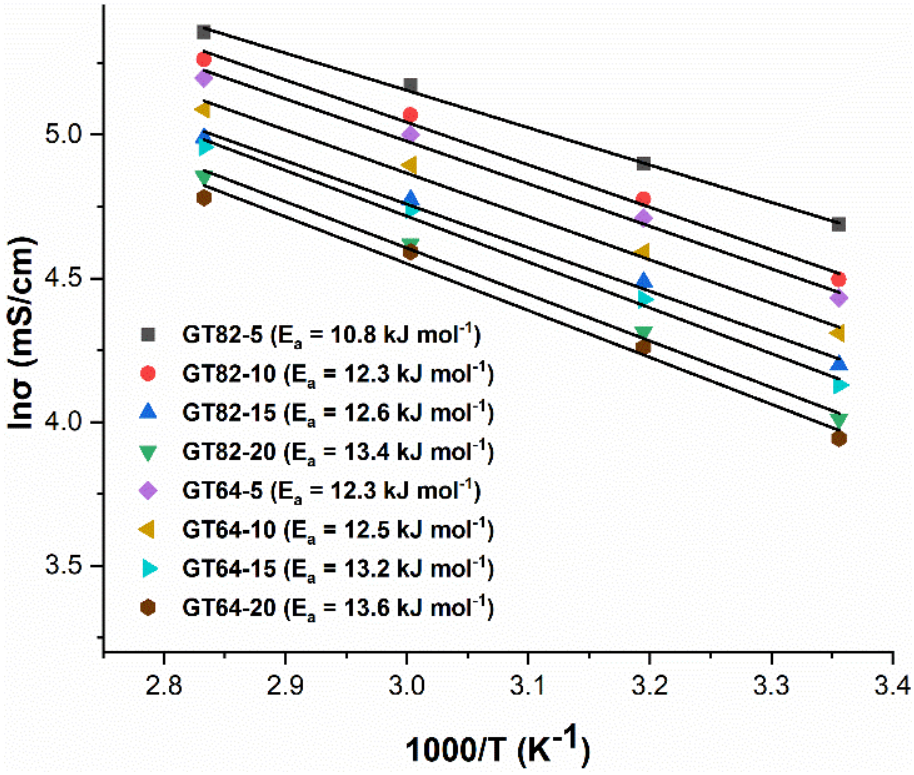


**Figure 3.10 – Arrhenius plot of ln(σ) vs. inverse temperature of cross-linked AEMs.**

The alkaline durability of the cross-linked polymers was almost identical to the non-cross-linked versions.[32, 45, 46] The cross-linked films were aged in 1 M NaOH for more than 1000 h and the conductivity was measured at regular intervals. Each data point was measured in triplicate and there was <0.5% deviation in the individual measurements. The loss in hydroxide ion conductivity was plotted as a function of aging time. As shown in Figure 3.11 (left), the AEMs had <1.5% loss in ionic conductivity over 1000 h. The alkaline stability was further confirmed by monitoring the structural change before and after the alkaline treatment using FT-IR spectroscopy. Figure 3.11 (right) shows the lack of appearance/disappearance of new/old peaks in the IR spectrum. The C-N stretching

frequencies at 911, 971, and 1483 cm-1 is unchanged, which indicates that the head-group moiety was intact after alkaline aging.[100, 104, 105]

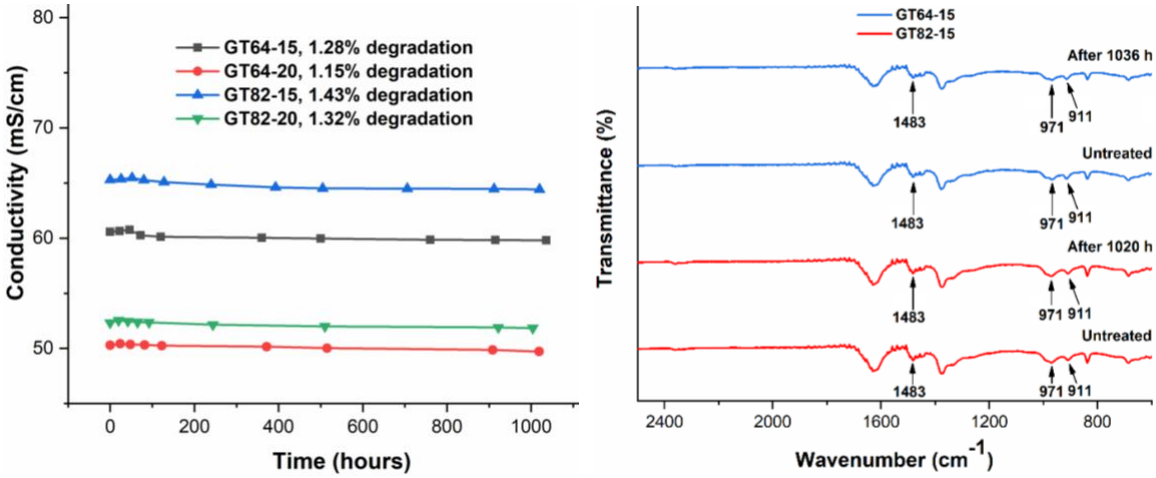


**Figure 3.11 – Alkaline stability analysis of cross-linked AEMs in 1 M NaOH solution at 80 °C. OH− conductivity loss over time (left). Structural characterization using FT-IR spectroscopy (right).**

### *3.3.3 Water uptake, hydration number, free and bound water molecules*

The conductivity of a film is closely related to its water uptake per ion because the water is needed for ion hydration and transport.[106] The WU of the cross-linked films was measured at room temperature and the results are shown in Table 3.2. Figure 3.12 shows a representative plot of water uptake and IEC vs. cross-linker concentration for GT82 series of films. WU decreased significantly with TMHDA concentration, although the IEC dropped marginally. Hence, it is clear that cross-linking is an effective strategy to mitigate WU without sacrificing IEC.

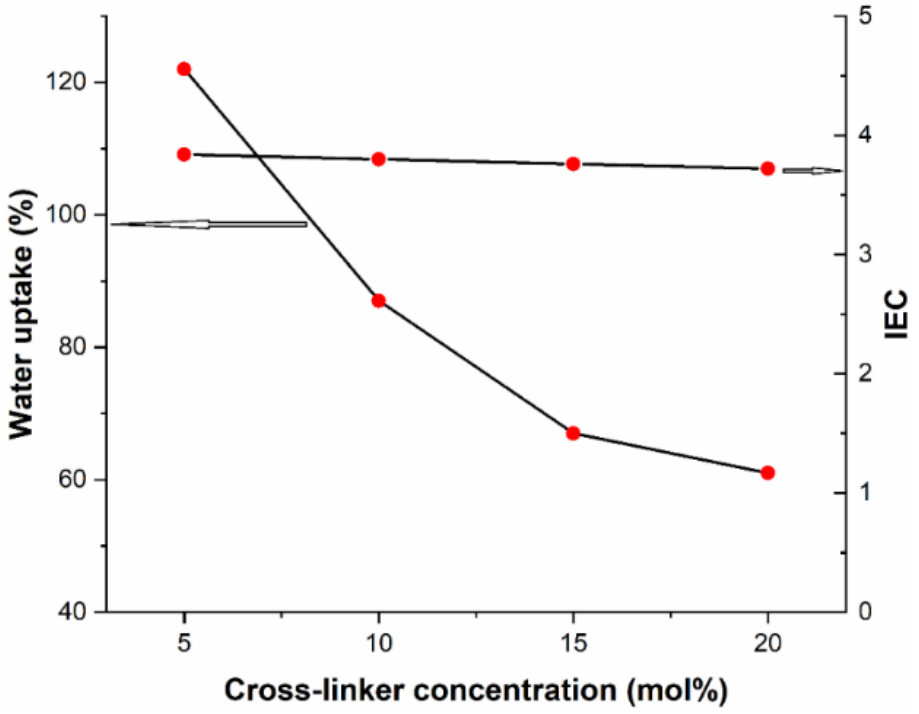


**Figure 3.12 – Variation of water uptake and IEC with TMHDA concentration of cross-linked GT82 AEMs.**

The trend observed in Figure 3.12 also followed the same trend observed in ionic conductivity vs. cross-linker concentration (Figure 3.8). To illustrate this point, the WU can also be viewed in terms of hydration number (λ), which is a measure of the number of water molecules per ionic pair. The number of bound or non-freezable ($N_{bound}$) water and unbound or freezable ($N_{free}$) water molecules per ion pair (i.e., anion-cation pair) were calculated from λ using DSC measurements for representative polymer series (GT64, GT66 and GT82) and are listed in Table 3.2. Increasing the TMHDA concentration primarily decreased the $N_{free}$ for each polymer series. For example, a heavily cross-linked membrane like GT82-20 had low $N_{free}$ and $N_{bound}$ waters (0 and 9, respectively). On the other hand, a lightly crosslinked film like GT82-5 had near optimal $N_{free}$ and $N_{bound}$ (7.6 and 10, respectively). This shows that the low mobility and conductivity of the ions in films

with high cross-linker concentrations is a result of lack of sufficient free water (which swell the ion conduction channels to maintain their size) because the film is more rigid and it is difficult for water molecules to populate inside.[45, 106]

### *3.3.4 Morphology*

SAXS was used to investigate the phase segregation and microstructure of the cross-linked poly(norbornene) membranes. During casting, the poly(norbornene) block copolymers phase segregate into ion conduction channels based on the thermodynamic dissimilarities between the halogenated and hydrophobic blocks. Once cross-linking begins to occur, the crosslinking agent further limits the self-assembly, thereby locking in the microstructure of the membrane upon curing. The inter-domain spacing (*d*-spacing), or the average separation length between inhomogeneities in the membranes, was determined from the Bragg spacing of the primary scattering peak in the SAXS spectra, as shown for a representative polymer series (GT66) in Figure 3.13. The inter-domain spacing values were determined by a Lorentz curve fitting function and are listed in Table 3.2. It was found that the domain size for the polymers with different cross-link densities were all similar, ranging only from 48.6 to 51.8 nm. From the previous section, it was found that the hydration number, specifically the number of free water molecules, decreases with increasing cross-linker concentration. This suggests that channel size is not dictated by cross-linker concentration however channel swelling becomes more restricted.[32]

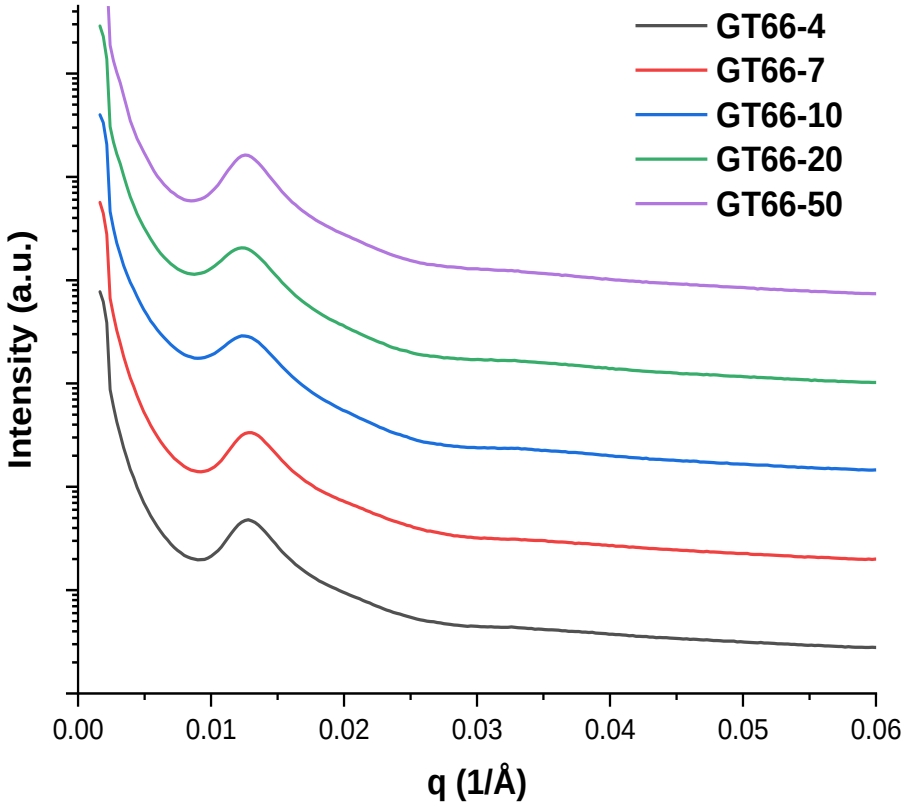


**Figure 3.13 – SAXS spectra of cross-linked tetrablock copolymer poly(norbornene) membranes in bromide form.**

## 3.4 Composite cross-linked poly(norbornene) AEMs

### *3.4.1 Physical properties and ion exchange capacity*

Thin membranes are desired to limit ohmic losses and improve water transport across the AEM. However, thin (<30 μm) membranes are often too fragile as free-standing films alone. Composite films were made with cross-linked high IEC, vinyl addition poly(norbornene) tetrablock copolymer a poly(tetrafluoroethylene) (PTFE) reinforcement layer by Xergy, Inc. (Harrington, DE).[32] The thin, proprietary PTFE reinforcement provides mechanical strength so that thin membranes can be easily handled.

The number average molecular weights, polydispersity and IEC of the precursor polymers (GT64, GT72, GT78 and GT82) used in composite membrane casting are listed in Table 3.1. This range of molecular weight and Đ was previously found to provide membranes with high conductivity and good mechanical strength. Cross-linked reinforced membranes with different amounts of TMHDA cross-linker (2.5 to 25 mol%) were made. The IEC of the membranes were calculated prior to reinforcement and decreased slightly with increasing TMHDA concentration as observed previously with other cross-linked polymers in Table 3.2.

The area specific resistance, water uptake (WU), swelling and storage modulus of a representative composite membrane series (GT64) are listed in Table 3.3 and are discussed in detail in the following subsections. The ratios of IEC/ASR and WU/ASR are discussed in Chapter 4. The properties of the other composite AEMs used in this thesis were inferred from their unreinforced counterparts listed in Table 3.2. These materials were used in the membrane electrode assemblies (MEA) of the fuel cells and electrolyzers in Chapters 4-7.

**Table 3.3 – Properties of composite cross-linked poly(norbornene) AEMs.**

| **Sample** | **Cross-linking (mol%)** | **IEC (meq/g)[a]** | **ASR (Ω-cm$^2$)[b]** | **Storage Modulus (MPa)[c]** | **Water Uptake (%)** | **Swelling (%)** | **IEC/ASR (meq/g Ω-cm$^2$)** | **WU/ASR (%/Ω-cm$^2$)** |
|---|---|---|---|---|---|---|---|---|
| GT64 | 0 | 3.37 | 0.038 | 66.8 | 88 | 68 | 3.33 | 2316 |
| GT64-2.5 | 2.5 | 3.36 | 0.056 | 75.4 | 82 | 45 | 3.30 | 1464 |
| GT64-5 | 5 | 3.34 | 0.041 | 119 | 65 | 39 | 3.30 | 1585 |
| GT64-10 | 10 | 3.31 | 0.033 | 129 | 35 | 24 | 3.28 | 1061 |
| GT64-15 | 15 | 3.28 | 0.020 | 175 | 29 | 14 | 3.26 | 1472 |
| GT64-20 | 20 | 3.25 | 0.025 | 458 | 24 | 11 | 3.23 | 968 |

| | | | | | | | | |
|---|---|---|---|---|---|---|---|---|
| GT64-25 | 25 | 3.22 | 0.025 | 553 | 18 | 7 | 3.20 | 735 |
| GT72-10 | 10 | 3.47 | ND | ND | ND | ND | ND | ND |
| GT78-5 | 5 | 3.70 | ND | ND | ND | ND | ND | ND |
| GT78-15 | 15 | 3.62 | 0.029 | ND | ND | ND | ND | ND |
| GT82-5 | 5 | 3.84 | ND | ND | ND | ND | ND | ND |
| GT82-10 | 10 | 3.80 | ND | ND | ND | ND | ND | ND |
| GT82-15 | 15 | 3.76 | ND | ND | ND | ND | ND | ND |
| GT82-20 | 20 | 3.72 | ND | ND | ND | ND | ND | ND |

[a] IEC calculated after the addition of TMHDA molecular weight; [b] Area specific resistance measured by EIS; [c] Storage modulus determined by DMA. ND = not determined.

### *3.4.2 Ionic area specific resistance*

The ionic area specific resistance (ASR) is an important membrane metric for electrochemical devices. This value represents the through-plane area resistance of the membrane. Resistance in this direction is especially important for composite membranes because the supporting material does not contribute to ionic conductivity. Through-plane hydroxide mobility also depends on the orientation of the pores in the reinforcement layer and membrane packing. The ASR values for the membranes in this study are listed in Table 3.3. The ASR was calculated from high frequency resistance (HFR) of the fully assembled fuel cell using electrochemical impedance spectroscopy (EIS). Figure 3.14 shows the Nyquist plots from the EIS measurements of MEAs containing GT64 membranes at a cell temperature of 60 °C with anode and cathode dew points set to 50 °C. The high frequency intercept in the plots represents the total series ohmic resistance of the system (i.e., time-independent resistances without a parallel capacitance). All of the membranes, with the exception of GT64-2.5, have an ASR less than or equal to 0.04 Ω-cm$^2$, which exceeds the ARPA-E IONICS (US Department of Energy) goal for fuel cell integration.

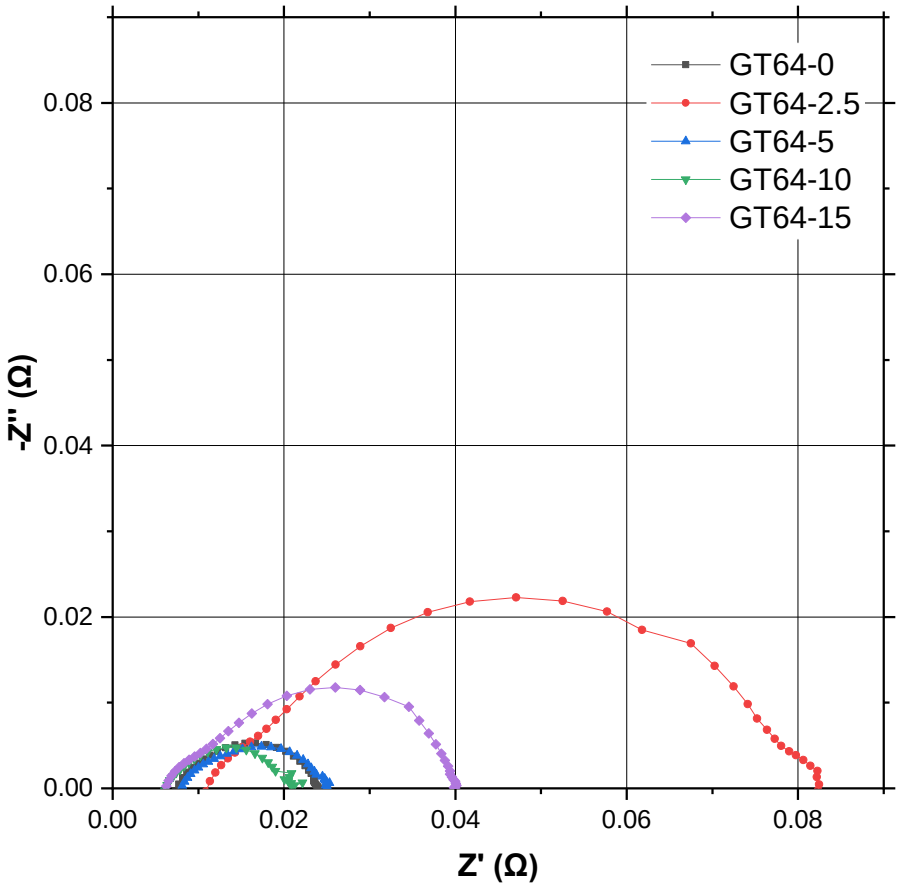


**Figure 3.14 – Nyquist plots of EIS measurements using five GT64 membranes with 0, 2.5, 5, 10, and 15 mol% cross-linker. Cell temperature was 60 °C with anode and cathode dew points set to 50 °C.**

### *3.4.3 Water uptake and swelling*

The water uptake and swelling of the GT64 composite membranes decreased with TMHDA concentration, Table 3.3. The water uptake and swelling were highest for the non-cross-linked composite membrane, 88% and 68%, respectively. A very small TMHDA concentration (2.5 mol%) significantly lowered the swelling due to a more tightly bound structure within the cross-linked polymer network. At higher TMHDA concentrations, ≥10%, the water uptake and swelling were both well below 50%, which is advantageous for reducing the physical deformation when integrated into a membrane electrode

assembly. The water uptake values are also much lower for the composite films than those of the free standing films without PTFE support, as reported previously.[45] For example, an unreinforced polymer membrane with 10 mol% TMHDA had 53% water uptake while GT64-10 had only 35% water uptake. At 20 mol% cross-linker, the effect is even more dramatic. The water uptake was 51% for the unreinforced membrane vs. 24% for the reinforced membrane. Furthermore, the water uptake of the non-cross-linked GT64 membrane without reinforcement could not even be measured due to excessive swelling and mechanical instability. This shows that the hydrophobic PTFE reinforcement (as well as the cross-linking) significantly contributes to limiting the water uptake in these membranes.

### *3.4.4 Mechanical properties*

The mechanical properties of the membranes were influenced by PTFE reinforcement and the degree of cross-linking, Table 3.3. The storage modulus of the membranes improved with the amount of cross-linking. The non-cross-linked membrane (GT64) had a storage modulus of only 66.8 MPa, which is similar to that of the PTFE reinforcement by itself. Very light cross-linking (2.5 mol% TMHDA) led to a small increase in modulus to 75.4 MPa. There was an 8-fold increase in storage modulus (553 MPa) for the membrane with the highest TMHDA concentration (25 mol%) compared to the uncross-linked sample. The higher modulus obtained with the cross-linked membranes provided further rigidity and mechanical strength so that they could be handled and used in very thin films which minimized the ohmic losses during device operation.

## 3.5 Summary

A series of tetrablock copolymers containing all-hydrocarbon backbone based on vinyl addition polymerization of norbornene were synthesized for anion-exchange membranes. To the author's knowledge, this is first anion exchange membrane based on vinyl addition-type poly(norbornene). These membranes displayed high thermal stability up to 400 °C. For GT32, the ionic conductivity was 122.7 mS/cm at 80 °C with an IEC (1.88 meq/g), which was less than GT46 (2.6 meq/g). This shows the importance of optimizing the bound and unbound water content in the membrane. Water content in GT32 was measured by DSC analysis and it was found that 6.7 unbound water molecules and 11.9 bound water molecules in the membrane leading to the best ionic conductivity among the synthesized samples. The long-term alkaline stability test in 1 M NaOH solution at 80 °C showed exceptional chemical stability with no detectable degradation (<1 %) over a 1200 h period.

Cross-linked anion conductive polymers synthesized via vinyl addition polymerization of norbornenes were also studied. The membranes had record high ionic conductivity, up to 212 mS/cm at 80 °C. It was found that only light cross-linking was needed to mitigate water swelling problems which have plagued other high-IEC AEMs. The dimensional stability was attributed to cross-link density, which can be tuned to balance the free and bound water content within the membrane. There were 7.8 free water molecules and 10.0 bound water molecules per ion pair within the most conductive membrane. Excellent alkaline stability in 1 M NaOH solution at 80 °C was demonstrated (<1.5 % conductivity loss in >1000 h at 80 °C). The cross-linked polymers were also cast

into composite membranes using a PTFE reinforcement, which improved the mechanical properties and dramatically decreased water uptake and swelling.

# CHAPTER 4. COMPOSITE POLY(NORBORNENE) ANION CONDUCTING MEMBRANES FOR ACHIEVING DURABILITY, WATER MANAGEMENT AND HIGH POWER IN HYDROGEN/OXYGEN ALKALINE FUEL CELLS

## 4.1 Motivation

Thin membranes are desired to minimize ohmic losses in the AEM. In this chapter, a composite block copolymer membrane made of poly(norbornene) (PNB) synthesized by vinyl addition polymerization and a poly(tetrafluoroethylene) (PTFE) reinforcement layer was used as the electrolyte in AEM fuel cells. The anion conductive PNB precursor material was previously shown to form chemically stable polymers with high conductivity.[32, 45, 46, 107] The proprietary PTFE reinforcement layer (Xergy, Inc.) was chemically inert and shown to be useful when casting thin yet mechanically robust membranes.[25, 76] In the past, similar approaches have been used to make composite AEMs for fuel cells that have achieved modest peak power densities of <350 mW/cm$^2$.[77, 78] The membranes in this chapter used light cross-linking of a high IEC polymer to balance conductivity, water uptake and dimensional stability and enable maximum fuel cell performance. Optimized cross-linker concentration in the AEM produced $H_2/O_2$ fuel cells with peak power density up to 3.4 W/cm$^2$ at 80 °C using $H_2/O_2$. This was 70% higher than the previous highest reported $H_2/O_2$ AEM fuel cell by Wang et al.[108] Optimization of the inlet gas dew points for the anode and cathode was also performed. The membranes were also operated reliably for over 500 h ($H_2/CO_2$ free air) with no change in membrane resistance and minimal loss of operating voltage.

## 4.2 Results

### *4.2.1 Effect of cross-linker concentration on peak power density*

The fuel cells in this chapter were constructed using the reinforced membranes with varying TMHDA cross-linker concentration from Table 3.3. Highly optimized electrodes were fabricated using the USC and NREL method described in Chapter 2. A set of fuel cells was operated with humidified $H_2$ and $O_2$ reacting gases, with the catalyst layer deposited onto 5% wetproofed Toray-H-60 GDLs, at a cell temperature of 60 °C. After a short break-in period where the anode and cathode RH were optimized, forward and reverse polarization scans were run on each cell to determine peak power density. The optimized anode and cathode dew points are listed in Table 4.1 using the notation (A/C), where the value of A represents the anode dewpoint and the value of C represents the cathode dew point in degrees Celsius. This notation will be used throughout this chapter. The power density and polarization curves for the cells with various TMHDA content in the AEM are shown in Figure 4.1 and the peak power densities are summarized in Table 4.1. The specific power and specific current values were also calculated based on the peak power density, current produced at peak power, and the metal loading of the electrodes in Table 4.1.

**Table 4.1 – AEM fuel cell performance highlights at 60 °C.**

| XL (mol%) | $H_2$ cross-over (mA/cm$^2$)[a] | OCV (V) | A/C dew point (°C) | HFR (mΩ-cm$^2$)[b] | Cell potential (V) | CD (A/cm$^2$) | PPD (W/cm$^2$) | PtRu/C load. (mg/cm$^2$)[c] | Pt/C load. (mg/cm$^2$)[c] | Spec. power (W/mg PtRu) | Spec. power (W/mg Pt) | Spec. current (mA/mg PtRu) | Spec. current (mA/mg Pt) |
|---|---|---|---|---|---|---|---|---|---|---|---|---|---|
| 0 | 40 | 0.881 | 50/50 | 38.0 | 0.555 | 2.497 | 1.39 | 0.472 | 0.424 | 2.94 | 3.27 | 5291 | 5890 |
| 2.5 | 25 | 0.873 | 55/55 | 55.5 | 0.547 | 2.270 | 1.24 | 0.331 | 0.313 | 3.75 | 3.97 | 6857 | 7251 |

| | | | | | | | | | | | | | |
|---|---|---|---|---|---|---|---|---|---|---|---|---|---|
| 5 | 5 | 0.950 | 48/52 | 40.5 | 0.554 | 3.431 | 1.90 | 0.948 | 0.490 | 2.01 | 3.88 | 3620 | 7003 |
| 10 | 54 | 0.882 | 40/40 | 35.0 | 0.555 | 3.417 | 1.89 | 0.730 | 0.515 | 2.56 | 3.68 | 4680 | 6634 |
| 15 | 12 | 0.930 | 40/40 | 31.0 | 0.537 | 4.097 | 2.20 | 0.986 | 0.560 | 2.23 | 3.93 | 4155 | 7316 |

[a] Hydrogen crossover measured by EIS; [b] High frequency resistance measured by EIS; [c] Metal loadings for specific power and current determined by XRF. All other values measured or calculated based on test station data. XL = cross-linker concentration; A/C = denotes anode (A) and cathode (C) dew points in degrees Celsius, respectively; CD = current density; PPD = peak power density.

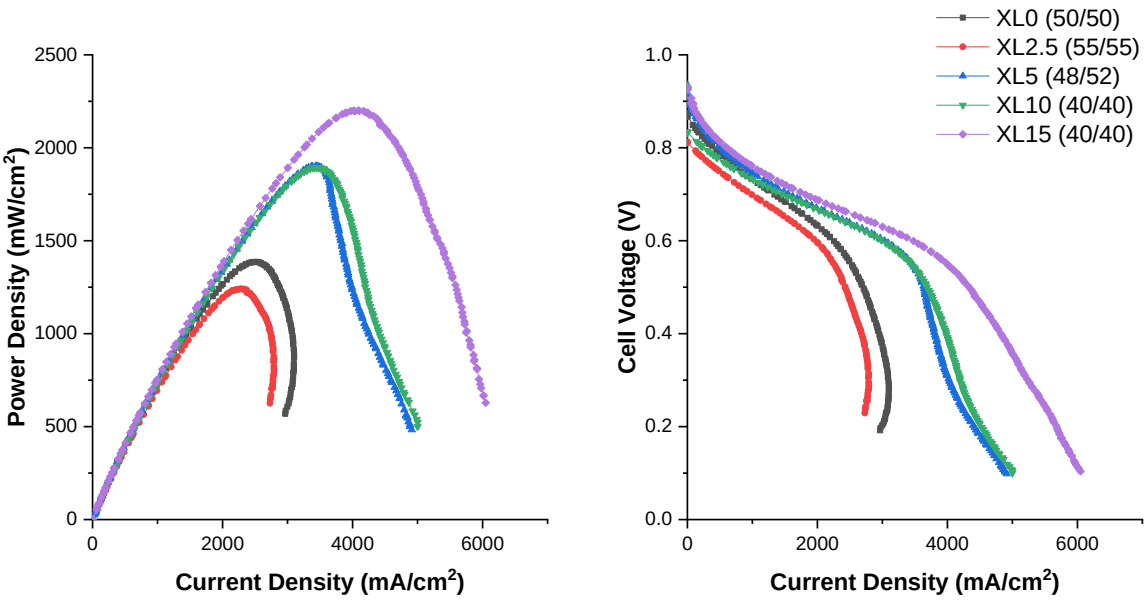


**Figure 4.1 – Comparison of peak performance after RH optimization. Cell temperature for all samples was 60 °C.**

The cell voltage at peak power for all samples at 60 °C was ca. 0.55 V. The peak power density generally increased with cross-linker concentration, although the peak power output for 0 and 2.5 mol% TMHDA, and 5 and 10 mol% TMHDA were very similar. Among the membranes tested, the lowest performing cells used membranes with 0 and 2.5 mol% TMHDA; 1.24 to 1.39 W/cm$^2$ peak power, respectively. Intermediate power levels were recorded for membranes with 5 and 10 mol% TMHDA: 1.89 and 1.90 W/cm$^2$, respectively. The highest peak power density was observed for the cell containing the GT64-15 membrane: 2.20 W/cm$^2$. The MEA with the GT64-2.5 membrane had the highest specific power density and current density due to its lower than average catalyst loading.

Even at 60 °C, this cell exceeded the previous best literature value for AEM fuel cell reported by Wang et al., which achieved 2.0 W/cm$^2$ at 80 °C.[108]

At 80 °C, the performance of the fuel cells significantly increased, as shown in Figure 4.2 and the peak power densities and optimal dew points are summarized in Table 4.2. The specific power and specific current values were also calculated based on the peak power density, current produced at peak power, and the metal loading of the electrodes in Table 4.2. Membranes with 10 and 15 mol% TMHDA were selected for testing at 80 °C because of their higher performance. The GDEs used in these tests and the testing method were slightly modified compared to the 60 °C experiments. Most notably, the catalyst layers were deposited onto Toray-H-60 with 20% wetproofing (vs. 5% wetproofing), and the dew point of the anode and cathode feed gases were optimized more granularly. As shown in Figure 4.2, there was less separation in power density among the four cells tested, and the power density produced was similar across a wide range of TMHDA concentrations. Just like the 60 °C experiments, the cells achieved peak power at ca. 0.54 V. Both GT64-10 and GT64-20 achieved a peak power density of ca. 3.0 W/cm$^2$ with similar optimal anode and cathode dew points. The peak power for GT64-25 was 3.27 W/cm$^2$. Again, GT64-15 showed the highest performance among all membranes tested with a peak power density of 3.37 W/cm$^2$. This performance at this cross-linker concentration also correlates the highest specific power density and current density in this chapter. This was also one of the highest performances reported for an AEM fuel cell to date, surpassing the previous record by 70%.[108]

**Table 4.2 – AEM fuel cell performance highlights at 80 °C.**

| XL (mol%) | OCV (V) | A/C dew point (°C) | HFR (mΩ-cm²)[a] | Cell voltage (V) | CD (A/cm²) | PPD (W/cm²) | PtRu/C loading (mg/cm²) | Pt/C loading (mg/cm²) | Spec. power (W/mg PtRu) | Spec. power (W/mg Pt) | Spec. current (mA/mg PtRu) | Spec. current (mA/mg Pt) |
|---|---|---|---|---|---|---|---|---|---|---|---|---|
| 10 | 1.001 | 68/74 | 35.1 | 0.514 | 5.940 | 3.06 | 0.70 | 0.60 | 4.36 | 5.09 | 8491 | 9906 |
| 15 | 1.016 | 67/74 | 25.3 | 0.524 | 6.425 | 3.37 | 0.70 | 0.60 | 4.81 | 5.61 | 9182 | 10712 |
| 20 | 1.009 | 68/75 | 7.60 | 0.536 | 5.588 | 3.00 | 0.70 | 0.60 | 4.28 | 4.99 | 7982 | 9313 |
| 25 | 0.996 | 68/76 | 28.7 | 0.528 | 6.179 | 3.27 | 0.70 | 0.60 | 4.66 | 5.44 | 8834 | 10307 |

[a] High frequency resistance measured by EIS; All other values measured or calculated based on test station data. XL = cross-linker concentration; A/C = denotes anode (A) and cathode (C) dew points in degrees Celsius, respectively; CD = current density; PPD = peak power density.

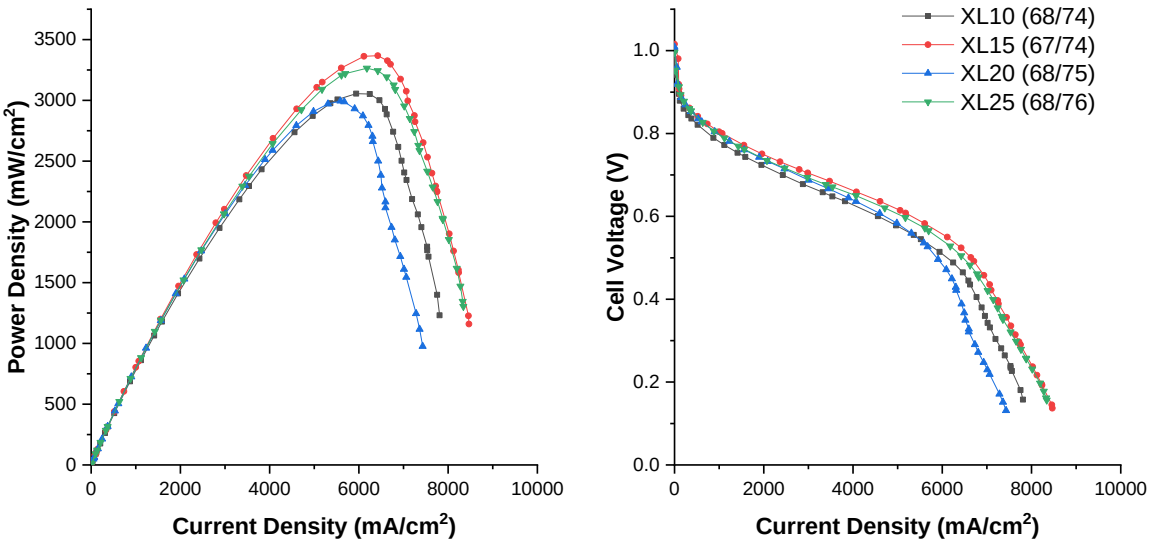


**Figure 4.2 – Comparison of peak performance after RH optimization. Cell temperature for all samples was 80 °C.**

### *4.2.2 Effect of cross-linker concentration on optimal inlet dewpoints*

Table 4.1 shows cells with higher TMHDA concentration displayed optimum performance with lower anode and cathode dewpoints. At 60 °C, the cells with ≥10 mol% TMHDA concentration operated at had a peak power density with anode and cathode dew points both at 40 °C. Optimal inlet dew points for AEMs with <10 mol% cross-linker

required significantly higher inlet dewpoints (>50 °C) to show optimal performance. At 80 °C (Table 4.2), the optimal dewpoints were similarly low for cross-linker concentrations ≥10 mol% and varied only by 1-2 °C on either the anode or cathode.

Figure 4.3 shows the RH optimization for the GT64-15 membrane at 60 °C cell temperature. At anode and cathode dew points of 50 °C, there is clearly too much water in the system which causes electrode flooding and lower power. The performance increased steadily as the humidity was reduced to a dew point of 40 °C for both feed streams. This trend continued for an intermediate TMHDA concentration (5 mol%), where the dew points at the highest peak power density were 48 °C for the anode and 52 °C for the cathode. At TMHDA concentration of ≤2.5 mol%, the best performance was achieved when the dew points for the anode and cathode were both at 50 °C. At dew points of 60 °C at both electrodes, lower power was observed due to cell flooding. At the opposite end of the spectrum (dew points at 50 °C), the membrane is too dry and low power is also observed. At dew points of 55 °C, significantly higher power is able to be achieved due to a better balance of input water and generated water. The optimal dew points for the membrane without any cross-linker are between 50 °C (for both electrodes) and 55 °C (for both electrodes). When the dew points were both set at 45 °C, lower power was observed due to a lack of hydration. Another interesting trend from the optimization data in Figure 4.3 is that the mass transport limited current increased with decreasing reacting gas dew points. This is a clear sign that water transport is performance-limiting during AEM fuel cell operation.

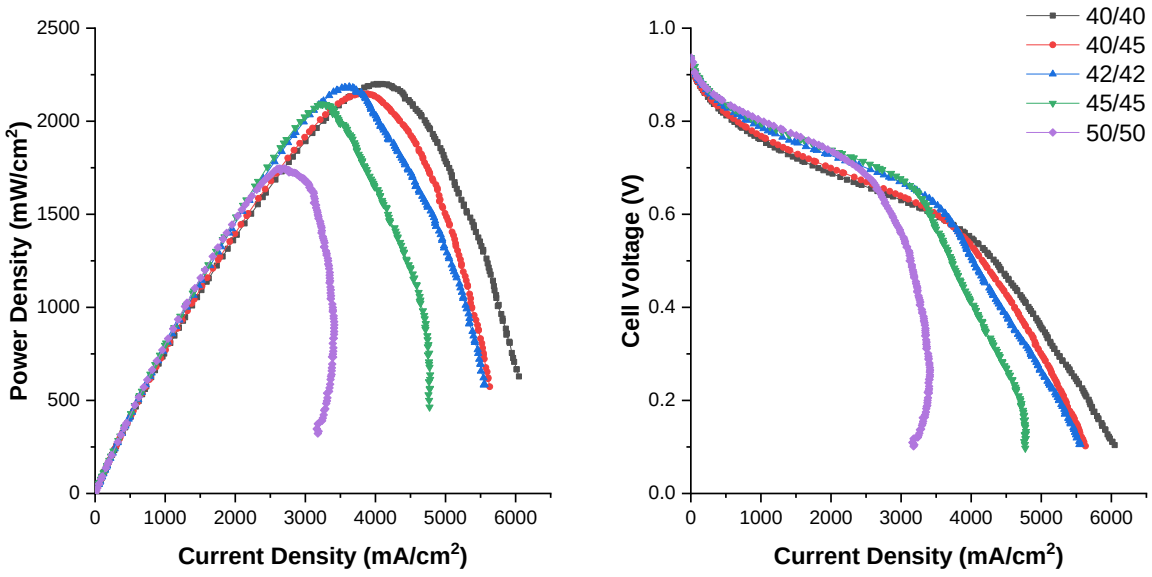


**Figure 4.3 – Polarization curves for GT64-15 at cell temperature of 60 °C with various anode and cathode inlet dew points.**

RH sensitivity was also investigated at a cell temperature of 80 °C. Figure 4.4 shows the RH optimization at 80 °C for an AEM fuel cell operated at 80 °C with a GT64-15 membrane. Although the overall water content at the inlet is higher at this elevated temperature, the same trend was observed. At 80 °C, water has a higher vapor pressure so the membrane dries out at a faster rate, thus requiring higher humidity in the feed streams. For a cross-linker concentration of 15 mol%, the cell performance benefited from lower anode and cathode dew points (66 °C and 74 °C, respectively) than the operating temperature. The effect of cell flooding can be seen starting at inlet dew points of 68 °C and 74 °C (anode and cathode, respectively) and became more severe at 70 °C and 76 °C (anode and cathode, respectively).

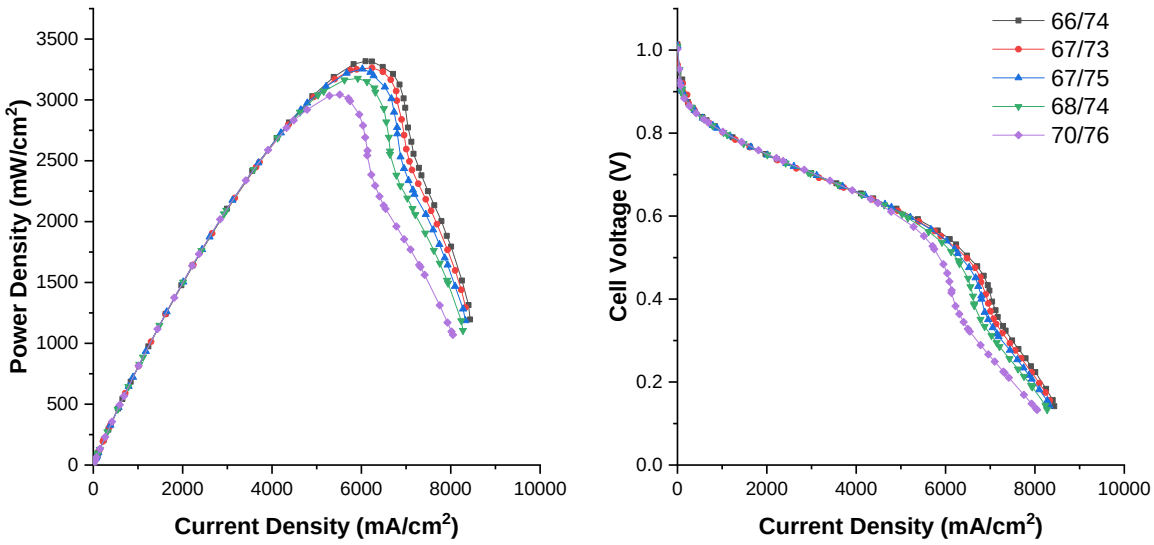


**Figure 4.4 – Polarization curves for GT64-15 at cell temperature of 80 °C with various anode and cathode inlet dew points.**

### *4.2.3 Long-term in-situ stability of composite cross-linked AEMs*

The fuel cells were generally operated for 24 h to ensure that dependable performance values were obtained and the AEMs had good stability in the highly alkaline environment. One long-term AEM fuel cell stability test was performed with the GT64-15 membrane at 80 °C using $CO_2$-free air and electrodes deposited onto a 5% wetproofed GDL. This cell was not fully optimized for the highest power density (like later cells) and its power density at 0.7 V was 1450 mW/cm$^2$. It is noted that the peak power of this cell with $H_2/O_2$ gas feeds was about 2.3 W/cm$^2$, which still exceeds the highest published cell to-date. This cell was selected for long-term aging and Figure 4.5 shows hourly data of the cell voltage vs. time at constant current, 600 mA/cm$^2$. It is noted that the cell power dropped to 31% of its $H_2/O_2$ value when air was used in place of oxygen. This reflects the lower activity of oxygen in air and also the importance of optimizing the electrode structure and relative humidity of the feed gas. These effects are currently under investigation and may

be the subject of future reports. The cell ran for 545 h without detectable membrane degradation, at which point the experiment was terminated. During the first 300 hours, the cell performance dropped by about 17%. This change in performance was likely caused by the cell water dynamics, where a net loss of water slowly occurred at the electrode over time, as evidenced by the increasing ASR. As such, the dew points of the anode and cathode were adjusted to 78 °C at the 300 h point to increase the water content in the cell. This increase in dew point restored the cell to its initial level of performance. After operating for an additional 150 h, the dew points of the anode and cathode were both increased to 79 °C and were held there for the remainder of the durability test. The cause of the change in the MEA that necessitated a higher dew point is not clear at this time. After adjusting the water content, the cell voltage and the HFR also returned to their initial values showing that proper hydration had been restored. The initial and final HFR values (0.043 $\Omega$-cm$^2$ and 0.042 $\Omega$-cm$^2$, respectively) were essentially the same showing that the AEM conduction properties did not change substantially and the membranes had very high in-situ stability.

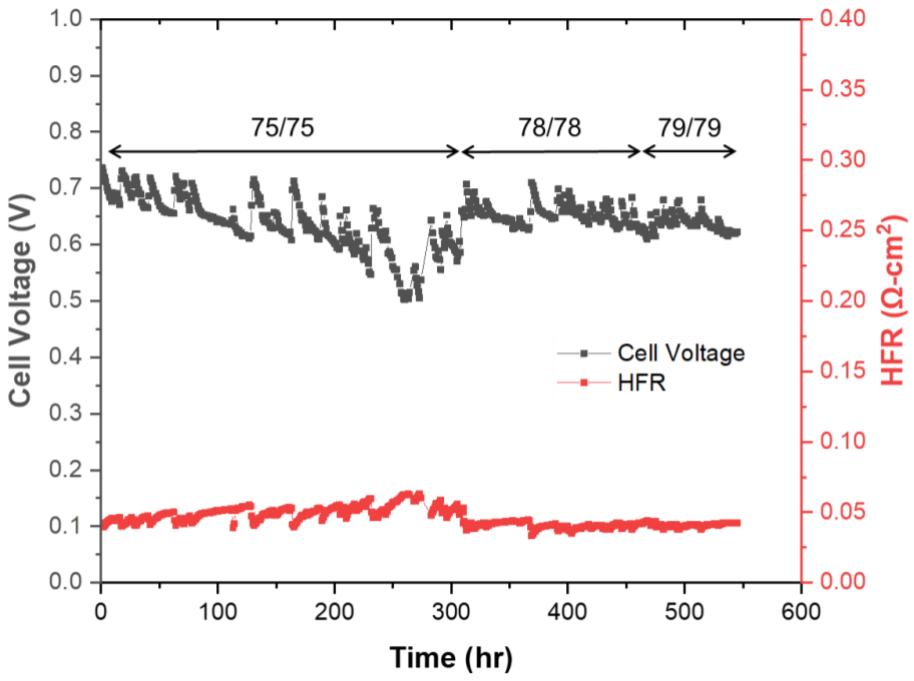


**Figure 4.5 – Cell voltage and HFR of GT64-15 over time at 80 °C under $H_2$ and $CO_2$-free air.**

## 4.3 Discussion

Figure 4.1 and Figure 4.2 both show that the maximum peak power density that achieved occurred in a cell with an AEM that did not have the highest hydroxide conductivity among those tested. Conductivity alone does not capture the deleterious effects of mechanical deformations on cell performance. From Table 3.1, GT64-5 (181 mS/cm) had higher in-plane hydroxide conductivity than GT64-15 (142 mS/cm) due to the presence of higher amounts of cross-linker which lowers the water uptake of the AEM. It was also observed that the fuel cells with these cross-linked membranes generally performed better with drier inlet gas feeds, particularly on the anode side where water is generated. This illustrates the disruptive nature of excessive WU and swelling within a fuel cell and the subtle interactions between conductivity, mechanical deformation and current

density. The achieved power density appears to be the result of off-setting trends of mechanical dimensional stability (better with higher TMHDA concentration) and lower conductivity, both of which may be related to lower WU.

The relative humidity of the anode and cathode feeds are known to play a critical role in alkaline exchange membrane fuel cell performance.[69] The water content in the hydrogen and oxygen input streams must be carefully balanced with the production of water at the anode, the diffusion of water through the membrane, and consumption of water at the cathode. Factors such as catalytic activity and loading can affect each electrode differently, which in turn affects the overall cell performance. As mentioned earlier, the three tiers of power output can be seen in Figure 4.1 based on the TMHDA concentration in the membrane. However, there is an additional trend that can be seen in this data. Not only did the performance go up with TMHDA concentration, but the amount of water fed to the cell in the reacting gases decreased (i.e., lower dew points). As reported previously, water uptake decreases with increasing TMHDA concentration in the polymer network.[45] As seen in the WU data in Table 3.2, the higher TMHDA concentration decreased the WU. However, the tighter and more rigid polymer network also appears to lock water inside the membrane, limiting the rate of dry-out.

For the composite membranes used in this work, the normalization of the water uptake (WU/ASR) and the IEC (IEC/ASR) by the area specific resistance, Table 3.3, gives insight into why certain TMHDA concentrations are better than others. The ASR normalized IEC (IEC/ASR) is analogous to conductivity per IEC (σ/IEC), which has been used to measure mobility or how efficient ion conducting groups are at transporting hydroxide ions.[32, 45, 46, 48] For membranes in this study, the IEC/ASR are all quite similar,

ranging from 3.20 to 3.33, showing that the movement of the hydroxide was not severely impacted by the more rigid structure of higher TMHDA concentrations. On the other hand, the WU/ASR showed that although the in-plane hydroxide conductivity (Table 3.3) decreased with TMHDA concentration, cell performance did not suffer much because the lower WU and swelling were ultimately more beneficial.

One potential concern that was found with the use of thin composite membranes is hydrogen crossover. Prior to the break-in procedure, a hydrogen crossover test was performed by flowing $H_2$ at the negative electrode (anode) and $N_2$ at the positive electrode (cathode). The hydrogen crossover current was measured by applying a voltage of 0.5 V across the cell and the resulting values are listed in Table 4.1. The hydrogen crossover was 5 to 54 $mA/cm^2$ but did not correlate with membrane thickness or cross-linker concentration, as would have been expected. The effect of the elevated crossover for the composite membranes can be observed in the lower open circuit voltage (OCV) values. The OCV ranged from 0.881 V to 0.950 V. Other fuel cells using similar electrode formulations had OCV values of ca. 1.1 V.[70, 108] From these results, it is suspected that crossover measurements may have been influenced by unintentional thin spots or fabrication defects in the membranes, although no obvious regions were seen.

The work of this chapter shows the importance of minimizing excess water uptake to achieve high performance in AEM fuel cells. Light membrane cross-linking preserves efficient ion transport and hydroxide mobility in the membrane and enables exceptionally high current density and power density fuel cell operation. The impact of dimensional stability on cell performance was found to be much greater than simply the reduction of ohmic losses and allowed for the efficient transport of anions throughout the entire

membrane electrode assembly. This study opens the way for advances in low-platinum and non-platinum electrodes operating at high power.

## 4.4 Conclusion

The behavior of high IEC, high conductivity composite AEMs were analyzed and used in alkaline $H_2/O_2$ fuel cells. The membranes were composed of a reinforced poly(norbornene) BCP. It was found that light cross-linking provided critical dimensional stability so that very high IEC could be used without penalty of excessive water uptake and swelling. The improvement in fuel cell performance was greater than simply minimizing the membrane ohmic losses through the use of thinner membranes. Mechanical stability of the membrane and electrode/membrane interface is exceedingly important to the efficient transport of ions within the cell. The fuel cells were sensitive to the relative humidity of the feed gases, and the reacting gas dew points needed to be optimized to yield the highest peak power. The optimum AEM (15 mol% TMHDA crosslinker) and cell operating conditions resulted in one of the highest reported peak power densities to-date (3.4 $W/cm^2$ at 80 °C). It was also shown that the AEMs were stable for long periods of time (>500 h) under load with no change in the membrane resistance.

# CHAPTER 5. THE IMPORTANCE OF WATER TRANSPORT IN HIGH CONDUCTIVITY AND HIGH-POWER ALKALINE FUEL CELLS

## 5.1 Motivation

Water management is a key factor in achieving high AEMFC performance. The AEM plays an important role in balancing the water content and distribution during device operation.[69, 70] It has been shown that a significant majority of the reacting water at the AEMFC cathode is provided by back-diffusion of water produced at the AEMFC anode.[71] This suggests that high AEM water permeability is beneficial in AEMFCs. However, excessive AEM water uptake can flood the ion conducting channels within the polymer and lead to membrane softening and mechanical failure.[43, 72] Thus, high water permeability without high water solubility appears to be a critical feature for AEMFCs. Waters of hydration are necessary for hydroxide ion conduction; however, excessive unbound (i.e., free) water leads to low hydroxide mobility and membrane distortion.[45] Hence, it is necessary to balance the amount of free and bound water inside the membranes to yield the maximum hydroxide mobility and water transport.[32, 45, 46] Cross-linking is an effective way to reduce water uptake and swelling.[35] However, AEMs with high cross-linking density can become too rigid, leading to worse ion mobility, mechanical properties and water diffusivity (i.e., high water solubility without high diffusivity).[73-75] In the case of polymers with high IEC, light cross-linking is an effective strategy to balance the high conductivity and water uptake (WU) without sacrificing IEC.[45, 46] In addition, thinner membranes can enable rapid water transport without high water uptake, and enable high current density

AEMFCs. Conveniently, light cross-linking also helps in the production of thin membranes with good mechanical properties.

AEM carbonation upon exposure to $CO_2$ is another important factor in AEMFC performance. When $CO_2$-containing air is fed to an operating AEMFC, the hydroxide anions produced by the reduction of oxygen at the positive electrode react with carbon dioxide to produce carbonated anions with lower mobility than hydroxide (i.e., carbonate or bicarbonate), increasing Ohmic-related losses.[81] Additionally, these carbonated anions can rapidly populate the AEM and AEMFC anode, leading to significant thermodynamic and kinetic-related losses.[71, 79] It has been stated that the adverse effects of membrane carbonation could be minimized by using AEMs with very high ionic conductivity so that the decrease in mobility upon carbonation can be mitigated and cell decarbonation during operation through the so-called "self-purging" mechanism can occur more rapidly. Hence, AEMs with very high conductivity are most desirable.[45]

In this chapter, the synthesis of chemically stable AEMs with record high conductivity, 212 mS/cm at 80 °C, and their implementation into AEMFCs are described. The polymer was cast into ultra-thin, composite membranes using a PTFE reinforcement layer. This AEM was used to enable record performance in a hydrogen/oxygen AEMFC with a peak power density of 3.5 W/cm$^2$ and maximum current density of 9.7 A/cm$^2$ at 0.15 V at 80 °C when water transport from the anode to cathode was controlled. Light cross-linking was used to control the WU at high IEC in this polymer, 3.88 meq/g. It is shown that thin, reinforced, high-conductivity membranes with excellent water transport are a critical component in producing high-power AEMFCs. A comparison of AEMFC

membrane thickness supports the hypothesis that water transport from anode to cathode is a critical factor in the achievable current and power density.

## 5.2 Results

### *5.2.1 Fuel cell performance of composite cross-linked poly(norbornene) AEMs with optimized electrodes*

GT82-15 was selected for detailed analysis in an alkaline fuel cell because of its high conductivity and balanced WU (Table 3.2). A reinforced GT82-15 membrane was loaded into a 5 $cm^2$ single cell AEMFC with identical electrodes to those published previously.[35] In these electrodes, a small amount of PTFE is added to both the anode and cathode electrodes in order to help with water management. This allows the results obtained in this study to be directly compared to the literature state-of-the-art. Polarization curves were collected with both $H_2/O_2$ and $H_2$/air ($CO_2$-free) feed gases entering the cell at a volumetric flowrate of 1 L/min, and the results are shown in Figure 5.1. Positively, the GT82-15 based AEMFC was able to achieve a power density of 3.5 $W/cm^2$ and a maximum current density of 9.7 $A/cm^2$ at 80 °C, making this cell the highest-performing AEMFC reported to-date.[35, 109, 110] The high performance was due to a combination of factors: (i) very high ionic conductivity (i.e., low internal resistance loss) and (ii) very high water transport through the AEM from the hydrogen anode to the oxygen cathode during operation. A critical current-limiting factor in AEMFC's is the rate of water transport from the water-producing negative electrode to the water-consuming positive electrode.[71]

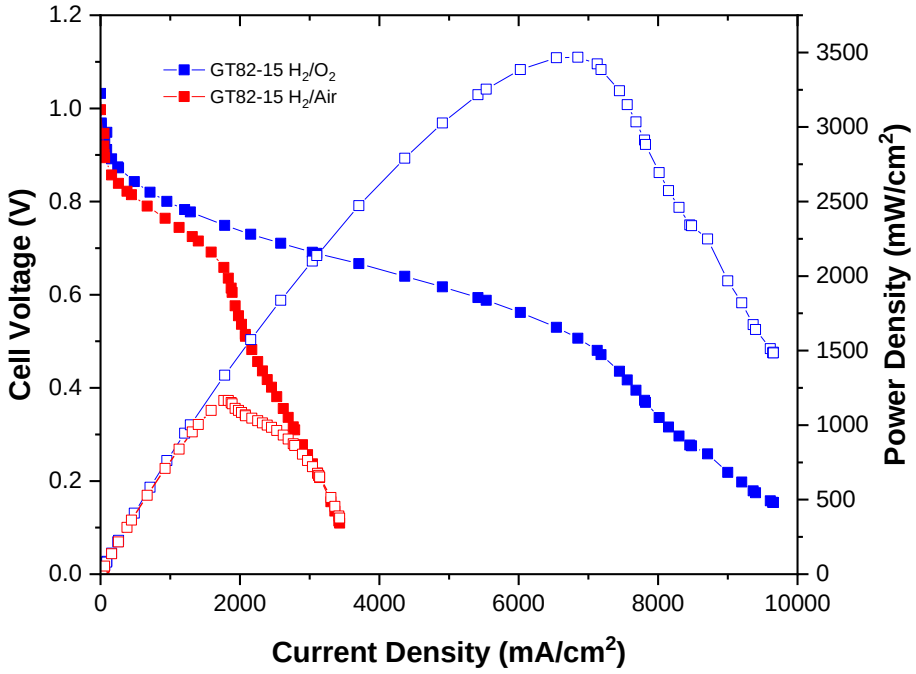


**Figure 5.1 – Current-voltage (filled) and current-power density (empty) curves for AEMFCs with a 10 µm GT82-15 AEM, operating with $H_2/O_2$ (blue) and $H_2$/air (red) feeds at 1 L/min. The cell temperature was 80 °C. The anode/cathode dew points for the cells operating with $O_2$ and air ($CO_2$-free) at the cathode were 66 °C /75 °C and 70 °C /78 °C, respectively. The Anode: 0.70 mgPtRu/cm$^2$; 0.05 MPa backpressure. Cathode: 0.60 mgPt/cm$^2$; 0.1 MPa backpressure.**

### *5.2.2 Effect of membrane thickness on water transport*

In order to show the influence of anode to cathode water transport on the achievable current density and peak power more definitively, two variables were changed in the following set of fuel cell tests. First, the electrode composition was changed to be identical to a previous study where no PTFE was added to the catalyst layers.[70] This is important because in these tests, the electrode itself does little to remove water from the anode. This places an even greater burden on the membrane to transport water from the anode to cathode. This change in the electrodes is expected to reduce the overall achievable current and power, but the purpose of this experiment is to show the importance of water transport

through the membrane, not just achieving the highest power density. Second, the membrane and membrane thickness were varied; GT78-15 membranes with thicknesses of 10 μm, 20 μm and 30 μm were used. Testing different thicknesses is important because the diffusional flux of water from the hydrogen anode to the oxygen cathode is inversely proportional to thickness. The cells were operated under various conditions and their performance and operating HFR were measured in order to understand the water transport behavior during operation. Figure 5.2 shows the results of AEMFC tests with GT78-15 AEMs with different thicknesses. The cell with the 10 μm membrane has a lower peak power density and achievable current than the cell in Figure 5.1, due to the experimental conditions noted above. However, the performance was still very high, and higher than other cells with identical electrodes.[70] The optimized dew points for the cell with the 10 μm AEM were 75 °C and 77 °C at the anode and cathode, respectively. The peak power density was 1.95 W/cm$^2$ and the cell was able to support a current density of 6.3 A/cm$^2$ at 0.1 V. Also, the average HFR during operation was 5.8 mΩ, which corresponds to an ASR of 0.029 Ω cm$^2$. The in-situ ASR of this membrane is also the lowest of any AEM reported to date in an operating AEMFC.

As shown in Figure 5.2, as the thickness of the AEM increased, the achievable peak power density significantly decreased. However, the decrease in current and power density were not caused by an increase in the voltage drop across the thicker membrane because the ASR of the 20 μm GT78-15 AEM was slightly lower (0.028 Ω cm$^2$) than the HFR of the 10 μm GT78-15 AEM (0.029 Ω cm$^2$). Although the ASR is proportional to the membrane thickness, the membrane conductivity depends on the WU. During operation in a fuel cell, the hydration state of the membrane varies across the membrane as water is

consumed at the cathode and produced at the anode. This means that the hydration number in an operating cell will have a spatial dependence with a lower value at the oxygen cathode and a higher value at the hydrogen anode. Thus, in an operating cell, very thin membranes can have higher HFR because the local hydration state is less favorable. This local hydration gradient is likely more exaggerated in very thin membranes than thicker membranes. This is supported by the observation that during operation, the HFR for the 30 μm was 80% higher than the HFR for the 20 μm AEM (i.e., 50% higher thickness led to 80% higher HFR). The gradient in hydration number does call into question the validity of ex-situ hydroxide aging of AEMs since the hydration number (i.e., local hydroxide concentration within the membrane) in operating cells is non-uniform and is likely to be low at the oxygen cathode. No degradation in performance with time was observed, however, and the long-term durability and of these AEMs is the subject of another study.[111]

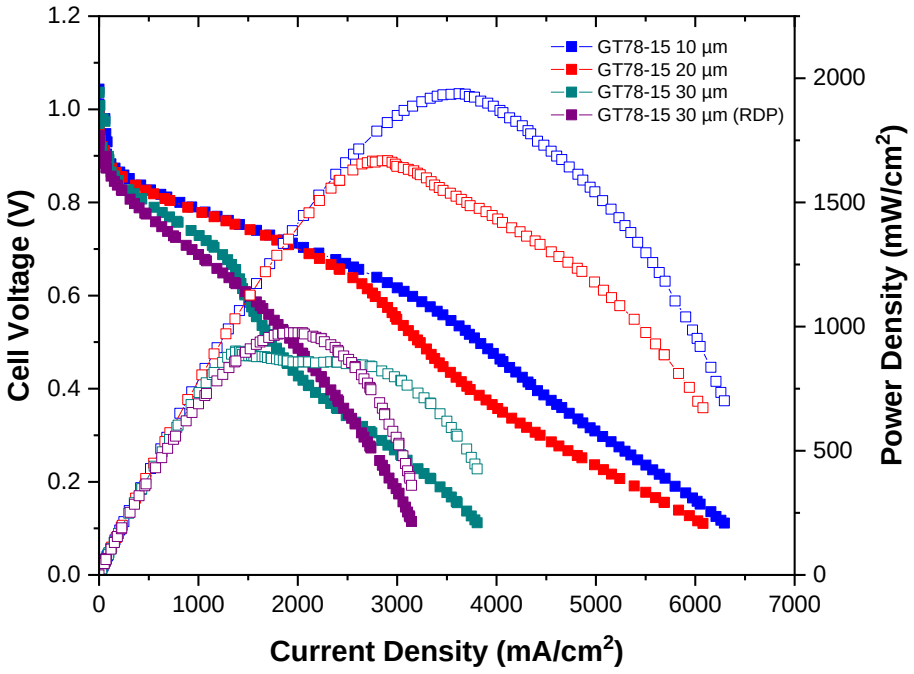


**Figure 5.2 – Current-voltage (filled) and current-power density (empty) curves for AEMFCs assembled with GT78-15 AEMs with three thicknesses: 10 µm, 20 µm and 30 µm. All cells were operated with $H_2/O_2$ reacting gases at 80 °C with no back pressurization. The anode and cathode catalyst loadings were 0.70 mgPtRu/cm$^2$ and 0.60 mgPt/cm$^2$, respectively. The AEMFCs operated with 10 µm (blue) and 20 µm (red) were operated at anode/cathode dew points of 75 °C/77 °C. AEMFCs assembled with the 30 µm AEM were operated at anode/cathode dew points of 75 °C/77 °C (cyan) and 70 °C/72 °C (purple).**

The values for the optimized dew points of the feed gases were different for the 10 µm and 20 µm thick membranes. Figure 5.2 showed the performance for all cells at the optimized dew points for the 10 µm AEM, 75 °C and 77 °C, respectively, for the anode and cathode. The optimized dew points for the 20 µm membrane were 70 °C for the anode and 73 °C for the cathode. The difference in the optimized dew points is important because the dew point helps to set the rate of water evaporation from the anode where water is produced. The water formed at the anode either evaporates into the anode reacting gas or diffuses across the membrane to the cathode. The lower the dew point of the incoming anode, the higher the rate of evaporation. If the rate of water removal from the anode is not

fast enough, anode flooding occurs. Combined with the lower achievable power density and lower current density for the thicker membrane, the lower values for the optimum dew points shows that the rate of water transport through the AEM is lower, resulting in lower water flux and current at the oxygen cathode. This is the first time that the AEM thickness and water transport rates have been linked, which is important for understanding the design and operation of AEMs and AEMFCs.

The distortion of the polarization and power curves (Figure 5.2) at higher thicknesses and higher dew points also suggests that water dynamics are playing a significant role in device performance. In the 30 μm thick AEM, there is an initial polarization that reaches an apparent mass transport limit at ca. 1.5 A/cm$^2$. Then, there is an inflection point as the cell passes 2 A/cm$^2$ where this limitation appears to be somewhat alleviated. This can be explained by observing the rate of water consumption at the cathode at high current. Water consumption at the cathode dries out the electrode and lowers the local hydration number of the AEM, but a higher water flux from the anode through the membrane allows the cell to support a higher current density without anode-flooding. It should be noted that the distorted current-voltage shape can be avoided by increasing the amount of water removed from the cell by lowering the oxygen dew point. Also shown in Figure 5.2 are polarization and power curves for a cell with the 30 μm GT78-15 AEM operated at anode and cathode dew points of 70 °C and 72 °C, respectively. The cell performance at the reduced reacting gas dewpoints curves is denoted as "GT78-15 30 μm (RDP)". As shown, the polarization curve has a more typical shape and a higher peak power density was achieved. Lowering the feed gas dew points in this cell does come at the expense of reduced performance in

the kinetic region and higher HFR (ca. 14 mΩ) and ASR (0.07 Ω $cm^2$) due to the relatively lower rate of water transport through the thicker AEM.

The dynamics between the cell performance at one static set of dew points and optimal dew points for each AEM thickness shows the dew points sensitivity of AEMFCs. In general, the thicker the AEM, the more sensitive the AEMFC performance was to the reacting gas dew points. With the thickest AEM tested here (30 μm), even the shape of the polarization curve changed when the reacting gas dew points were too high. In addition, the distorted shape was still prevalent when the anode and cathode dew points were each only 2 °C higher that their optimized values. With thinner AEMs, the shapes of the polarization curves were less sensitive to the dew points, as was the achievable current and peak power density. For example, when the dew points for the 20 μm AEMs were increased by 2 °C, the peak power density decreased by ca. 5% from its maximum value and the current density at 0.1 V was nearly identical. It was only when the dew points were increased by 6 °C to 8 °C that the peak power and achievable current density were significantly affected. For the cells operating with the 10 μm AEM, their performance was slightly more sensitive to the dew point values than the 20 μm membranes, but the shape of the polarization curve did not change as a result of altering the dew points. For these cells, if the dew points were either raised or lowered by 2 °C, there was around a 10% drop in the peak power density, although the achievable current density at 0.1 V was similar.

Finally, in-situ stability is an important factor in all fuel cells. Constant-current, short term durability tests were performed with the GT82-15 membrane-based AEMFC, Figure 5.3 (identical configuration to the cell in Figure 5.1). Remarkably, at a constant current density of 600 mA/$cm^2$ under $H_2$/air ($CO_2$-free), the cell voltage loss was negligible over

100 h. The cell voltage fluctuation at the 80 h point was due to a change in the feed dew points caused by automatic filling of cold water into the test station humidifier. The high frequency resistance (HFR) of the cell was nearly constant over the entire experiment. The extremely stable HFR suggests very little, if any, degradation of the GT82-15 membrane during testing, which is in good agreement with the ex-situ chemical stability tests for this AEM, discussed above. The most likely reason for the drop in the maximum current with air (about 3.5 A/cm$^2$) compared to the maximum current density with pure oxygen (about 9.5 A/cm$^2$) is permeation of oxygen through the ionomer at the positive electrode.

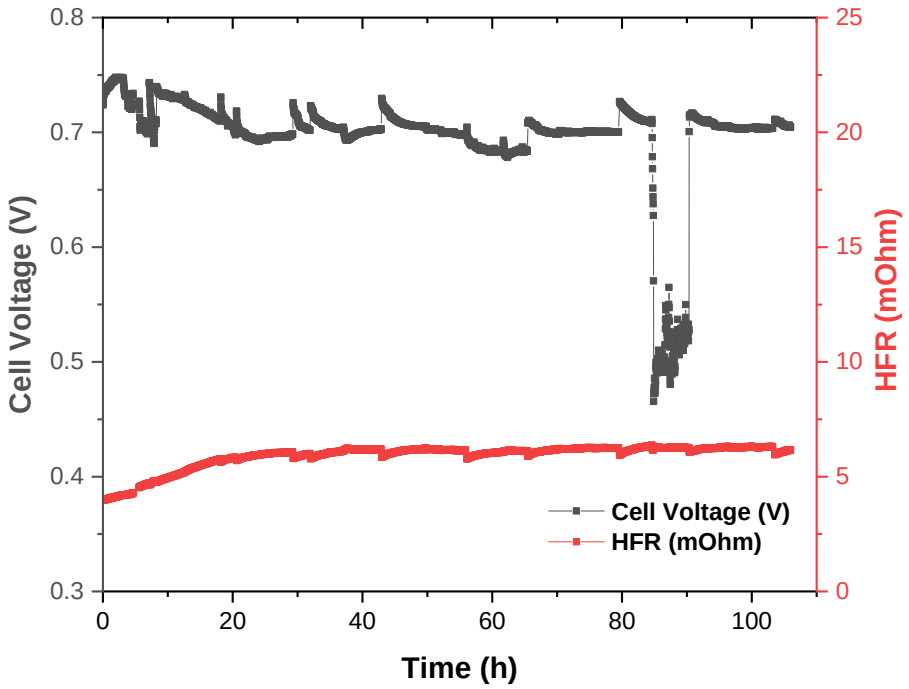


**Figure 5.3 – Cell voltage at constant current (left axis) and HFR (right axis) for AEMFC with GT82-15.**

### *5.2.3 Mitigating effects of carbonation using high conductivity AEMs*

The effect of carbonation has an impact in fuel cell operation because the mobility of carbonate is significantly lower than hydroxide. Very high ionic conductivity AEMs like

the ones reported in this study can potentially mitigate the adverse effects of electrolyte carbonation from ambient air. Unreinforced GT64-5 and GT64-10 (Table 3.2) were selected for study of the carbonate conductivity because they have a good balance of conductivity and water uptake. The comparison of $OH^-$ and $CO3^{2-}$ conductivity for GT64-5 and GT64-10 with temperature is shown in Figure 5.4 (left). The $OH^-$ conductivity for GT64-5 was 84 mS/cm and 181 mS/cm at 25 °C and 80 °C, respectively. In the $CO_3^{2-}$ form, the conductivity of GT64-5 was 18 mS/cm and 54 mS/cm at 25 °C and 80 °C, respectively. For GT64-10, the conductivity before and after carbonation was 74 mS/cm vs. 15 mS/cm at 25 °C, and 162 mS/cm vs. 47 mS/cm at 80 °C. The activation energy ($E_a$) for $OH^-$ and $CO_3^{2-}$ transport was calculated from the $\ln\sigma$ vs. 1/T for GT64-5 and GT64-10, Figure 5.4 (right). The $E_a$ values were 12.3 kJ/mol (OH-) and 17.6 kJ/mol ($CO_3^{2-}$) for GT64-5, and 12.6 kJ/mol ($OH^-$) vs. 18.4 kJ/mol ($CO_3^{2-}$) for GT64-10.

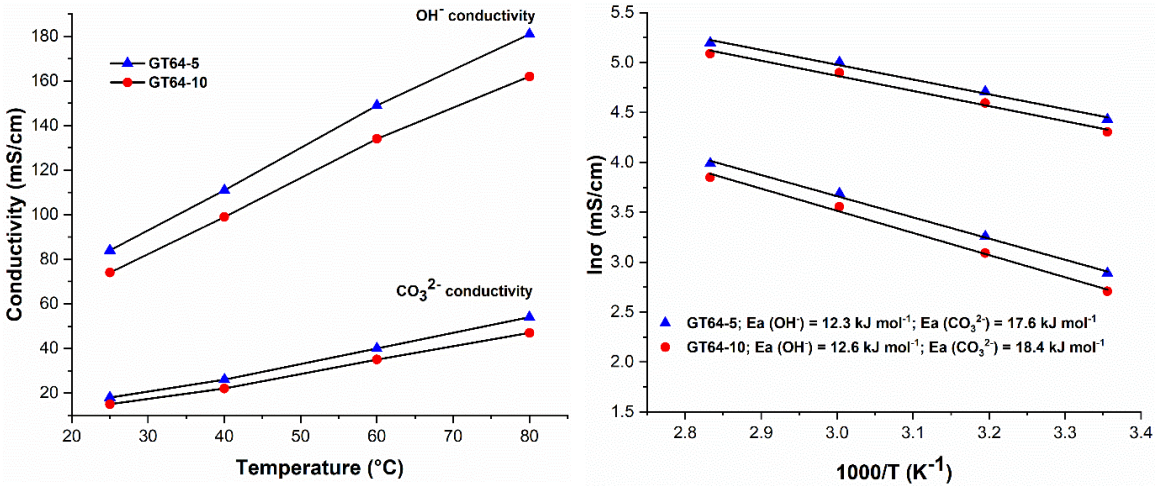


**Figure 5.4 – The measurement of $OH^-$ and $CO_3^{2-}$ conductivity as a function of temperature (left), Arrhenius plot of ln(σ) vs. inverse temperature for cross-linked AEMs in $OH^-$ and $CO_3^{2-}$ form (right).**

Other examples of membranes with very high hydroxide conductivities (e.g., >200 mS/cm at 80 °C) have been reported in the literature. A comparison of this work to other high conductivity AEMs is shown in Table 5.1. The anion conducting films synthesized in this study are still the only stable AEMs with little or no degradation (<1.5% degradation over 1000 h at 80 °C in 1 M NaOH) with >200 mS/cm ionic conductivity at 80 °C. Previously, Wang et al. synthesized radiation-grafted HDPE and LDPE AEMs with high hydroxide conductivity, 202 to 214 mS/cm at 80 °C; however, there was 6.2 to 8% decrease in conductivity after 500 h ex-situ aging.[108, 110] Later, Zhu et al. developed crossed-linked, comb-shaped PPO films with ionic conductivity of 200 mS/cm (80 °C) that showed a 27% decrease in conductivity after 500 h aging.[50] Recently, Zhu et al. reported an AEM able to achieve 201 mS/cm (80 °C) and 15.8% loss in conductivity over 1000 h with poly(olefin)-based AEMs.[112] Jannasch reported QPip-tethered PPO based AEMs with high ionic conductivity of 221 mS/cm at 80 °C, but 15% degradation occurred after only 240 h.[113] Recently, we have reported the synthesis of poly(norbornene) films by vinyl addition and

ROMP.[45, 46] The films have high ionic conductivity, ca. 200 mS/cm (80 °C), and no detectable loss in ionic conductivity in ex-situ aging at 80 °C .

**Table 5.1 – Properties (hydroxide ion conductivity, alkaline stability, water uptake etc.) of highly conducting (>190 mS/cm at 80 °C) AEMs.**

| Membrane | $OH^-$ Conductivity (mS/cm)[b] | IEC (meq/g)[d] | Water Uptake (%)[e] | Alkaline Stability[f] | Reference |
|---|---|---|---|---|---|
| Cross-linked membranes using VA poly(norbornene) | 198 | 3.43 | 69 | <1.5% degradation after 1000 h | [45] |
| Cross-linked membranes using ROMP poly(norbornene) | 195 | 4.51 | 115 | Retained its initial conductivity after 792 h | [46] |
| Cross-linked membranes using VA poly(norbornene)[a] | 212 | 3.84 (3.76) | 122 | <1.5% degradation after 1000 h | This work |
| HDPE-based radiation-grafted AEM | 214[c] | (2.44) | 155 | 8% drop in ionic conductivity after 500 h | [110] |
| LDPE-based radiation-grafted AEM | 202[c] | (2.54) | 149 | 6.2% drop in ionic conductivity after 500 h | [108] |
| Crossed-linked comb-shaped PPO membranes | 200 | 2.63 (2.35) | 144 | 27% decrease in conductivity for similar membrane after 500 h | [50] |
| Poly(olefin)-based AEMs | 201 | 2.76 (2.41) | 193 | 15.8% degradation after 1000 h | [112] |
| AEM Based on QPip-Tethered PPO | 221 | 2.8 (2.6) | 115 | 15% degradation after 240 h[g] | [113] |

[a] Block copolymers using bromobutyl norbornene (BBNB) as the halogenated block. [b] $OH^-$ conductivity was measured at 80 °C. [c] Measured at 100% relative humidity. [d] Theoretical IECs was determined by $^1H$ NMR or feed ratio, numbers in the brackets indicate the IECs by titration. [e] Water uptake was measured at room temperature. [f] Stability assessment was performed at 80 °C in 1 M NaOH or 1 M KOH. [g] Measurement was performed at 90 °C. VA = vinyl addition; ROMP = ring-opening metathesis polymerization.

## 5.3 Discussion

High ionic conductivity, rapid water transport, long-term alkaline stability and the ability to make thin, robust membranes are the key properties that are needed from AEMs in AEMFCs. The work of this chapter shows that the critical AEM features responsible for the leap in fuel cell performance shown here are the mechanical properties (i.e., ability to fabricate ultra-thin membranes) and water transport (i.e., transporting water from the anode to the water-consuming cathode). Water removal from the anode is critical for preventing anode flooding and supplying water to the oxygen cathode. Humidification or dehumidification of the feed gases alone is not sufficient for achieving high current density because the inner portion of the electrodes (closest to the AEM) are the most active regions. Thus, high water flux from the anode to the cathode is the most effective means of mitigating anode flooding and supplying the water to the cathode. Ultra-thin membranes facilitate high flux rates for water and minimize the parasitic voltage drop across the membrane. Very light cross-linking in the AEMs used here provided enough control over WU so that very high IEC values could be used without mechanical distortion of the membranes.

The effect of carbonation has a significant impact in fuel cell operation because the mobility of carbonate is significantly lower than hydroxide. The ratio of the $OH^-$ to $CO_3^{2-}$ mobility was 4.7 (GT64-5) and 4.9 (GT64-10) at 25 °C (Figure 5.4). This is in agreement with a previous reported mobility ratio of 5.[79] That is, carbonate has only about 20% to 22% of the mobility of hydroxide at 25 °C. At 80 °C, the mobility ratio decreased to 3.4 and 3.7 for GT64-5 and GT64-10, respectively (Figure 5.4). Hence, the adverse effect of carbonation on anion mobility becomes comparatively less significant at fuel cell-relevant

temperatures. The anionic conductivity of the AEMs discussed in this work and others (Table 5.1) display record high hydroxide conductivities (e.g., >200 mS/cm at 80 °C). However, to reach an acceptably high $CO_3^{2-}$ conductivity (>100 mS/cm) for a fuel cells, the ionic conductivity of the AEMs would likely still need to double if the polymer electrolyte becomes completed carbonated from $CO_2$ exposure. It is noted AEMFC carbonation has other negative effects on fuel cell performance, such as lowering the pH at the negative electrode, inducing kinetic losses at the anode, and build-up of $CO_2$ in the hydrogen fuel if it is recirculated.[71, 79]

## 5.4 Conclusion

A series of highly conductive cross-linked poly(norbornene) membranes were used in AEMFCs. The precursor polymers were cross-linked with a hexyl diamine (TMHDA) in different mol% with respect to the halogenated monomer in the polymer chain. It was found that the mechanical properties and ability to form ultra-thin membranes was critical to obtaining high fuel cell performance by enabling efficient water transport from anode to cathode. Light cross-linking was found to be effective for mitigating the effect of high IECs towards high water uptake and low mechanical stability. The 10.1 bound water molecules and 7.6 free water molecules were optimum for hydration and effective conduction of ions through the film (GT82-5) to produce maximum ionic conductivity. Record high ionic conductivity of 212 mS/cm at 80 °C was achieved with only <1.5% loss in ionic conductivity over 1000 h of aging in 1 M NaOH at 80 °C and were stable up to 400 °C. The $H_2/O_2$ fuel cell performance at 80 °C showed a peak power density of 3.5 W/cm$^2$ and maximum current density of 9.7 A/cm$^2$, the highest reported to date.

# CHAPTER 6. IONOMER OPTIMIZATION FOR WATER UPTAKE AND SWELLING IN ANION EXCHANGE MEMBRANE ELECTROLYZER: OXYGEN EVOLUTION ELECTRODE

## 6.1 Motivation

Solid polymer electrolyte electrolysis based on alkaline exchange membranes (AEM) seeks to combine the advantages of conventional alkaline electrolysis (AEL) and proton exchange membrane electrolysis (PEMEL).[28, 42, 114-117] A schematic of an AEM electrolysis (AEMEL) cell is shown in Figure 6.1 along with its half-reactions. Like AEL, AEM electrolysis systems have facile OER kinetics and electrodes that can use no (or little) platinum group metals. The polymer membranes used in AEM-based systems have been advanced in recent years, with development of high conductivity, stable and low-cost membranes used in hydrogen/oxygen AEM fuel cells. Fuel cells with up to 3.5 W/cm$^2$ at peak power density have been demonstrated.[2, 32, 35, 36, 45, 46, 108, 111, 118] Furthermore, AEMELs do not require circulation of a highly concentrated alkaline electrolyte. Rather, the solid polymer electrolysis process uses a liquid water feed which may contain a dilute salt for pH control and may be recirculated.[116, 119]

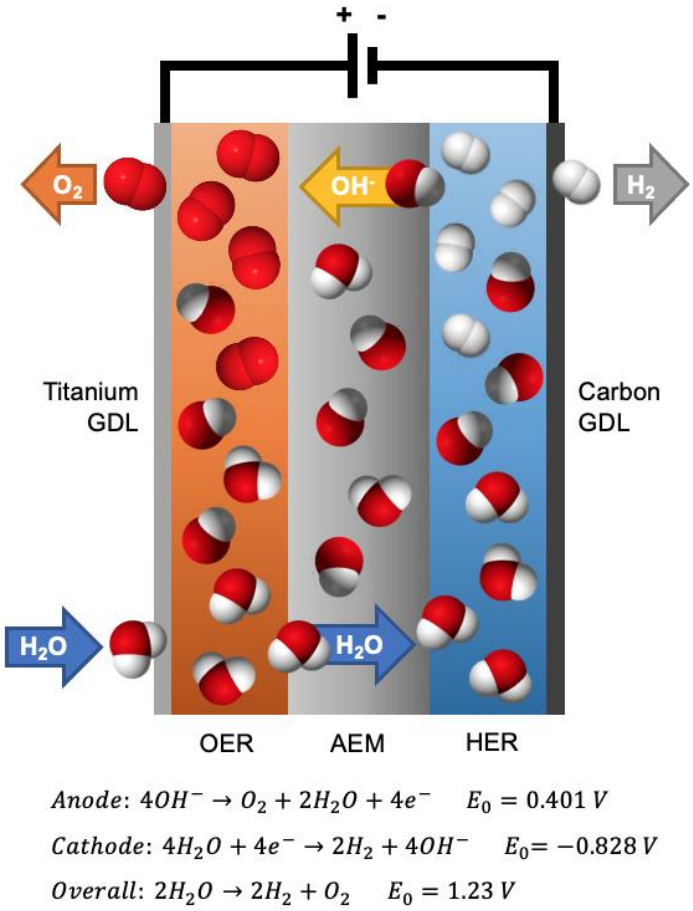


**Figure 6.1 – Schematic of the low-temperature AEM electrolysis cell configuration and associated half-reactions used in this study.**

While AEM performance has advanced in recent years, less attention has been paid to the anion conductive ionomer (ACI) in the catalyst layers, especially with regards to AEMEL. Both fuel cell and electrolyzer electrodes are often fabricated via the catalyst-coated substrate (CCS) method by spraying a slurry of catalyst, ionomer and solvent directly onto a gas diffusion layer (GDL). The deposited catalyst and ionomer mixture form the catalyst layer on the surface of the GDL after solvent evaporation. The main functions of the ionomer are to provide an ionic pathway between the catalyst sites and AEM and provide adhesion of the components within the electrode. High ionic conductivity and

chemical stability are important attributes of the electrolyzer ACI.[42, 120] The ionomers do not need to form free-standing films so mechanical strength and polymer chain entanglement are less of an issue, compared to AEMs.[82] Adhesion of the catalyst and ionomer to the current collector within the electrode is especially important in electrolyzers where liquid water is present and gas is vigorously evolved at the electrodes. The gaseous hydrogen and oxygen products may form bubbles between the membrane catalyst layer which can cause MEA delamination.[121] This is not as important in fuel cells where reactants are supplied in gas form and catalyst detachment is less of an issue. High ion exchange capacity (IEC) ionomers are favored because they have higher ionic conductivity and are generally stickier than low IEC ionomers. However, water management and excessive water uptake (WU) within the electrodes has been found to be a critical factor in achieving high performance in AEM fuel cells.[36, 69, 70, 122] Electrode swelling due to excessive WU can disrupt the three-phase boundary between the catalyst, ionomer and current collector. Improved fuel cell performance was achieved by optimizing ionomer properties through a trade-off between conductivity and WU.[17, 123, 124] Hydrophobic additives have also been shown to be a useful tool for controlling water uptake within the catalyst layer in AEM fuel cells.[35]

In this chapter, a series of poly(norbornene) tetrablock copolymers and homopolymers were used as the OER ionomer in AEMEL to investigate the trade-offs between WU and conductivity. Cross-linking within the ACI was used to control its hydrophilicity and water uptake so that the benefits of high conductivity ionomers could be realized without the penalty of excess water swelling. To the author's knowledge, this work demonstrates the first application of a cross-linked OER ionomer in an AEM water

electrolyzer and explains the balance between ionic conductivity and WU in achieving optimal device performance.

## 6.2 Results

### *6.2.1 Optimization of OER ionomer content*

The ACI content in the oxygen-evolving anode was first evaluated by comparing MEAs with four levels of GT25 (Table 3.1) ionomer content: 15%, 25%, 30% and 45%. Steady state electrolysis tests were performed at 1A/cm$^2$ with 3 wt% carbonate in the anode water feed. The resulting cell voltage at 1A/cm$^2$ was 1.76 V, 1.70 V, 1.73 V and 1.89 V for the MEAs with 15%, 25%, 30% and 45% ionomer content, respectively. The area specific resistance for the four MEAs was 0.33 Ohm-cm$^2$ (15% ionomer), 0.30 Ohm-cm$^2$ (25% ionomer), 0.38 Ohm-cm$^2$ (30% ionomer) and 0.38 Ohm-cm$^2$ (45% ionomer). Figure 6.2 shows a comparison of the polarization curves of the MEAs with the different wt% ionomer in the OER catalyst layer. Figure 6.3 shows the steady state response while the cell was operated at constant current density of 1 A/cm$^2$. The highest ionomer content, 45%, showed a significant increase in cell voltage with time due to disruption in the ionic and gas pathways. Based on this set of experiments, 25% ionomer content was used in the anode for the remainder of the study, unless otherwise noted.

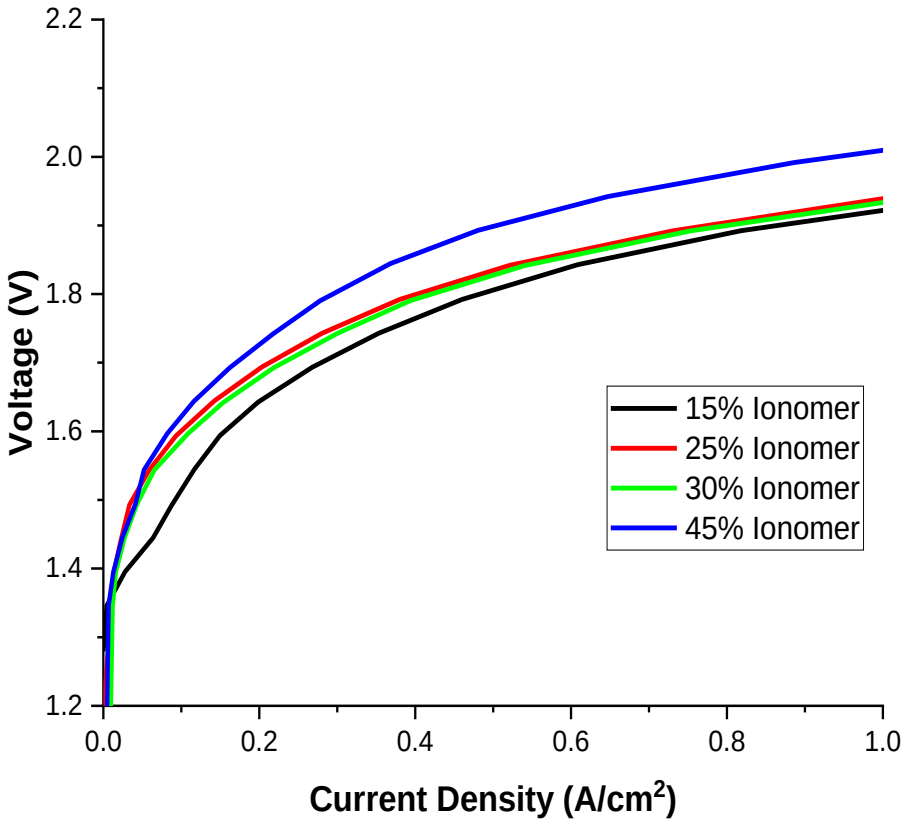


**Figure 6.2 – Comparison of polarization curves of MEAs with various OER ionomer content after break-in. The AEM was radiation grafted ETFE (25 µm thick). The anode ionomer was GT25 and catalyst was $PbRuO_x$. The cathode ionomer was GT73 (20 wt%) and catalyst was PtNi.**

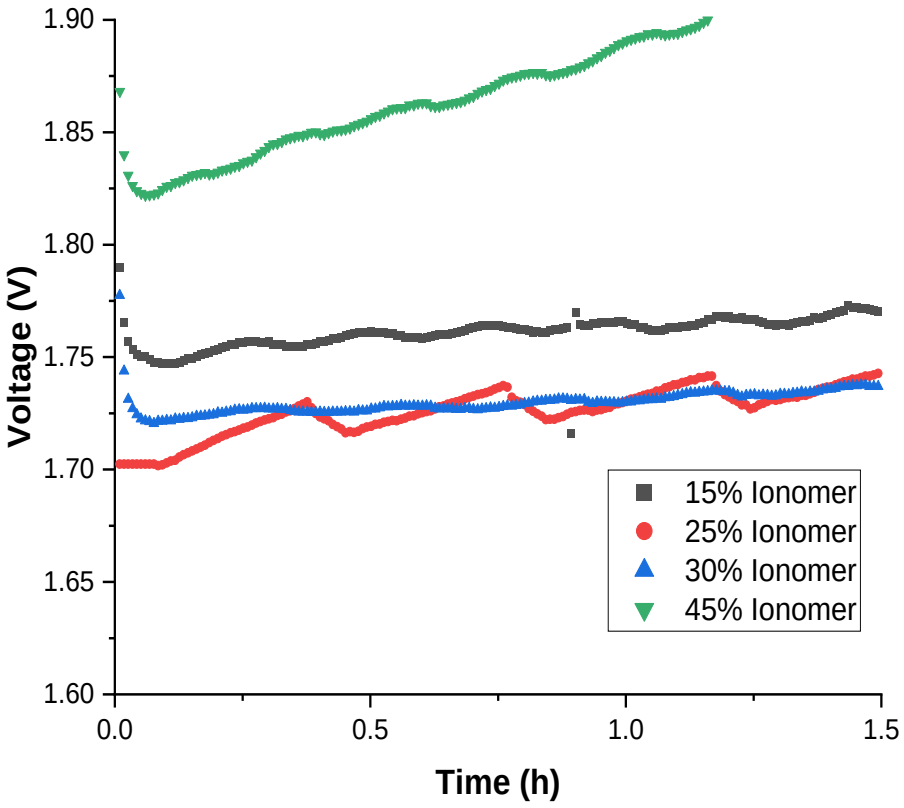


**Figure 6.3 – Cell voltage vs. time of MEAs with various OER ionomer content at 1 A/cm$^2$. The AEM was radiation grafted ETFE (25 µm thick). The anode ionomer was GT25 and catalyst was PbRuO$_x$. The cathode ionomer was GT73 (20 wt%) and catalyst was PtNi.**

### *6.2.2 Effect of OER ionomer ion exchange capacity*

Six ionomers with different IEC values (GT0, GT18, GT32, GT75, GT82, GT100) were investigated in the oxygen-evolving anode using $IrO_2$ catalyst (Table 3.1). The samples were divided into four groups based on their IEC and hydrophilicity, namely (i) non-ionic homopolymer (GT0), (ii) low IEC tetrablock copolymer (GT18, GT32), (iii) high IEC tetrablock copolymer (GT75, GT82), and (iv) fully ionic homopolymer (GT100).

Figure 6.4 shows a comparison of the polarization curves for MEAs from 0 to 450 mA/cm$^2$ for the six ionomers. The MEAs containing low IEC tetrablock copolymers ACIs (i.e., GT18, GT32), showed the best (lowest) cell voltage among the six ionomers tested. The MEA with GT18 had the lowest cell voltage (1.59 V and 1.86 V for 100 mA/cm$^2$ and 500 mA/cm$^2$, respectively). The MEA with the GT32 ionomer had a slightly higher cell voltage (1.62 V and 1.98 V for 100 mA/cm$^2$ and 500 mA/cm$^2$, respectively). The MEA with the zero IEC ionomer (GT0) had a slightly higher cell voltage, 1.69 V and 2.46 V for 100 mA/cm$^2$ and 500 mA/cm$^2$, respectively, even though it had no ionic conductivity. The ionomers with the highest IEC (i.e., GT75, GT82 and GT100) showed the worst performance among the six non-cross-linked ACI samples tested. The MEA with the hydrophilic ionomer (GT100) had a cell voltage of 1.83 V and 2.67 V at 100 mA/cm$^2$ and 500 mA/cm$^2$, respectively. The MEA with the GT75 ionomer had a more extreme cell voltage of 2.08 V at for 100 mA/cm$^2$. At 450 mA/cm$^2$, the cell voltage was greater than 3 V. In addition, catalyst detachment from the GDL occurred with electrode material observed coming out of the anode gas exhaust. The is likely the cause of the rapid rise in voltage over the first hour of operation for the GT75 and GT82 MEAs. Lastly, the MEA with the GT82 ionomer had a cell voltage of 2.11 V at 100 mA/cm$^2$, which was the highest among the non-cross-linked ACI samples tested. The trends observed in the polarization curves are consistent with the constant current results at both low current density (100 mA/cm$^2$) and high current density (500 mA/cm$^2$), Figure 6.5.

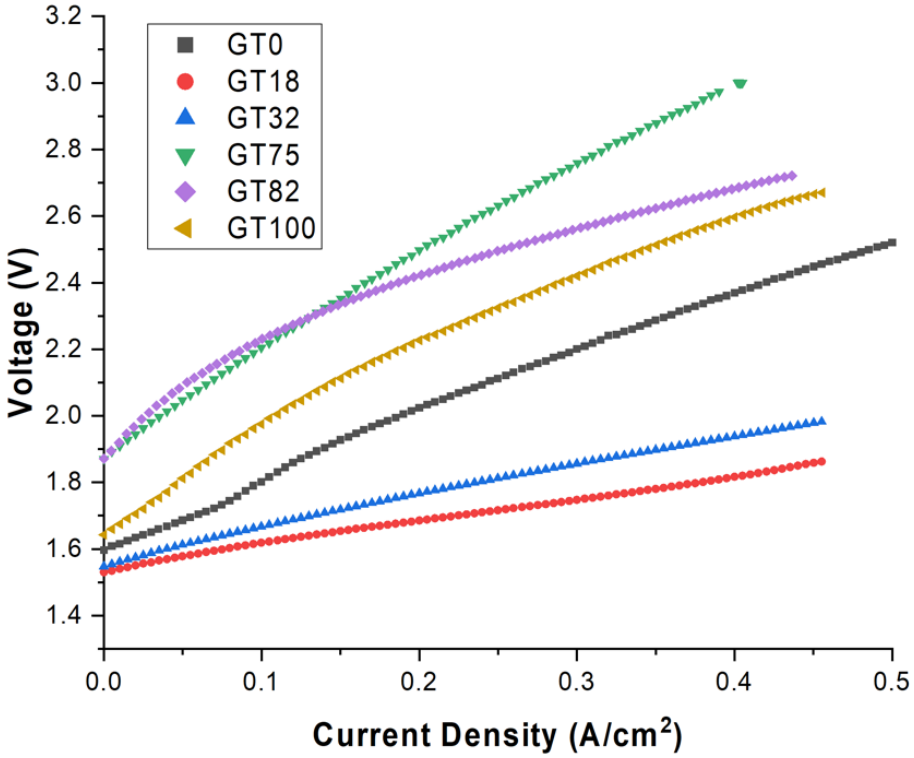


**Figure 6.4 – Comparison of polarization curves of MEAs with OER ionomers of various ion exchange capacities after break-in. The AEM was GT74 with a PTFE reinforcement layer (50 µm thick, 5 mol% cross-linking). The anode catalyst was $IrO_2$. The cathode ionomer was GT32 (20 wt%) and catalyst was Pt/C.**

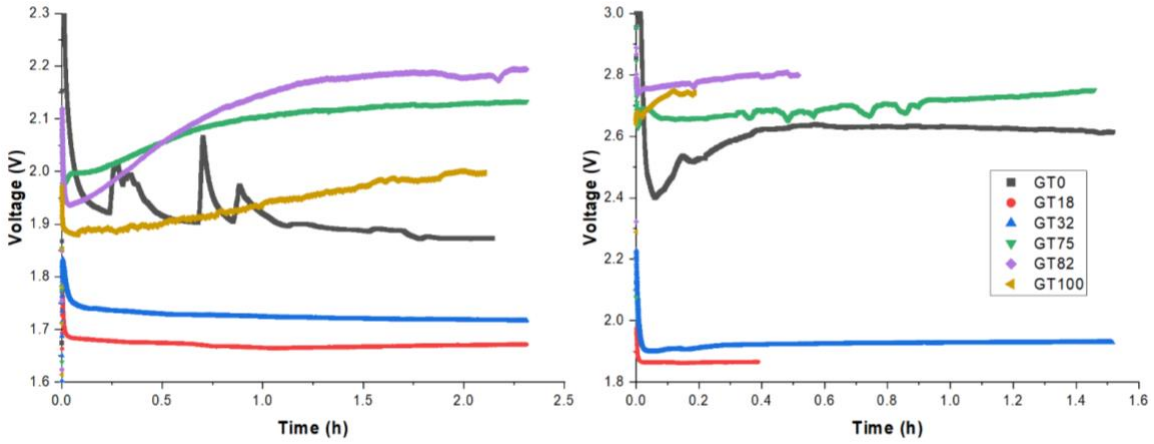


**Figure 6.5 – Cell voltage vs. time for MEAs with OER ionomers of various ion exchange capacity at 100 mA/cm$^2$ (left) and 500 mA/cm$^2$ (right). The AEM was GT74 with a PTFE reinforcement layer (50 µm thick, 5 mol% cross-linking). The anode catalyst was $IrO_2$. The cathode ionomer was GT32 (20 wt%) and catalyst was Pt/C.**

### *6.2.3 Effect of hydrophobic additive*

The selection of 25% ACI loading discussed above was retested with GT11 (Table 3.1) ionomer in the oxygen evolving anode to confirm that the loading was optimum for different IEC ionomers. Four levels of ionomer loaded were used. A baseline anode (25% ionomer) was made using the same ionomer-to-catalyst ratio as the above-mentioned experiments using GT11 as the ionomer and $IrO_2$ as the OER catalyst. Two variations of this anode electrode were fabricated with higher (50%) and lower (12.5%) ionomer content. A fourth anode type (denoted as "25% Ionomer + 8% PTFE") was constructed to test the effect of adding a small amount of hydrophobic PTFE (8 wt% with respect to the dry mass of solids) to the baseline anode composition. The addition of PTFE to the ionomer slurry is known to make the electrode more hydrophobic. The amount of catalyst in these formulations was kept the same as the baseline to isolate the effect of the anode ionomer

loading. Figure 6.6 shows the polarization curves from 0 to 1 A/cm$^2$ taken after 1 hr of operation at 100 mA/cm$^2$. The cell voltage over time at 100 mA/cm$^2$ is shown in Figure 6.7. Among the four cells tested, the more hydrophobic MEA with added PTFE showed the best overall performance with stable operation at 100 mA/cm$^2$ with a cell voltage of 1.71 V. The MEA with 25% ionomer content had a slightly higher cell voltage, 1.76 V, at the same current density, although it was the best non-PTFE cell. The cell voltage with less ionomer (12.5%) was the worst performing electrode within this set. The electrode with higher ionomer (50%) was worse than the 25% ionomer electrode but better than the 12.5% ionomer electrode. This shows that choking-off the ionic and gas pathways with too much ionomer (50% ionomer) has a penalty, and not providing enough ionic conductivity (12.5% ionomer) also has a penalty. In addition, the cell with 12.5% ionomer content showed an initial cell voltage of 1.84 V and increased over time. The cell with 50% ionomer showed stable operation but had the highest cell voltage among the four MEAs (1.89 V at 100 mA/cm$^2$).

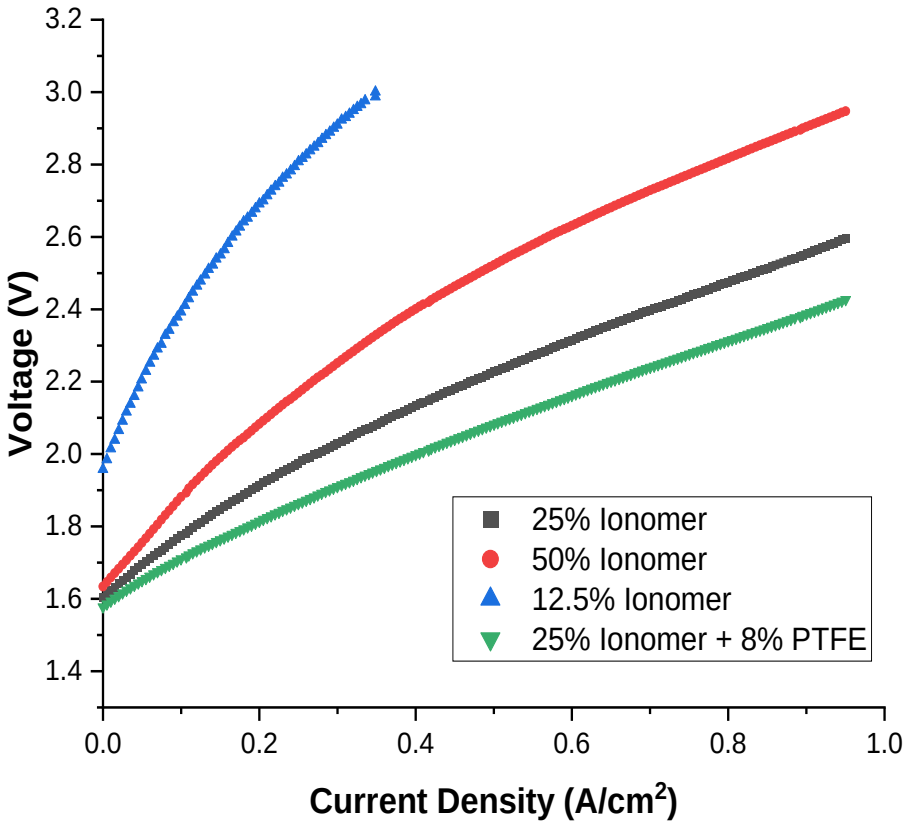


**Figure 6.6 – Comparison of polarization curves of MEAs with various amounts of OER ionomer and PTFE after break-in. The AEM was GT74 with a PTFE reinforcement layer (35 µm thick, 5 mol% cross-linker). The anode ionomer was GT11 and catalyst was $IrO_2$. The cathode ionomer was GT32 (20 wt%) and catalyst was Pt/C.**

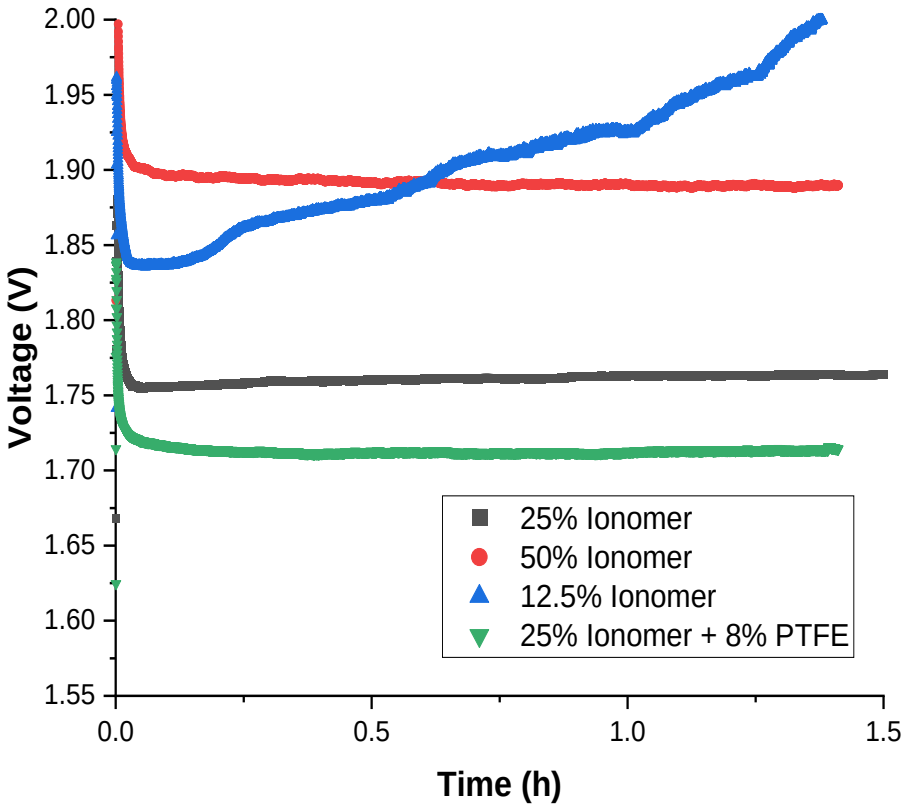


**Figure 6.7 – Cell voltage vs. time for MEAs with various OER ionomer content and PTFE at 100 mA/cm$^2$. The AEM was GT74 with a PTFE reinforcement layer (35 µm thick, 5 mol% cross-linking). The anode ionomer was GT11 and catalyst was $IrO_2$. The cathode ionomer was GT32 (20 wt%) and catalyst was Pt/C.**

To understand the effect of the addition of PTFE, electrochemical impedance spectroscopy was performed on the four cells. The Nyquist plots for the four MEAs are shown in Figure 6.8. The high frequency resistance (HFR) (i.e., area specific resistance) and low frequency resistance (LFR) values are tabulated in Table 6.1. The apparent, total charge transfer resistance ($R_{ct}$) was also calculated by subtracting the HFR from the LFR. The HFR values for all four cells range from 0.39 to 0.45 Ohm-cm$^2$. The average $R_{ct}$ of the cells without PTFE was 4.71 Ohm-cm$^2$. This result suggests that water content of the anode ionomer is the critical factor determining OER performance because PTFE has a significant

effect on electrode hydrophobicity and not conductivity, or the PTFE changed the ionomer distribution in some way so as to improve the effective conductivity.

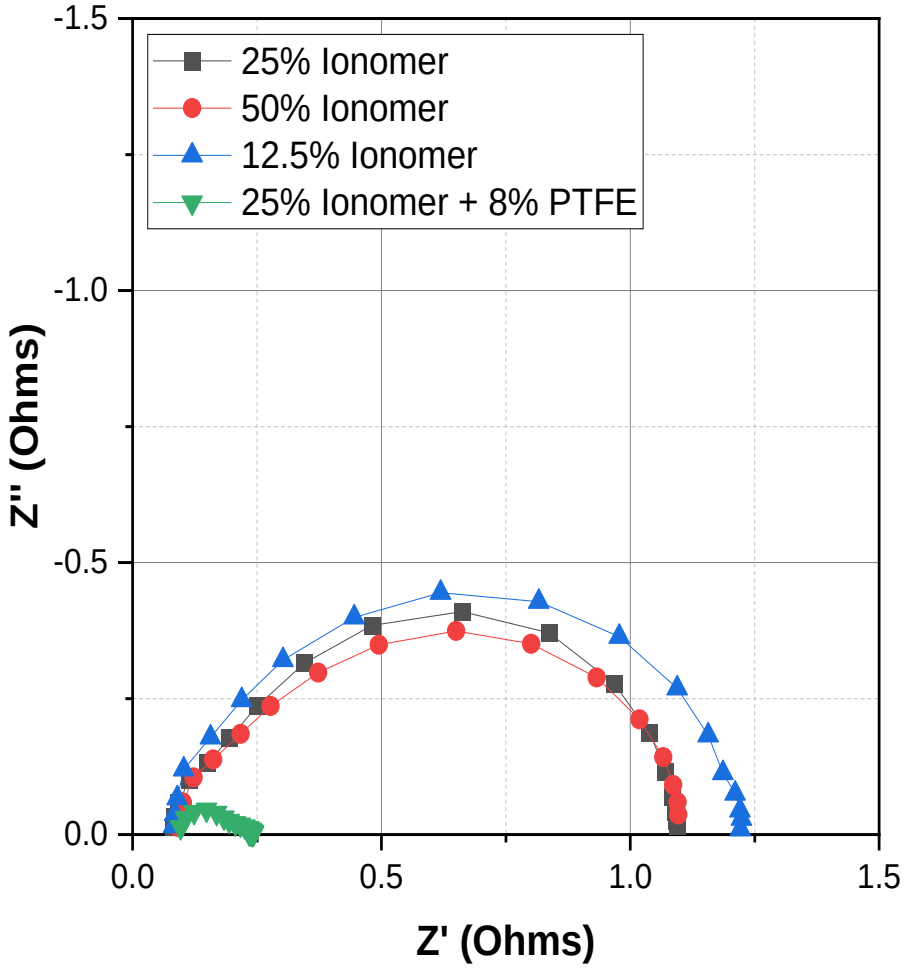


**Figure 6.8 – Comparison of Nyquist plots of MEAs with various amounts of OER ionomer and PTFE. The AEM was GT74 with a PTFE reinforcement layer (35 µm thick, 5 mol% cross-linking). The anode ionomer was GT11 and catalyst was $IrO_2$. The cathode ionomer was GT32 (20 wt%) and catalyst was Pt/C.**

**Table 6.1 – EIS data of MEAs with various amounts of GT11 ionomer and PTFE.**

| Sample (Ionomer wt%) | HFR ($Ohm\text{-}cm^2$) | LFR ($Ohm\text{-}cm^2$) | $R_{ct}$ ($Ohm\text{-}cm^2$) |
|---|---|---|---|
| 25% | 0.39 | 5.27 | 4.88 |
| 50% | 0.44 | 5.27 | 4.84 |
| 12.5% | 0.39 | 4.80 | 4.40 |
| 25% + 8% PTFE | 0.45 | 1.10 | 0.65 |

### *6.2.4 Effect of OER ionomer water uptake*

The WU of the OER electrode was investigated and the electrode performance was improved by controlling the water swelling of the ionomer via polymer cross-linking. MEAs with cross-linked, high IEC ionomers were used because they have excellent ionic conductivity without excessive WU. A high IEC tetrablock copolymer, GT72 (Table 3.1), was selected as the baseline polymer for the cross-linked ACI experiments. Three levels of cross-linking (5 mol%, 10 mol%, and 15 mol%) were used. The properties of the cross-linked ionomers are listed in Table 3.2. GT72 had a high degree of swelling without any cross-linking and with a WU of over 1000%. The WU of the cross-linked ionomers was much lower, 96% WU, by adding a small amount of TMHDA (5 mol%). Increasing the amount of cross-linker further lowered the WU to 78% and 66% for 10 mol% and 15 mol% cross-linker, respectively. The conductivity of the cross-linked ionomers also remained high (>130 mS/cm) with a slight decrease at higher cross-linker content.

Figure 6.9 shows the cell voltage vs. time at 1 A/cm$^2$ for MEAs fabricated with different OER ionomers. MEAs constructed with GT11 and GT38 OER ionomers (same catalyst system) are also shown for comparison to previous tests. The MEA with GT11 had an initial cell voltage of 1.79 V at 1 A/cm$^2$ but increased gradually over time. The cells with cross-linked ionomer had the lowest cell voltage among all samples tested. The 10 mol% cross-linked ionomer performed slightly better than the other two cross-linked ionomers, with an initial cell voltage of 1.75 V at 1 A/cm$^2$. The MEAs with 5 mol% and 15 mol% cross-linked ionomers had cell voltages of 1.77 V and 1.78 V, respectively. This results shows that the high conductivity of GT72 ionomer can only be used if its WU can be controlled.

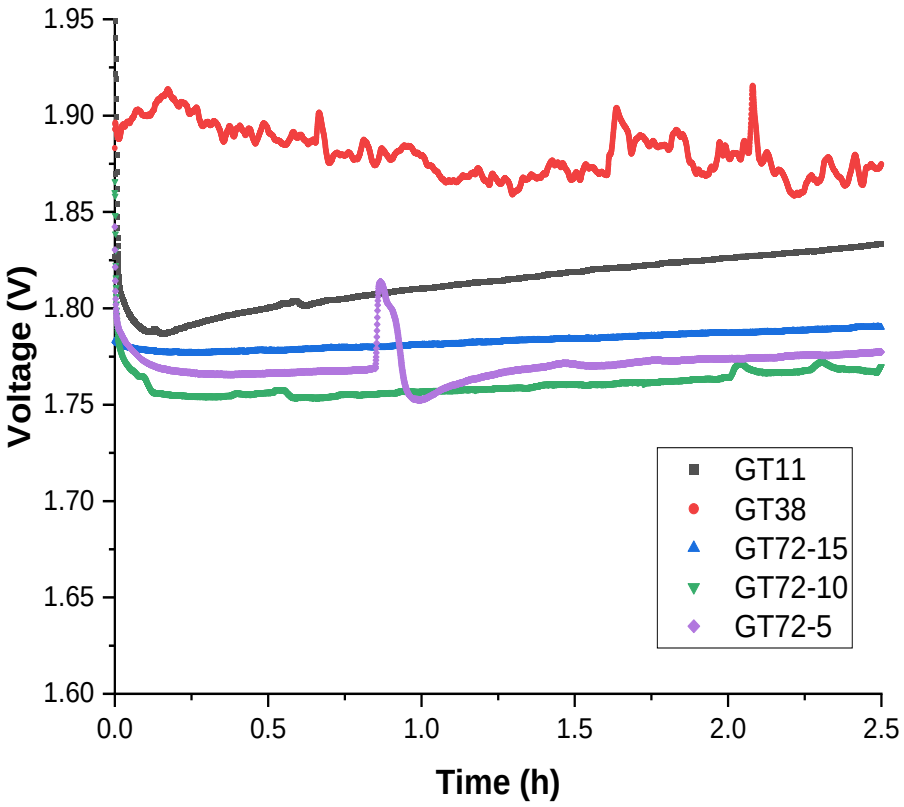


**Figure 6.9 – Cell voltage vs. time for OER ionomers at 1 A/cm$^2$ constant current. The anode catalyst was $PbRuO_x$. The cathode ionomer was GT74 (20 wt%) and the catalyst was PtRu on ECS-3701.**

## 6.3 Discussion

The results from the survey of OER ionomers with different IEC values and the addition of PTFE show that MEA performance is strongly influenced by WU. Although high ionic conductivity is an advantage, it can only be used if WU is controlled. The cells with low IEC ionomer had significantly better performance than any of the non-cross-linked, high IEC ionomers. Furthermore, the MEA containing the nonconductive ionomer (GT0) outperformed the MEAs with high IEC ionomer because it did not undergo excessive WU. In this case, ion conductivity between the AEM and catalyst was supplied by the carbonate containing water feed to the anode. Cells with low IEC ionomer (GT18

and GT32) had similar performance even though the number average molecular weight of GT32 was three times higher than that of GT18. Thus, the molecular weight of the anode ionomer does not appear to have been a major factor in performance.

The critical factor in anode performance is the WU of the OER electrode, in the form of hydrated ACI. The electrodes with high IEC ionomers all had very high WU (>1000%) which causes the material to swell and negates the benefit of high ionic conductivity. It is noted that the volume fraction of *hydrated* ionomer in the electrode is significantly greater in the case of electrodes with high IEC ionomer compared to low IEC ionomers, even though the dry mass of the ionomer was the same. Excess WU can swell the ionomer and disrupt the three-phase boundary needed in the electrode. It is also possible that high ionomer swelling can decrease the void volume between the catalyst particles. An electrically insulating film of residual ionomer can form around the catalyst particles leading to a higher contact resistance and kinetic overpotential as suggested by Bernt et al.[125] In the case of GT0, hydroxide ions are transported through the ionomer via diffusion only. The oxygen evolution reaction can take place at catalyst sites that are supplied with hydroxide via the ionomer or the carbonate water feed at the anode. GT18 and GT32 have higher conductivity than GT0 and modest water uptake (15% and 63%, respectively). By increasing the IEC from GT0 to GT18 or GT32, hydroxide ions can be more efficiently shuttled to catalyst sites which resulted in improved cell performance.[126] Without proper management of the WU in the electrode, the benefits of having even higher ionic conductivity (e.g., GT75 and GT82) are negated due to ionomer swelling, as occurred in the high IEC, non-cross-linked ionomer.

The high IEC ionomer with excessive WU also had a detrimental effect on catalyst durability. In Figure 6.5, the rapid rise in cell voltage over the first hour of operation for both the GT75 and GT82 MEAs is attributed to catalyst detachment from the GDL, as was observed in the anode gas exhaust. Similarly, the MEA containing the highest IEC ionomer (GT100) had a high cell voltage and showed an undesirable rise in cell voltage over time due to catalyst detachment. Catalyst detachment was observed while operating at both low and high current density. The high IEC ionomers have excessive swelling and are more soluble in water which causes the ionomer and catalyst to lose adhesion and be washed away by the water feed during operation. Thus, even though the high IEC OER ionomers were stickier (a desirable attribute in electrode fabrication), the high WU negated the benefit.

Figure 6.8 demonstrates that the water content in the OER electrode can be managed successfully via the introduction of hydrophobic additives. Adding PTFE to the anode ink improved the cell voltage and charge transfer resistance due to a reduction in water content within of the OER catalyst layer. However, the results also highlight the sensitivity of cell resistance to the ionomer-to-catalyst ratio. The addition of PTFE increases the effective ionomer/binder-to-catalyst ratio slightly (up from 25% to 31%) which resulted in a 17% increase in the HFR from the baseline. A similar trend was observed in the MEA where the OER ionomer content was increased (50% ionomer). The cell voltage at 100 $mA/cm^2$ was 7% higher than the baseline cell because the HFR was increased by 13% due to the insulating effect of the higher ionomer volume fraction. On the other hand, the electrode showed severe durability issues when there was an inadequate amount of binder. The MEA with reduced ionomer content (12.5% ionomer) showed that

insufficient binder led to catalyst detachment accompanied by a rise in cell voltage over time. Many reports have previously shown that 10 to 20 wt% is the optimal amount of binder for AEM electrolyzers.[8, 125] The results of this study suggest the need to manage WU without modifying the ionomer to catalyst ratio, and it is more important to consider the hydrated mass of the ACI rather than its dry mass.

Modification of the molecular structure of the ionomer to reduce water uptake has been achieved in the past through cross-linking.[45, 46] The addition of the cross-linker significantly lowers WU of the ionomer while only marginally affecting the IEC and ionic conductivity of the ionomer. To enable the use of a high IEC ACI while maintaining reasonable water uptake, light cross-linking was introduced to limit the swelling of the ionomer. Restricting the ionomer WU increased the density of quaternary ammonium head groups in the hydrated ionomer and facilitated more efficient ion conduction. The WU of the high IEC cross-linked ionomers was similar to the WU of the non-cross-linked GT38 ionomer, yet the conductivity of the cross-linked, high IEC ionomer was 28 to 72% higher. Figure 6.9 shows that all three of the MEAs containing cross-linked ionomers had a lower cell voltage than any of the non-cross-linked ionomer electrodes. The average cell voltage of the cross-linked ionomer samples was similar (1.77 V at 1 A/cm$^2$), showing that cell performance has low sensitivity to the amount of cross-linker present in the OER electrode, within the range tested. It is also noted that the cell performance of 1.77 V at 1 A/cm$^2$ is very favorable compared to state-of-the-art performance.[127]

These results demonstrate that the use of light cross-linking provides a way to use their high ionic conductivity without inducing excessive WU and destructive swelling. It also shows that the dry weight of the ionomer is a misleading metric when constructing

MEAs, when excessive WU can occur. The results also suggest that other means, such as polymer molecular structure and highly hydrophobic monomers, can be used to control ionomer hydrophobicity in high ionic conductivity ionomers without altering the ionomer-to-catalyst ratio.

## 6.4 Conclusion

A series of poly(norbornene) tetrablock copolymers and homopolymers with widely varying ion exchange capacities were synthesized and used in the fabrication of oxygen evolving electrodes in low-temperature AEM electrolyzers. It was found that ionomers with low or zero IEC outperformed ionomers with very high IEC and ionic conductivity. Excessive swelling of the high IEC ionomer was identified as the cause of poor performance. Uncontrolled WU caused an increase in ionic and electronic resistance and also caused durability issues in the form of catalyst detachment. Control over the water content in the catalyst layer was first achieved through the addition of a small amount of a PTFE hydrophobic agent. However, the ionomer-to-catalyst ratio was found to be a particularly sensitive parameter for maintaining a proper water balance and adhesive properties. Light cross-linking within the OER ionomer was a more effective way to limit swelling of the ACI and allowed the conductivity benefits of high IEC ionomers to be used in the oxygen evolving electrode. The cross-linked, high IEC ionomers had comparable WU to non-cross-linked, low IEC ionomers. They showed an improvement of over 150 mV in cell voltage, demonstrating that the benefits of higher conductivity could be used as long as WU was properly managed. Overall, modification of the ionomer structure was found to be the preferred method of reducing WU. The results of this study provide guidance for optimizing OER electrodes in AEM electrolyzers to achieve maximum ionic

conductivity while properly managing water content. Optimization of the ionomer in the HER electrode in AEM electrolyzers will be the focus of a future study.

# CHAPTER 7. IONOMER OPTIMIZATION FOR WATER UPTAKE AND SWELLING IN ANION EXCHANGE MEMBRANE ELECTROLYZER: HYDROGEN EVOLUTION ELECTRODE

## 7.1 Motivation

In the previous chapter, the ACI in the oxygen evolution electrode (OER) was optimized through a trade-off between conductivity and WU.[128] In this study, a family of poly(norbornene) tetrablock copolymers were synthesized and used to investigate the properties of the hydrogen evolution reaction (HER) ionomer in low-temperature AEM electrolysis cells. The ion exchange capacity (IEC) of the ionomers (1.49 to 3.60 meq/g) was adjusted by controlling the ratio of ion conducting to non-ion conducting norbornene monomers in the ACI and used to control the hydrophilicity and water uptake within the cathode catalyst layer. Ionic conductivity and swelling due to WU are especially important at the negative electrode because water is used as a reactant in the HER. Light cross-linking of the ionomer was used to maintain adequate WU in high IEC ionomers without the penalty of excessive swelling or dry-out. Optimization of the ionomer loading was also performed. This work compliments the previous chapter on the use of cross-linked high IEC OER ionomer in an AEM water electrolyzer and highlights for the first time the differences in ionomer requirements between the OER and HER electrodes.[129]

## 7.2 Results

### *7.2.1 Optimization of HER ionomer content*

The ACI content in the hydrogen-evolving cathode was first investigated by comparing MEAs with four GT74 (Table 3.1) ionomer loadings: 10%, 15%, 20% and 30%. The tests were performed at 1 A/cm$^2$ and identical anodes. The resulting cell voltage using the four ACIs was 1.80 V, 1.82 V, 1.82 V and 1.86 V for the MEAs with 10%, 15%, 20% and 30% HER ionomer content, respectively. The area specific resistances of the four MEAs were similar, though there was a slight increase with ionomer content: 0.83 Ω-cm$^2$ (10% ionomer), 0.84 Ω-cm$^2$ (15% ionomer), 0.86 Ω-cm$^2$ (20% ionomer) and 0.87 Ω-cm$^2$ (30% ionomer). Figure 7.1 shows a comparison of the polarization curves of the MEAs with the different ionomer content in the HER catalyst layer. Figure 7.2 shows the steady state response for these MEAs operated at 1 A/cm$^2$. This set of results shows that the electrode with 10% ionomer gave the best performance, although there was not a sharp drop-off from 10% to 20% ionomer. Electrodes with less than 10% ionomer content did not perform as well. It is also noted that higher ionomer content (i.e., 30% in Figure 7.2) showed an increase in current with time indicative of electrode flooding.

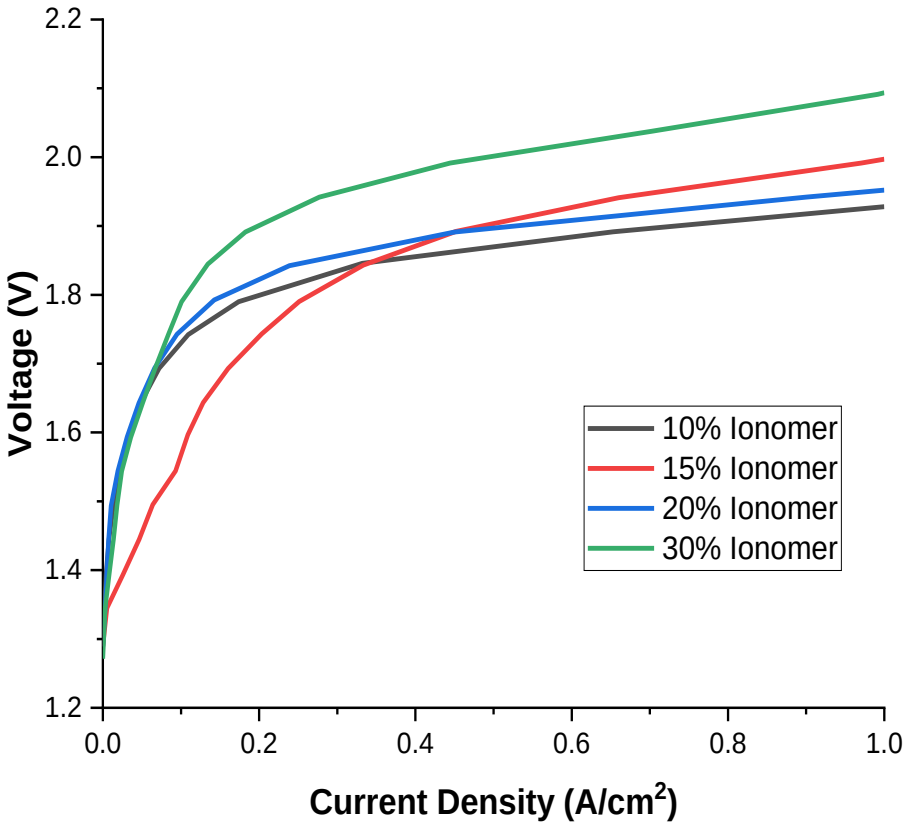


**Figure 7.1 – Comparison of polarization curves of MEAs with various HER ionomer content. The AEM was GT69 with a PTFE reinforcement (40 µm thick, 15 mol% cross-linking). The anode ionomer was GT25 (25 wt%) and catalyst was $PbRuO_x$. The cathode ionomer was GT74 and the catalyst was PtNi.**

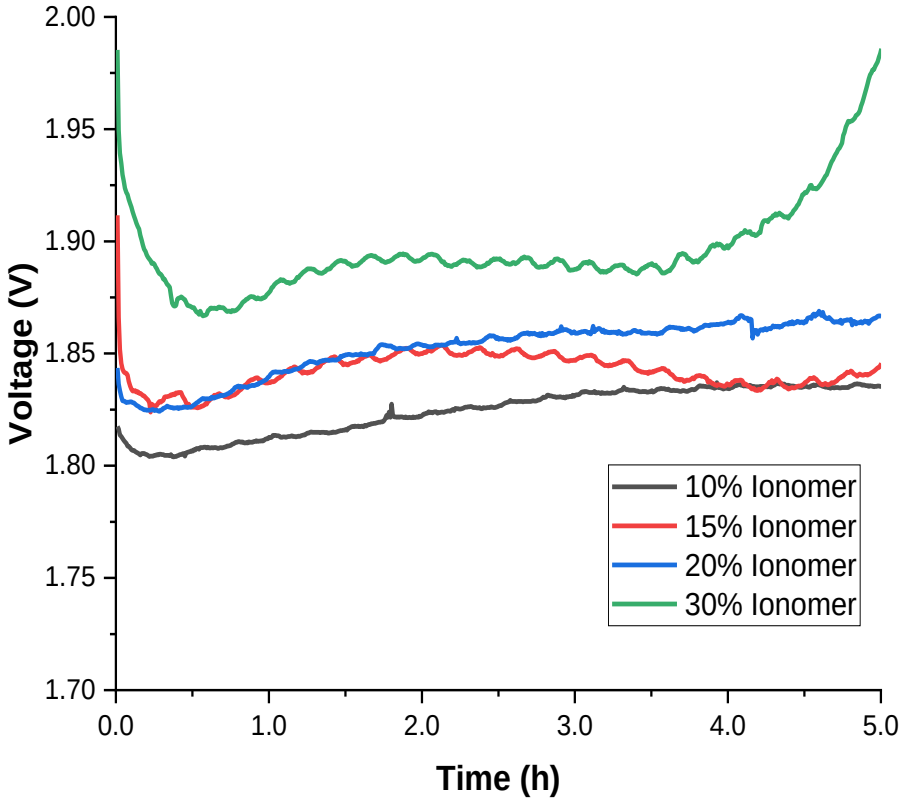


**Figure 7.2 – Cell voltage vs. time for MEAs with various HER ionomer content at 1 A/cm$^2$. The AEM was GT69 with a PTFE reinforcement (40 µm thick, 15 mol% cross-linking). The anode ionomer was GT25 (25 wt%) and catalyst was $PbRuO_x$. The cathode ionomer was GT74 and catalyst was PtNi.**

### *7.2.2 Effect of HER ionomer ion exchange capacity*

Next, the effect of HER ionomer IEC was investigated at a constant ionomer loading of 20 wt%. Figure 7.3 shows polarization curves from 0 to 500 mA/cm$^2$ for AEMELs with cathode ionomers from Table 3.1 with relative low IEC (GT32) and high IEC (GT74). From the polarization curve, both MEAs performed similarly at low current density (100 mA/cm$^2$). At 100 mA/cm$^2$, where the reaction kinetics dominate, the two MEAs had very similar cell voltage, 1.68 V and 1.67 V for cathodes containing GT32 and GT74, respectively. However, at a higher current density of 500 mA/cm$^2$, the cell voltage of the MEA with GT74 in the cathode was 100 mV lower than the MEA with GT32 in the

cathode (2.11 V vs. 2.21 V). Figure 7.4 shows the cell voltage vs. time for these two MEAs at 500 mA/cm$^2$ constant-current operation. The electrode with GT74 trended toward lower cell voltage with time, down to 2.05 V while GT32 trended up to 2.26 V. The upward trend of GT32 with time may be indicative of electrode dry out as the electrode consumes water. These trends indicate that water balance in the HER electrode is a critical factor with dry-out possible with GT32 (i.e., rising voltage with time) and GT74 showing adequate water retention to support 500 mA/cm$^2$.

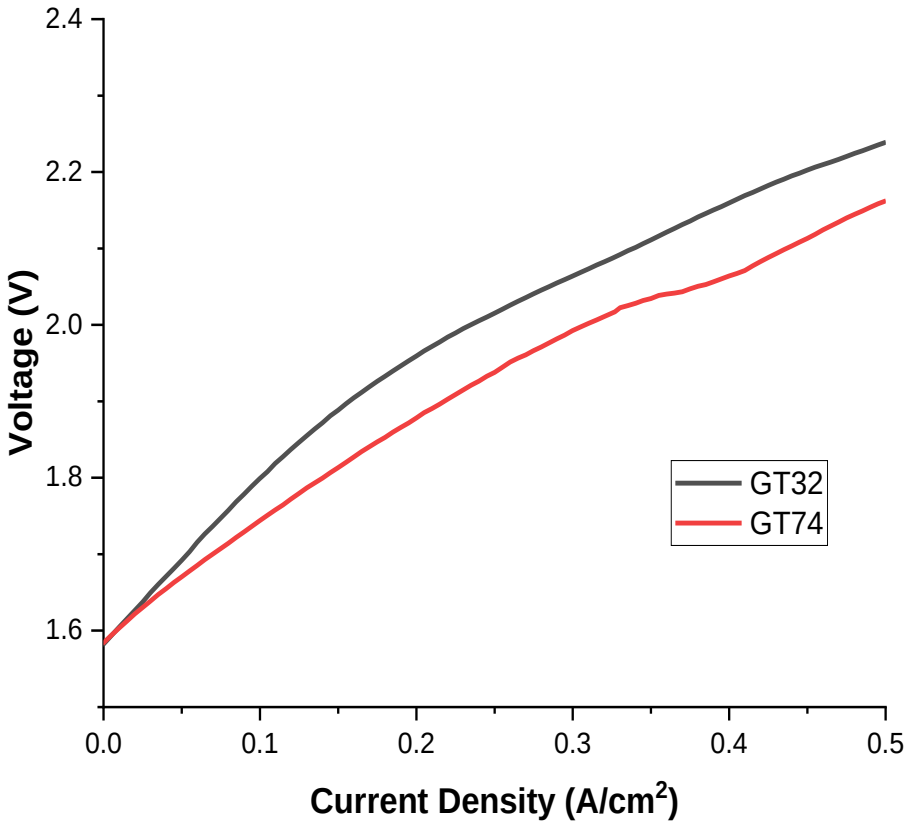


**Figure 7.3 – Comparison of polarization curves of MEAs with HER ionomers of high and low ion exchange capacities. The AEM was unreinforced GT74 (54 µm thick, 5 mol% cross-linking). The cathode catalyst was Pt/C. The anode ionomer was GT38 (25 wt%) and the catalyst was IrO2.**

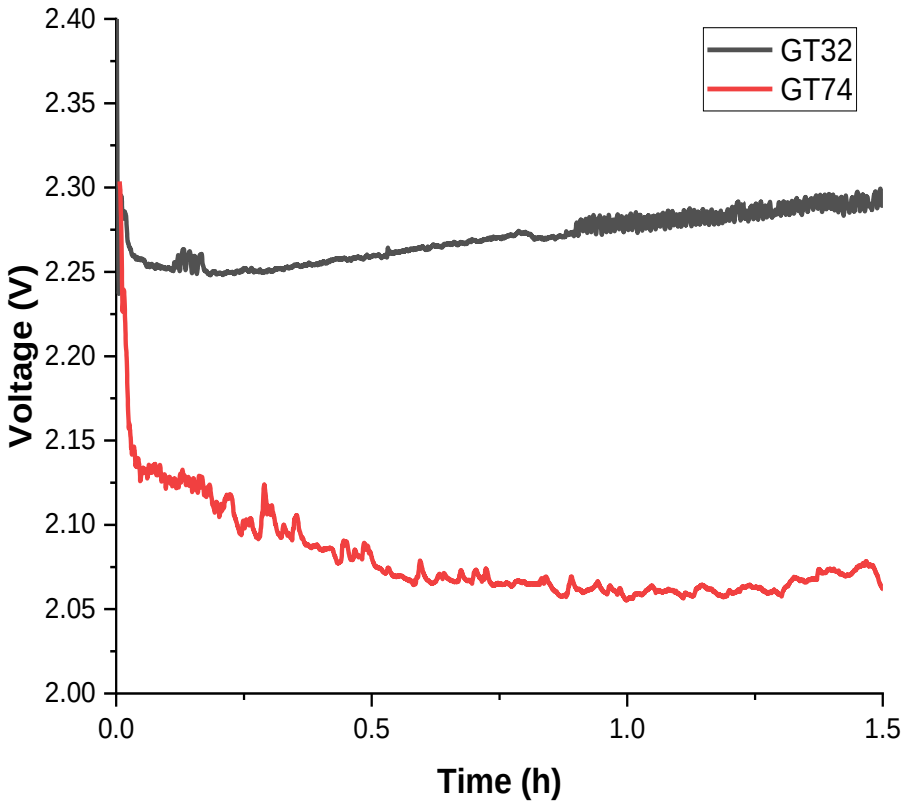


**Figure 7.4 – Cell voltage vs. time for MEAs with high and low IEC HER ionomers at 500 mA/cm$^2$. The AEM was unreinforced GT74 (54 µm thick, 5 mol% cross-linking). The cathode catalyst was Pt/C. The anode ionomer was GT38 (25 wt%) and the catalyst was $IrO_2$.**

### *7.2.3 Effect of HER ionomer water uptake*

The effect of ionomer WU in the HER electrode was investigated by controlling the swelling in the ACI polymer through polymer cross-linking. Cross-linked, high IEC ionomers were used because they have high ionic conductivity and high WU which is the established HER preference (above). A high IEC tetrablock copolymer, GT72 (Table 3.1), was selected as the baseline polymer for the cross-linked HER ACI experiments. Four levels of cross-linking (1 mol%, 3 mol%, 5 mol% and 10 mol%) were used. The physical and electrochemical properties of the cross-linked ionomers were measured and are listed

in Table 3.2. The hydroxide conductivity of GT72, GT72-1 and GT72-3 could not be measured because there was insufficient cross-linker to form a mechanically stable, free-standing film for measurement, although the polymers could be used as ionomer. GT72 had a high degree of swelling without any cross-linking and the estimated WU was greater than 1000%. The WU decreased significantly with increasing cross-linker content. The WU of GT72-1 was less than half that of the uncross-linked version (502%). Further increases in the cross-linker content lowered the WU to 198% (GT72-3), 96% (GT72-5) and 78% (GT72-10). The IEC of the cross-linked samples not significantly affected by cross-linker content, ranging from 3.47 (GT72-10) to 3.54 meq/g (GT72). The conductivity of the cross-linked ionomers remained high (>150 mS/cm) but decreased slightly with cross-linker content.

Figure 7.5 shows the polarization curves for AEMELs deploying the cross-linked ionomers from 0 to 500 mA/cm$^2$. At low current density (100 mA/cm$^2$), the performance of all of the MEAs was nearly identical. The difference in performance was more distinguishable at high current density (500 mA/cm$^2$). The trend observed at 1 A/cm$^2$, Figure 7.6, matched the trend in the polarization curves. The MEA with 10 mol% cross-linker had the highest steady-state cell voltage among all samples tested (1.89 V). The MEA with 5 mol%, and 1 mol% cross-linker had cell voltages of 1.84 V and 1.80 V, respectively. The MEA with no cross-linker had a cell voltage of 1.83 V. The MEA with 3 mol% cross-linker had the best constant-current cell voltage among all samples tested, 1.77 V, which was an improvement of 120 mV over the MEA with 10 mol% crosslinker. The constant-current cell voltage (at 1 A/cm$^2$) and water uptake as a function of the amount of

cross-linker are plotted in Figure 7.7. A minimum in-cell voltage at 3 mol% cross-linker was observed with a corresponding water uptake of 198%.

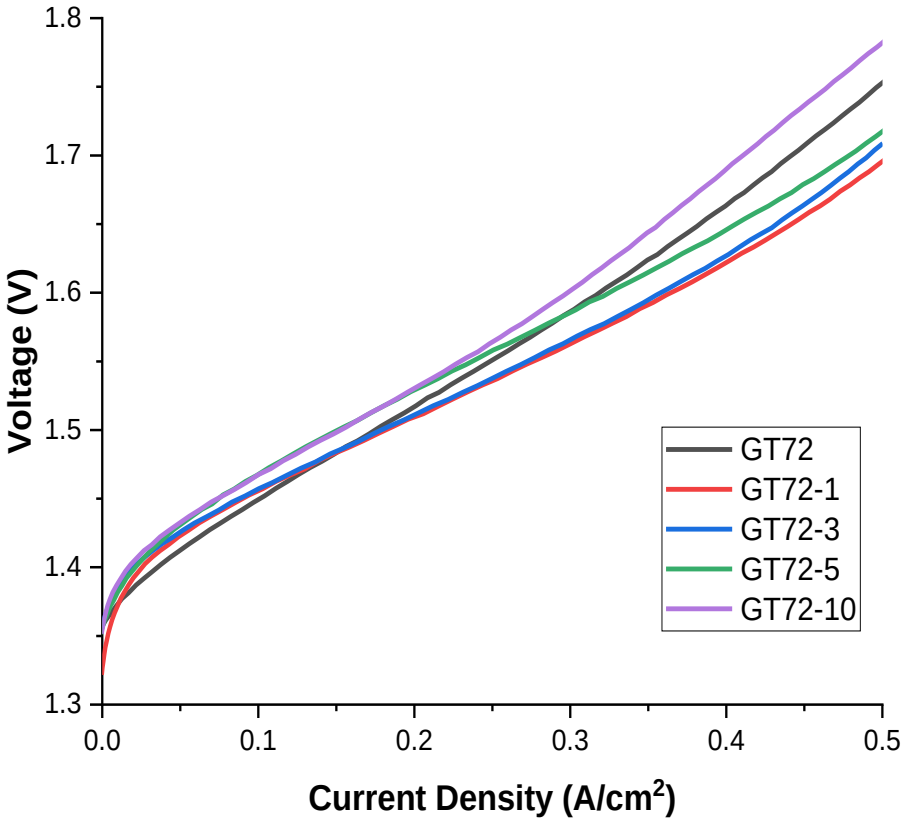


**Figure 7.5 – Comparison of polarization curves of MEAs with cross-linked HER ionomers. The AEM was GT72 with PTFE reinforcement (30 µm thick, 10 mol% cross-linking). The anode ionomer was GT72-10 (25 wt%) and catalyst was $PbRuO_x$. The cathode catalyst was PtNi.**

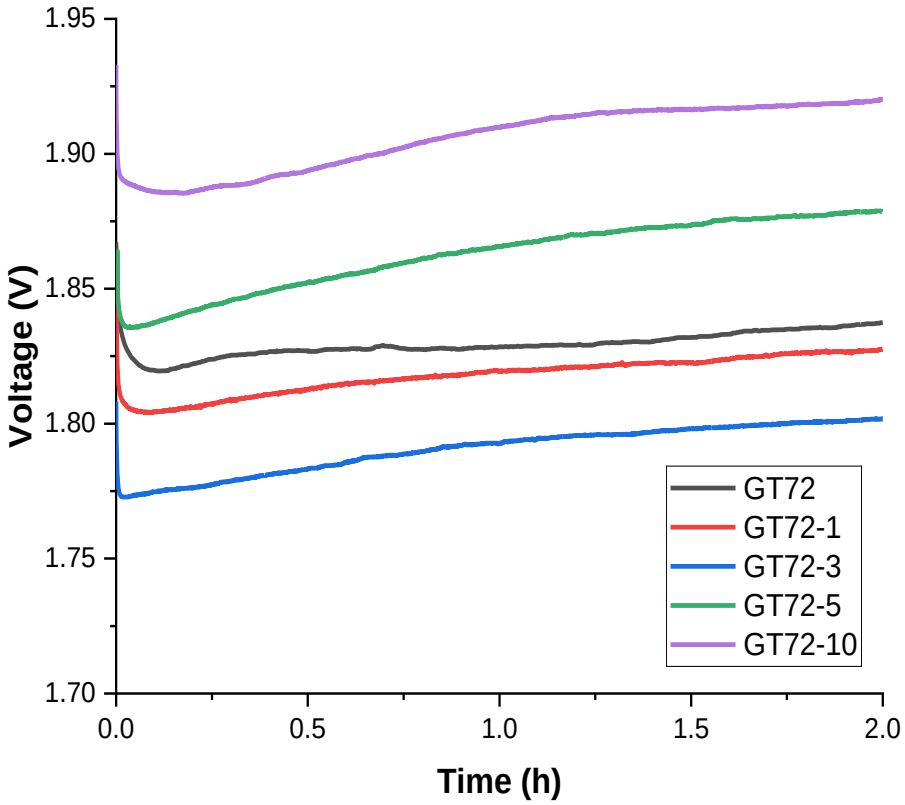


**Figure 7.6 – Cell voltage vs. time for MEAs with cross-linked, high IEC HER ionomers at 1 A/cm$^2$. The AEM was GT72 with PTFE reinforcement (30 µm thick, 10 mol% cross-linking). The anode ionomer was GT72-10 (25 wt%) and catalyst was $PbRuO_x$. The cathode catalyst was PtNi.**

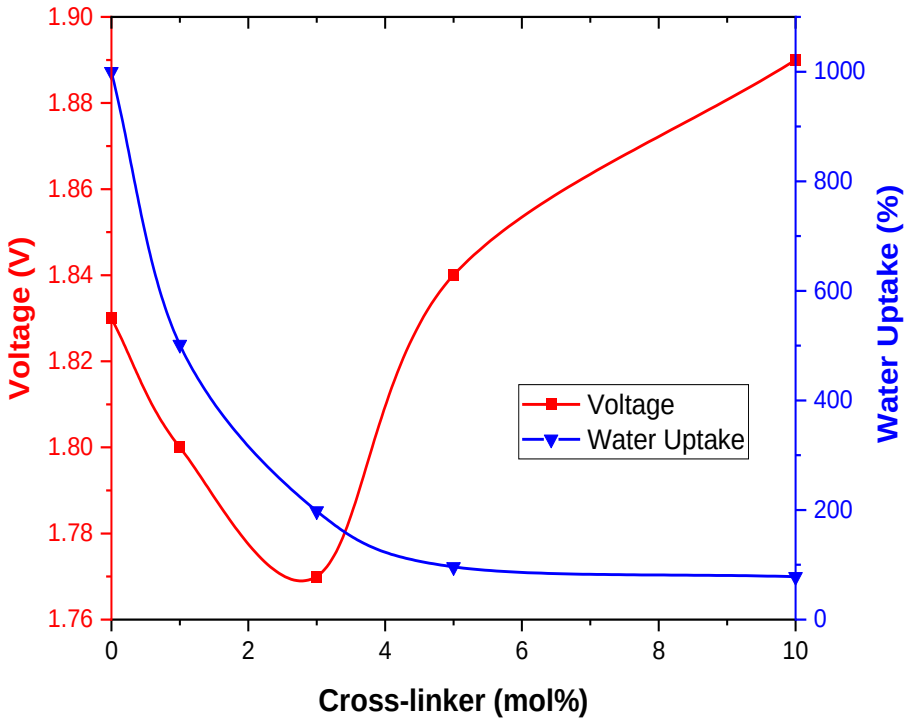


**Figure 7.7 – Cell voltage at 1 A/cm$^2$ (red) and water uptake (blue) vs. cross-linker concentration. The AEM was GT72 with PTFE reinforcement (30 µm thick, 10 mol% cross-linking). The anode ionomer was GT72-10 (25 wt%) and catalyst was PbRuO$_x$. The cathode catalyst was PtNi.**

The effect of ACI molecular weight was tested by comparing the performance of the GT72 ionomers with GT74 (Table 3.1), a low molecular weight ionomer with similar IEC. GT74 had a number average molecular weight of 40.4 kDa, IEC of 3.60 meq/g and WU of >1000%. In comparison, GT72 had a number average molecular weight of 68.2 kDa, IEC of 3.54 meq/g and WU of >1000%. The performance of a cross-linked version of the lower molecular weight ionomer, GT74-3, with 3% TMHDA was also compared with GT72-3. GT74-3 and GT72-3 (Table 3.2) had similar IEC (3.58 vs. 3.52 meq/g) and WU (219% vs. 198%). Figure 7.8 shows the cell voltage vs. time at 1 A/cm$^2$ for the MEAs fabricated with high and low molecular weight ACI at the same cross-link density. The cell voltage of the MEA with GT74 was 1.82 V, which was similar in performance to the MEA

with GT72 (1.83 V). The addition of cross-linker to GT74 showed an 18 mV increase in cell voltage compared to its non-cross-linked form.

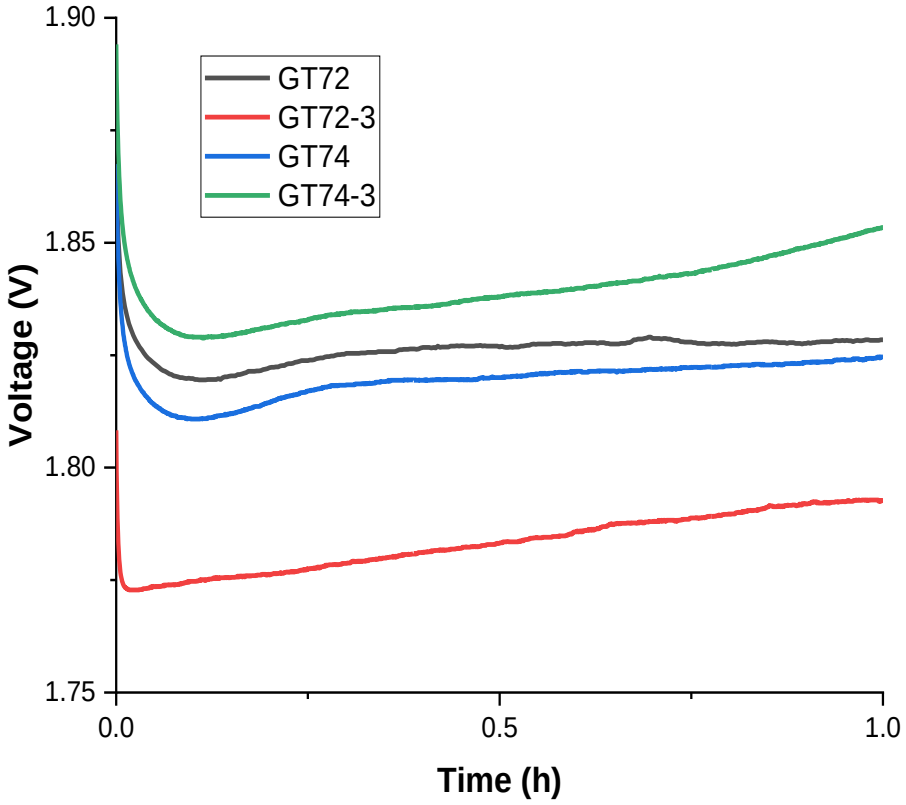


**Figure 7.8 – Cell voltage vs. time for MEAs with HER ionomers at 1 A/cm$^2$. The AEM was GT72 with PTFE reinforcement (30 µm thick, 10 mol% cross-linking). The anode ionomer was GT72-10 (25 wt%) and catalyst was $PbRuO_x$. The cathode catalyst was PtNi.**

## 7.3 Discussion

The comparison between HER ionomers with high and low IEC, and the amount of cross-linking shows that performance is improved with ionic conductivity if excessive WU is avoided. There was a dramatic improvement in cell voltage (approximately 200 mV at 500 mA/cm$^2$ constant-current operation) when using high IEC ionomer compared to low IEC ionomer in the HER electrode. This result is contrary to previous observations for the

OER ionomer where low IEC ionomers (with low conductivity and WU) outperformed high IEC ionomers in the absence of polymer cross-linking.[128] In the case of the OER electrode, WU was the critical factor in performance because excess swelling in the water-fed electrode negated the benefits of high ionic conductivity. Conductivity still played a role in cell performance, but it was a weak factor when there was high WU, especially in the flooded anode. The HER electrode, on the other hand, requires a higher local water activity because water is consumed at the HER electrode to form hydrogen and hydroxide ions, and is supplied only by diffusion from the water reservoir at the anode. The HER electrode is also a drier environment than the anode because it is not being supplied externally with liquid water. These results show that a more hydrophilic environment is needed at the HER electrode than at the OER electrode for optimal cell performance.

Figure 7.2 shows that cell performance was improved when the water content was changed by lowering the amount of high-IEC ionomer in the HER electrode. The volume fraction of water in the electrode (in the form of hydrated ionomer) decreases when the ionomer-to-catalyst ratio is decreased. The MEA with the lowest amount of ionomer (10%) showed the best performance among the four cells tested. Electrodes with <10% ionomer were not usable because of issues with catalyst detachment due to insufficient binder content. The MEA with the highest ionomer content (30%) showed the highest cell voltage and displayed performance stability issues after four hours of constant current operation. These results show that although a higher water content is preferred at the HER, excess swelling in the HER electrode can be detrimental to both performance and stability.

The addition of a cross-linker to the ACI significantly lowered WU by limiting the swelling of the ionomer yet minimally affected the IEC and ionic conductivity. Restricting

the swelling in the hydrated ionomer increased the density of quaternary ammonium head groups and facilitated more efficient ion conduction, compared to ionomers with a high degree of swelling. Figure 7.7 shows that the HER electrode was sensitive to the amount of cross-linker in the ionomer. This degree of sensitivity was not observed previously in an OER electrode.[128] This is most likely due the different operating environment where the anode is fully flooded and the cathode is much drier. The optimal amount of cross-linker was found to be 3 mol% TMHDA, which corresponds to a water uptake of 198%. A favorable cell performance of 1.77 V at 1 A/cm$^2$ was achieved using optimized HER and OER electrodes with a less conductive electrolyte (1 wt% vs. 3 wt% $Na_2CO_3$ in water), compared to the previous study.[128] This cell configuration is competitive with Nafion-based PEMELs and outperforms AEMELs built with other commercially available AEMs at higher operating temperature and NaOH electrolytes.[127, 130] Increasing or decreasing the amount of cross-linker in the HER ACI adversely affected the performance of the cell. The cell voltage rose by 30 to 60 mV when the HER ionomer cross-linker content was less than 3 mol% and WU was >500%. This behavior is similar to the flooded cathode behavior observed previously when the ionomer content in the HER was increased. On the other hand, when the WU was decreased to <100% using a higher level of polymer cross-linker, the cell voltage rose by 70 to 120 mV. In this case, performance suffered more severely when there was a lower water content in the hydrogen evolving cathode due to low local water activity. It should also be noted that GT72-10, which was previously found to be the best performing ionomer for the OER electrode, was the worst performing cross-linked ionomer for the HER electrode, among those compared.

Finally, the molecular weight of the ACI also had an impact on the effectiveness of the cross-linker. Non-cross-linked HER ionomers with comparable IEC performed similarly despite their differences in molecular weight. This observation was consistent with the previous report regarding non-cross-linked OER ionomers.[128] However, the shorter chain ionomer (GT74-3) did not show the same jump in performance as the longer chain ionomer (GT72-3) when the same amount of cross-linker was added. The performance of the MEA with GT74-3 was more similar to that of the non-cross-linked, higher molecular weight ionomer (GT72). This suggests that the molecular structure of cross-linked, higher molecular weight ionomers is more favorable for ion conduction. Chain entanglement within high molecular weight polymers may be responsible for the improved ion conduction.

The results from this study show that water management is needed in the HER electrode to a greater extent than in the OER electrode. These results also highlight the importance of using asymmetric ionomers that optimize the water content for the reactions at each electrolyzer electrode to achieve maximum cell performance.

## 7.4 Conclusion

Poly(norbornene) tetrablock copolymers with different ion exchange capacity were synthesized and used in the fabrication of hydrogen evolving electrodes in low-temperature AEM electrolyzers. It was found that ionomers with high IEC had better performance than ionomers with low IEC due to their higher ionic conductivity. The results also show that the HER electrode requires an ionomer that maintains high water activity. Optimization of the ionomer-to-catalyst ratio in the cathode electrode showed that better performance and

durability could be achieved by limiting the water content in cathode and by lowering the amount of ionomer present. Light cross-linking of the ionomer was used to manage the swelling of the ACI while maintaining high IEC and ionic conductivity. It was found that lowering the water uptake through cross-linking improved performance of the electrolyzer. Further reduction of the HER ionomer WU to below 200% had detrimental effects on cell performance. The highest achievable performance was 1.77 V at 1 A/cm$^2$ at 50 °C. The results of this study, as well as the results of the companion study on the OER ionomer, demonstrate the importance of managing water content in both AEM electrolyzer electrodes. These two studies also suggest the use of asymmetric ionomers to optimize the water content for the reactions at each electrode to achieve optimal cell performance.

# APPENDIX A. METHODS OF SYNTHESIS AND CROSS-LINKING OF VINYL ADDITION POLY(NORBORNENE) ANION CONDUCTING POLYMERS

The purpose of this appendix is to provide the reader with a background on the common synthesis and cross-linking methods of the poly(norbornene) anion conductive polymers characterized in Chapter 3. The synthesis and processing of these materials was performed entirely by Dr. Mrinmay Mandal (Georgia Tech) for the purposes of this work.

## A.1 Materials

1-hexene, 5-bromo-1-pentene and dicyclopentadiene were purchased from Alfa Aesar and used as-received. The monomers, butyl norbornene (BuNB) and bromopropyl norbornene (BPNB), were synthesized via a Diels-Alder reaction at high-temperature according to a published procedure.[107] In later work, the monomers butyl norbornene (BuNB), bromobutyl norbornene (BBNB) and bromopropyl norbornene, were supplied by Promerus, LLC (Brecksville, OH). Prior to polymerization, the monomers were purified by distillation over sodium and degassed by three freeze-pump-thaw cycles. All polymerization reactions were performed under a dry argon atmosphere in a glove box with rigorous care to avoid moisture and air. Toluene was dried by heating under reflux for 6 h over sodium and benzophenone. Toluene was freshly distilled prior to use. Triisopropylphosphine and $[(\eta^3\text{-allyl})\text{Pd(Cl)}]_2$ were purchased from Sigma-Aldrich and used as-received. The catalyst, (allyl)palladium(triisopropylphosphine)chloride ($(\eta^3\text{-allyl})\text{Pd}(^i\text{Pr}_3\text{P})\text{Cl}$), was prepared according to a previously published report.[131] Lithium

tetrakis(pentafluorophenyl)-borate·(2.5$Et_2O$) (Li[FABA]) was purchased from Boulder Scientific Co. and used as-received. N,N,N′,N′-Tetramethyl-1,6-hexanediamine (TMHDA), anhydrous toluene (99.9 %), anhydrous α,α,α-trifluorotoluene (TFT, ≥ 99 %) and tetrahydrofuran (THF) were purchased from Sigma-Aldrich and used as-received.

## A.2 Synthesis

### *A.2.1 Synthesis of poly(norbornene) tetrablock copolymer*

The tetrablock copolymer, [Poly(BuNB-b-BPNB-b-BuNB-b-BPNB)], consisting of alternating butyl norbornene (BuNB) and bromopropyl norbornene (BPNB) blocks (two blocks each) is described in Scheme A.1. The polymer was synthesized by the sequential addition of the monomers (one after the other) at room temperature in an inert atmosphere glove box. The monomers were divided into four round-bottomed flask (two for each monomer) and toluene was added to make a 5 wt% solution in each flask. The catalyst solution was prepared separately in a vial by dissolving ($\eta^3$-allyl)Pd($^i$Pr$_3$P)Cl (12 mg, 0.03 mmol) and Li[FABA] (28 mg, 0.03 mmol) in a solution composed of 0.5 g toluene and 0.5 g TFT. The catalyst solution was stirred for 20 min. BuNB (0.45 g, 3.00 mmol) and toluene (10 mL) were added to a 100 mL round-bottomed flask fitted with a magnetic stir bar. The catalyst solution was injected into the flask under vigorous stirring. After 20 min the BuNB polymerization was complete. A small aliquot was removed and quenched with $CH_3CN$ for gel permeation chromatography (GPC) analysis. Then, a mixture of BPNB (0.64 g, 3.00 mmol) and toluene (12 mL) was added to the reaction flask, still containing the catalyst, and stirred for 3 h to incorporate the BPNB block onto the BuNB polymer. After the 3 h reaction time (complete consumption of BPNB), a small aliquot was taken out and

quenched with $CH_3CN$ for GPC analysis. Next, BuNB (0.45 g, 3.00 mmol) and toluene (10 mL) were added to the reaction flask and allowed to react for 20 min for incorporation of the third block. A small aliquot was again taken out and quenched with $CH_3CN$ for GPC analysis. Finally, a mixture of BPNB (0.64 g, 3.00 mmol) and toluene (12 mL) was added to the flask and stirred for 3 h to incorporate the fourth block onto the polymer. After completion, the reaction mixture was quenched and the polymer precipitated by addition of methanol. The resulting polymer was dissolved in THF and stirred over activated charcoal. The solution was passed through an alumina filter to remove any palladium residue. The resulting product was precipitated from THF by addition of methanol. The polymer product was dried under vacuum at 60 °C. Tetrablock copolymers with different hydrophobic and hydrophilic chain lengths were synthesized by changing the monomer to catalyst feed ratio depending on the target ion exchange capacity (IEC). A tetrablock copolymer labeled as GT66 contains 34 mol% of hydrophobic blocks and 66 mol% halogenated blocks (GT = Georgia Tech, XX = mole percent of combined halogenated blocks). Similarly, a tetrablock copolymer labeled as GT64 (GT = Georgia Tech, XX = mole percent of combined halogenated blocks) is made with 64 mol% halogenated monomer.

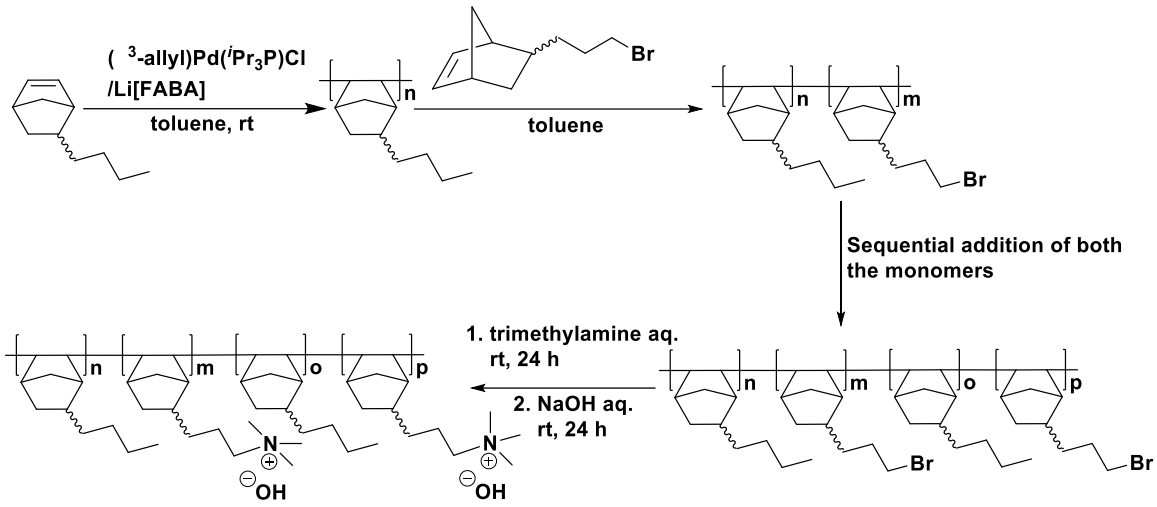


**Scheme A.1 – Synthesis of poly(norbornene) tetrablock copolymer.**

### *A.2.2 Cross-linking of poly(norbornene) tetrablock copolymer*

Light cross-linking was carried out by adding a cross-linking agent, *N,N,N',N'*-Tetramethyl-1,6-hexanediamine (TMHDA), to the polymer/solvent solution as depicted in Scheme A.2. The mole percent of TMHDA relative to the number of head-groups such as 1 mol%, 2.5 mol%, 3 mol%, 5 mol%, 10 mol%, 15 mol%, 20 mol% and 25 mol%. For example, a tetrablock copolymer labeled as GT64-5 (GT = Georgia Tech, XX = mole percent of combined halogenated blocks, Y = mole percent of cross-linker) has 5 mol% TMHDA with respect to the moles of brominated head-groups within the BCP.

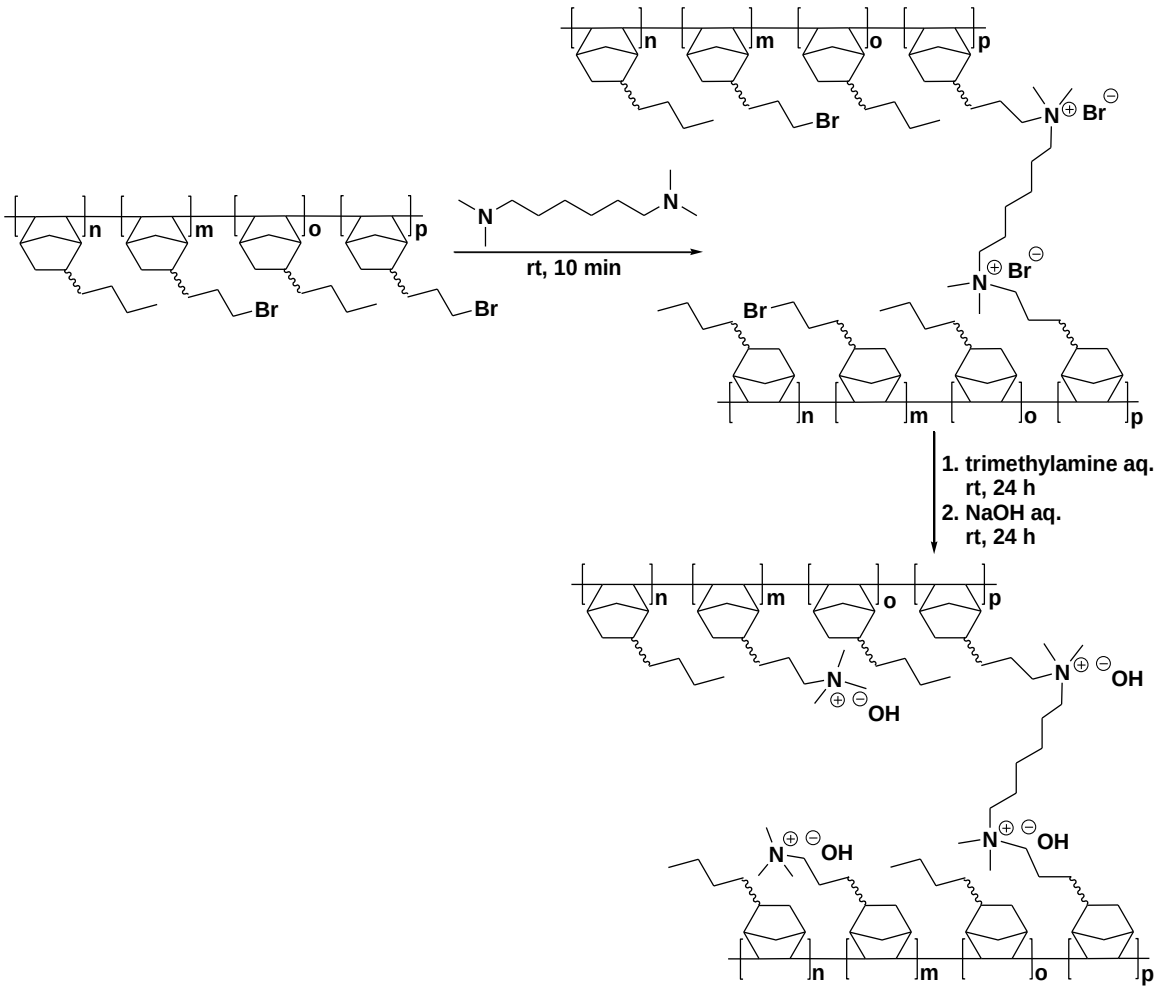


**Scheme A.2 – Cross-linking of poly(norbornene) tetrablock copolymer.**

## A.3 Membranes

### *A.3.1 Membrane casting and ion-exchange*

The tetrablock copolymer (0.20 g) was dissolved in 5 mL chloroform and the resulting solution was filtered through a 0.2 µm poly(tetrafluoroethylene) (PTFE) membrane syringe filter into a 4 cm diameter aluminum dish. The solvent was evaporated at room temperature in a nitrogen gas stream. The membrane was dried overnight under vacuum. The membranes were colorless, flexible and free-standing with a thickness of ca.

50 µm. Next, the bromobutyl headgroup was quaternized by immersion of the membrane in 45 wt% aqueous trimethylamine solution for 48 h at room temperature. The quaternized membrane with bromide counter-ion was removed from solution and washed thoroughly with DI water. The membranes were then soaked in 1 M NaOH solution under nitrogen for 24 h to exchange the bromide ions for hydroxide ions. The membranes were stored in DI water after being washed with DI water three times.

### *A.3.2 Cross-linked membrane casting*

The tetrablock copolymer (0.1 g) was taken up in 5 mL of chloroform. In-situ cross-linking was performed by adding a crosslinking agent to the polymer/solvent mixture when the membrane was cast, followed by reaction after casting. The cross-linking agent, TMHDA, was added to the solution at different mole ratios (e.g., 1 mol%, 3mol%, 4 mol%, 5 mol%, 7 mol%, 10 mol%, 20 mol% and 50 mol%) with respect to the moles of brominated monomer in the polymer (i.e., those monomers which were capable of forming a quaternary ammonium head-group). The cross-linker concentration in this thesis is given in terms of mol% TMHDA crosslinker added to the polymer. For example, 5 mol% TMHDA means that the up to 10% of the available head-groups are consumed by TMHDA cross-linker. It is noted that even if all the cross-linker were to react, the fraction of intramolecular cross-linking vs. intermolecular cross-linking would be difficult to evaluate. The solution was filtered through a 0.45 µm poly(tetrafluoroethylene) (PTFE) membrane syringe filter and a film was cast and dried at 60 °C for 24 h. The film was colorless, transparent, and flexible. The membranes were aminated by immersed in 50 wt% aqueous trimethylamine solution (48 h at room temperature). The quaternized membranes were

washed with DI water. The bromide ions were converted to hydroxide ions by soaking the membranes in 1 M NaOH solution under nitrogen for 24 h.

### *A.3.3 Composite cross-linked membrane casting*

Reinforced membranes were formed by dissolving the synthesized precursor polymer in toluene, forming a 10 wt% solution. Toluene was used rather than chloroform to better control the evaporation rate of the composite membranes, however the casting solvent did not affect the quality of the film or membrane. The cross-linking agent, TMHDA, was added to the solution in different molar ratios (e.g., 5 to 20 mol%) with respect to the moles of halogenated monomer in the polymer (determined by $^{1}$H NMR). After stirring for 30 min at room temperature until homogenous and translucent, the solution was filtered through a 0.45 μm PTFE membrane syringe filter. The precursor polymer solution was applied to a proprietary thin, microporous PTFE support material for reinforcement by Xergy, Inc. (Harrington, DE, United States) to form a composite film. The membranes, nominally 10 μm thick, were formed by drying at room temperature. The membranes were quaternized with 50 wt% aqueous trimethylamine solution for 48 h at room temperature to convert the bromobutyl/bromopropyl moieties to quaternary ammonium head-groups. The quaternized membranes were ion-exchanged from bromide ions to hydroxide ions by immersion in 1 M NaOH solution under nitrogen for 24 h. The quaternized membranes were washed thoroughly with DI water and stored in DI water until they were ready to be used.

## A.4 Ionomers

### *A.4.1 Ionomer fabrication and processing*

Poly(norbornene) anion conductive ionomers (ACI) without cross-linking were made by soaking the dried polymer powder in 50 wt% aqueous TMA solution at room temperature for 48 h to convert the bromoalkyl sites to quaternary ammonium head-groups. The majority of solvent was allowed to evaporate off in a fume hood over a hot plate (60 °C) over several days. The remaining solvent was evaporated in a vacuum oven (0.5 atm) at 60 °C.

### *A.4.2 Cross-linked ionomer fabrication and processing*

Ionomers with light cross-linking were made by adding 1, 3, 5 or 10 mol% of a cross-linking agent, N,N,N',N'-tetramethyl-1,6-hexanediamine (TMHDA), with respect to the number of available bromoalkyl sites in the polymer. The polymer and cross-linker solution were cast into a shallow aluminium dish and allowed to dry overnight in a tube furnace. The polymer was then soaked in 50 wt% aqueous TMA solution at room temperature for 48 h to convert the remaining uncross-linked bromoalkyl sites to quaternary ammonium head-groups. The remaining solvent was evaporated in a vacuum oven (0.5 atm) at 60 °C. The dried, quaternized ACI was milled into fine powder using a high-speed grinder with dry ice.

# REFERENCES


1. Steele, B. C. H.; Heinzel, A., Materials for fuel-cell technologies. *Nature* **2001,** *414*, 345.

2. Varcoe, J. R.; Atanassov, P.; Dekel, D. R.; Herring, A. M.; Hickner, M. A.; Kohl, P. A.; Kucernak, A. R.; Mustain, W. E.; Nijmeijer, K.; Scott, K.; Xu, T.; Zhuang, L., Anion-exchange membranes in electrochemical energy systems. *Energy & Environmental Science* **2014,** *7* (10), 3135-3191.

3. Li, N.; Guiver, M. D., Ion Transport by Nanochannels in Ion-Containing Aromatic Copolymers. *Macromolecules* **2014,** *47* (7), 2175-2198.

4. Mekhilef, S.; Saidur, R.; Safari, A., Comparative study of different fuel cell technologies. *Renewable and Sustainable Energy Reviews* **2012,** *16* (1), 981-989.

5. L, C.; K, A. F.; U, S., Fuel Cells – Fundamentals and Applications. *Fuel Cells* **2001,** *1* (1), 5-39.

6. Winter, M.; Brodd, R. J., What Are Batteries, Fuel Cells, and Supercapacitors? *Chemical Reviews* **2004,** *104* (10), 4245-4270.

7. Hickner, M. A.; Herring, A. M.; Coughlin, E. B., Anion exchange membranes: Current status and moving forward. *Journal of Polymer Science Part B: Polymer Physics* **2013,** *51* (24), 1727-1735.

8. Li, D.; Park, E. J.; Zhu, W.; Shi, Q.; Zhou, Y.; Tian, H.; Lin, Y.; Serov, A.; Zulevi, B.; Baca, E. D.; Fujimoto, C.; Chung, H. T.; Kim, Y. S., Highly quaternized polystyrene ionomers for high performance anion exchange membrane water electrolysers. *Nature Energy* **2020**.

9. Ren, X.; Price, S. C.; Jackson, A. C.; Pomerantz, N.; Beyer, F. L., Highly Conductive Anion Exchange Membrane for High Power Density Fuel-Cell Performance. *ACS Applied Materials & Interfaces* **2014,** *6* (16), 13330-13333.

10. Debe, M. K., Electrocatalyst approaches and challenges for automotive fuel cells. *Nature* **2012,** *486* (7401), 43-51.

11. Hickner, M. A.; Ghassemi, H.; Kim, Y. S.; Einsla, B. R.; McGrath, J. E., Alternative Polymer Systems for Proton Exchange Membranes (PEMs). *Chemical Reviews* **2004,** *104* (10), 4587-4612.

12. Lu, S.; Pan, J.; Huang, A.; Zhuang, L.; Lu, J., Alkaline polymer electrolyte fuel cells completely free from noble metal catalysts. *Proceedings of the National Academy of Sciences* **2008,** *105* (52), 20611-20614.

13. Yu, E. H.; Wang, X.; Krewer, U.; Li, L.; Scott, K., Direct oxidation alkaline fuel cells: from materials to systems. *Energy & Environmental Science* **2012,** *5* (2), 5668-5680.

14. Varcoe, J. R.; Slade, R. C. T., Prospects for Alkaline Anion-Exchange Membranes in Low Temperature Fuel Cells. *Fuel Cells* **2005,** *5* (2), 187-200.

15. Zhou, J. F.; Joseph, K.; Ahlfield, J. M.; Park, D. Y.; Kohl, P. A., Poly(arylene ether) Ionomers with Pendant Quinuclidium Groups and Varying Molecular Weight for Alkaline Electrodes. *Journal of the Electrochemical Society* **2013,** *160* (6), F573-F578.

16. McLean, G. F.; Niet, T.; Prince-Richard, S.; Djilali, N., An assessment of alkaline fuel cell technology. *International Journal of Hydrogen Energy* **2002,** *27* (5), 507-526.

17. Dekel, D. R., Review of cell performance in anion exchange membrane fuel cells. *Journal of Power Sources* **2018,** *375*, 158-169.

18. Park, D.-Y.; Kohl, P. A.; Beckham, H. W., Anion-Conductive Multiblock Aromatic Copolymer Membranes: Structure–Property Relationships. *The Journal of Physical Chemistry C* **2013,** *117* (30), 15468-15477.

19. Carrette, L.; Friedrich, K. A.; Stimming, U., Fuel Cells - Fundamentals and Applications. *Fuel Cells* **2001,** *1* (1), 5-39.

20. Li, N.; Yan, T.; Li, Z.; Thurn-Albrecht, T.; Binder, W. H., Comb-shaped polymers to enhance hydroxide transport in anion exchange membranes. *Energy & Environmental Science* **2012,** *5* (7), 7888-7892.

21. Varcoe, J. R.; Slade, R. C. T.; Wright, G. L.; Chen, Y., Steady-State dc and Impedance Investigations of H2/O2 Alkaline Membrane Fuel Cells with Commercial Pt/C, Ag/C, and Au/C Cathodes. *The Journal of Physical Chemistry B* **2006,** *110* (42), 21041-21049.

22. Mohanty, A. D.; Bae, C., Mechanistic analysis of ammonium cation stability for alkaline exchange membrane fuel cells. *Journal of Materials Chemistry A* **2014,** *2* (41), 17314-17320.

23. Liu, L.; Ahlfield, J.; Tricker, A.; Chu, D.; Kohl, P. A., Anion conducting multiblock copolymer membranes with partial fluorination and long head-group tethers. *Journal of Materials Chemistry A* **2016,** *4* (41), 16233-16244.

24. Mohanty, A. D.; Tignor, S. E.; Sturgeon, M. R.; Long, H.; Pivovar, B. S.; Bae, C., Thermochemical Stability Study of Alkyl-Tethered Quaternary Ammonium Cations for Anion Exchange Membrane Fuel Cells. *J Electrochem Soc* **2017,** *164* (13), F1279-F1285.

25. Merle, G.; Wessling, M.; Nijmeijer, K., Anion exchange membranes for alkaline fuel cells: A review. *Journal of Membrane Science* **2011,** *377* (1), 1-35.

26. Couture, G.; Alaaeddine, A.; Boschet, F.; Ameduri, B., Polymeric materials as anion-exchange membranes for alkaline fuel cells. *Progress in Polymer Science* **2011,** *36* (11), 1521-1557.

27. Wang, Y.-J.; Qiao, J.; Baker, R.; Zhang, J., Alkaline polymer electrolyte membranes for fuel cell applications. *Chemical Society Reviews* **2013,** *42* (13), 5768-5787.

28. Leng, Y.; Chen, G.; Mendoza, A. J.; Tighe, T. B.; Hickner, M. A.; Wang, C.-Y., Solid-State Water Electrolysis with an Alkaline Membrane. *Journal of the American Chemical Society* **2012,** *134* (22), 9054-9057.

29. Zeng, K.; Zhang, D., Recent progress in alkaline water electrolysis for hydrogen production and applications. *Progress in Energy and Combustion Science* **2010,** *36* (3), 307-326.

30. Alotto, P.; Guarnieri, M.; Moro, F., Redox flow batteries for the storage of renewable energy: A review. *Renewable and Sustainable Energy Reviews* **2014,** *29*, 325-335.

31. Liu, L.; Kohl, P. A., Anion conducting multiblock copolymers with different tethered cations. *Journal of Polymer Science Part A: Polymer Chemistry* **2018,** *56* (13), 1395-1403.

32. Mandal, M.; Huang, G.; Kohl, P. A., Anionic multiblock copolymer membrane based on vinyl addition polymerization of norbornenes: Applications in anion-exchange membrane fuel cells. *Journal of Membrane Science* **2019,** *570-571*, 394-402.

33. Gottesfeld, S.; Dekel, D. R.; Page, M.; Bae, C.; Yan, Y.; Zelenay, P.; Kim, Y. S., Anion exchange membrane fuel cells: Current status and remaining challenges. *Journal of Power Sources* **2018,** *375*, 170-184.

34. Arges, C. G.; Zhang, L., Anion Exchange Membranes' Evolution toward High Hydroxide Ion Conductivity and Alkaline Resiliency. *ACS Applied Energy Materials* **2018,** *1* (7), 2991-3012.

35. Huang, G.; Mandal, M.; Peng, X.; Yang-Neyerlin, A. C.; Pivovar, B. S.; Mustain, W. E.; Kohl, P. A., Composite Poly(norbornene) Anion Conducting Membranes for Achieving Durability, Water Management and High Power (3.4 W/cm2) in Hydrogen/Oxygen Alkaline Fuel Cells. *Journal of The Electrochemical Society* **2019,** *166* (10), F637-F644.

36. Mandal, M.; Huang, G.; Hassan, N. U.; Peng, X.; Gu, T.; Brooks-Starks, A. H.; Bahar, B.; Mustain, W. E.; Kohl, P. A., The Importance of Water Transport in High Conductivity and High-Power Alkaline Fuel Cells. *Journal of The Electrochemical Society* **2019,** *167* (5), 054501.

37. Miyatake, K.; Shimura, T.; Mikami, T.; Watanabe, M., Aromatic ionomers with superacid groups. *Chemical Communications* **2009,** (42), 6403-6405.

38. Li, N.; Wang, C.; Lee, S. Y.; Park, C. H.; Lee, Y. M.; Guiver, M. D., Enhancement of Proton Transport by Nanochannels in Comb-Shaped Copoly(arylene ether sulfone)s. *Angewandte Chemie International Edition* **2011,** *50* (39), 9158-9161.

39. Tanaka, M.; Fukasawa, K.; Nishino, E.; Yamaguchi, S.; Yamada, K.; Tanaka, H.; Bae, B.; Miyatake, K.; Watanabe, M., Anion Conductive Block Poly(arylene ether)s: Synthesis, Properties, and Application in Alkaline Fuel Cells. *Journal of the American Chemical Society* **2011,** *133* (27), 10646-10654.

40. Wang, L.; Hickner, M. A., Highly conductive side chain block copolymer anion exchange membranes. *Soft Matter* **2016,** *12* (24), 5359-5371.

41. Li, Y.; Liu, Y.; Savage, A. M.; Beyer, F. L.; Seifert, S.; Herring, A. M.; Knauss, D. M., Polyethylene-Based Block Copolymers for Anion Exchange Membranes. *Macromolecules* **2015,** *48* (18), 6523-6533.

42. Ahlfield, J.; Huang, G.; Liu, L.; Kaburagi, Y.; Kim, Y.; Kohl, P. A., Anion Conducting Ionomers for Fuel Cells and Electrolyzers. *Journal of The Electrochemical Society* **2017,** *164* (14), F1648-F1653.

43. Pan, J.; Chen, C.; Li, Y.; Wang, L.; Tan, L.; Li, G.; Tang, X.; Xiao, L.; Lu, J.; Zhuang, L., Constructing ionic highway in alkaline polymer electrolytes. *Energy & Environmental Science* **2014,** *7* (1), 354-360.

44. Wang, J.; Gu, S.; Xiong, R.; Zhang, B.; Xu, B.; Yan, Y., Structure–Property Relationships in Hydroxide-Exchange Membranes with Cation Strings and High Ion-Exchange Capacity. *ChemSusChem* **2015,** *8* (24), 4229-4234.

45. Mandal, M.; Huang, G.; Kohl, P. A., Highly Conductive Anion-Exchange Membranes Based on Cross-Linked Poly(norbornene): Vinyl Addition Polymerization. *ACS Applied Energy Materials* **2019,** *2* (4), 2447-2457.

46. Chen, W.; Mandal, M.; Huang, G.; Wu, X.; He, G.; Kohl, P. A., Highly Conducting Anion-Exchange Membranes Based on Cross-Linked Poly(norbornene): Ring Opening Metathesis Polymerization. *ACS Applied Energy Materials* **2019,** *2* (4), 2458-2468.

47. Dang, H.-S.; Jannasch, P., Alkali-stable and highly anion conducting poly(phenylene oxide)s carrying quaternary piperidinium cations. *Journal of Materials Chemistry A* **2016,** *4* (30), 11924-11938.

48. Liu, L.; Huang, G.; Kohl, P. A., Anion conducting multiblock copolymers with multiple head-groups. *Journal of Materials Chemistry A* **2018,** *6* (19), 9000-9008.

49. Mamlouk, M.; Horsfall, J. A.; Williams, C.; Scott, K., Radiation grafted membranes for superior anion exchange polymer membrane fuel cells performance. *International Journal of Hydrogen Energy* **2012,** *37* (16), 11912-11920.

50. Zhu, L.; Zimudzi, T. J.; Li, N.; Pan, J.; Lin, B.; Hickner, M. A., Crosslinking of comb-shaped polymer anion exchange membranes via thiol–ene click chemistry. *Polymer Chemistry* **2016,** *7* (14), 2464-2475.

51. Chen, C.; Pan, J.; Han, J.; Wang, Y.; Zhu, L.; Hickner, M. A.; Zhuang, L., Varying the microphase separation patterns of alkaline polymer electrolytes. *Journal of Materials Chemistry A* **2016,** *4* (11), 4071-4081.

52. Zhang, X.; Shi, Q.; Chen, P.; Zhou, J.; Li, S.; Xu, H.; Chen, X.; An, Z., Block poly(arylene ether sulfone) copolymers tethering aromatic side-chain quaternary ammonium as anion exchange membranes. *Polymer Chemistry* **2018,** *9* (6), 699-711.

53. Shi, Q.; Chen, P.; Zhang, X.; Weng, Q.; Chen, X.; An, Z., Synthesis and properties of poly(arylene ether sulfone) anion exchange membranes with pendant benzyl-quaternary ammonium groups. *Polymer* **2017,** *121*, 137-148.

54. Weiber, E. A.; Meis, D.; Jannasch, P., Anion conducting multiblock poly(arylene ether sulfone)s containing hydrophilic segments densely functionalized with quaternary ammonium groups. *Polymer Chemistry* **2015,** *6* (11), 1986-1996.

55. Akiyama, R.; Yokota, N.; Nishino, E.; Asazawa, K.; Miyatake, K., Anion Conductive Aromatic Copolymers from Dimethylaminomethylated Monomers: Synthesis, Properties, and Applications in Alkaline Fuel Cells. *Macromolecules* **2016,** *49* (12), 4480-4489.

56. Shimada, M.; Shimada, S.; Miyake, J.; Uchida, M.; Miyatake, K., Anion conductive aromatic polymers containing fluorenyl groups: Effect of the position and number of ammonium groups. *Journal of Polymer Science Part A: Polymer Chemistry* **2016,** *54* (7), 935-944.

57. Mohanty, A. D.; Tignor, S. E.; Krause, J. A.; Choe, Y.-K.; Bae, C., Systematic Alkaline Stability Study of Polymer Backbones for Anion Exchange Membrane Applications. *Macromolecules* **2016,** *49* (9), 3361-3372.

58. Fujimoto, C.; Kim, D.-S.; Hibbs, M.; Wrobleski, D.; Kim, Y. S., Backbone stability of quaternized polyaromatics for alkaline membrane fuel cells. *Journal of Membrane Science* **2012,** *423-424*, 438-449.

59. Nuñez, S. A.; Hickner, M. A., Quantitative 1H NMR Analysis of Chemical Stabilities in Anion-Exchange Membranes. *ACS Macro Letters* **2013,** *2* (1), 49-52.

60. Arges, C. G.; Ramani, V., Two-dimensional NMR spectroscopy reveals cation-triggered backbone degradation in polysulfone-based anion exchange membranes. *Proceedings of the National Academy of Sciences* **2013,** *110* (7), 2490-2495.

61. Chempath, S.; Boncella, J. M.; Pratt, L. R.; Henson, N.; Pivovar, B. S., Density Functional Theory Study of Degradation of Tetraalkylammonium Hydroxides. *The Journal of Physical Chemistry C* **2010,** *114* (27), 11977-11983.

62. Chempath, S.; Einsla, B. R.; Pratt, L. R.; Macomber, C. S.; Boncella, J. M.; Rau, J. A.; Pivovar, B. S., Mechanism of Tetraalkylammonium Headgroup Degradation in Alkaline Fuel Cell Membranes. *The Journal of Physical Chemistry C* **2008,** *112* (9), 3179-3182.

63. Hibbs, M. R., Alkaline stability of poly(phenylene)-based anion exchange membranes with various cations. *Journal of Polymer Science Part B: Polymer Physics* **2013,** *51* (24), 1736-1742.

64. Long, H.; Kim, K.; Pivovar, B. S., Hydroxide Degradation Pathways for Substituted Trimethylammonium Cations: A DFT Study. *The Journal of Physical Chemistry C* **2012,** *116* (17), 9419-9426.

65. Pan, J.; Li, Y.; Han, J.; Li, G.; Tan, L.; Chen, C.; Lu, J.; Zhuang, L., A strategy for disentangling the conductivity–stability dilemma in alkaline polymer electrolytes. *Energy & Environmental Science* **2013,** *6* (10), 2912-2915.

66. Lee, W.-H.; Mohanty, A. D.; Bae, C., Fluorene-Based Hydroxide Ion Conducting Polymers for Chemically Stable Anion Exchange Membrane Fuel Cells. *ACS Macro Letters* **2015,** *4* (4), 453-457.

67. Ono, H.; Kimura, T.; Takano, A.; Asazawa, K.; Miyake, J.; Inukai, J.; Miyatake, K., Robust anion conductive polymers containing perfluoroalkylene and pendant ammonium groups for high performance fuel cells. *Journal of Materials Chemistry A* **2017,** *5* (47), 24804-24812.

68. Lee, W.-H.; Kim, Y. S.; Bae, C., Robust Hydroxide Ion Conducting Poly(biphenyl alkylene)s for Alkaline Fuel Cell Membranes. *ACS Macro Letters* **2015,** *4* (8), 814-818.

69. Omasta, T. J.; Wang, L.; Peng, X.; Lewis, C. A.; Varcoe, J. R.; Mustain, W. E., Importance of balancing membrane and electrode water in anion exchange membrane fuel cells. *Journal of Power Sources* **2018,** *375*, 205-213.

70. Omasta, T. J.; Park, A. M.; LaManna, J. M.; Zhang, Y.; Peng, X.; Wang, L.; Jacobson, D. L.; Varcoe, J. R.; Hussey, D. S.; Pivovar, B. S.; Mustain, W. E., Beyond catalysis and membranes: visualizing and solving the challenge of electrode water accumulation and flooding in AEMFCs. *Energy & Environmental Science* **2018,** *11* (3), 551-558.

71. Gerhardt, M. R.; Pant, L. M.; Weber, A. Z., Along-the-Channel Impacts of Water Management and Carbon-Dioxide Contamination in Hydroxide-Exchange-Membrane Fuel Cells: A Modeling Study. *J Electrochem Soc* **2019,** *166* (7), F3180-F3192.

72. Hossain, M. M.; Wu, L.; Liang, X.; Yang, Z.; Hou, J.; Xu, T., Anion exchange membrane crosslinked in the easiest way stands out for fuel cells. *Journal of Power Sources* **2018,** *390*, 234-241.

73. Lin, C. X.; Zhuo, Y. Z.; Hu, E. N.; Zhang, Q. G.; Zhu, A. M.; Liu, Q. L., Crosslinked side-chain-type anion exchange membranes with enhanced conductivity and dimensional stability. *Journal of Membrane Science* **2017,** *539*, 24-33.

74. Lee, K. H.; Cho, D. H.; Kim, Y. M.; Moon, S. J.; Seong, J. G.; Shin, D. W.; Sohn, J.-Y.; Kim, J. F.; Lee, Y. M., Highly conductive and durable poly(arylene ether sulfone) anion exchange membrane with end-group cross-linking. *Energy & Environmental Science* **2017,** *10* (1), 275-285.

75. Wang, J.; He, G.; Wu, X.; Yan, X.; Zhang, Y.; Wang, Y.; Du, L., Crosslinked poly (ether ether ketone) hydroxide exchange membranes with improved conductivity. *Journal of Membrane Science* **2014,** *459*, 86-95.

76. Quartarone, E.; Angioni, S.; Mustarelli, P., Polymer and Composite Membranes for Proton-Conducting, High-Temperature Fuel Cells: A Critical Review. *Materials (Basel, Switzerland)* **2017,** *10* (7), 687.

77. Zhang, F.; Zhang, H.; Ren, J.; Qu, C., PTFE based composite anion exchange membranes: thermally induced in situ polymerization and direct hydrazine hydrate fuel cell application. *Journal of Materials Chemistry* **2010,** *20* (37), 8139-8146.

78. Zhao, Y.; Yu, H.; Yang, D.; Li, J.; Shao, Z.; Yi, B., High-performance alkaline fuel cells using crosslinked composite anion exchange membrane. *Journal of Power Sources* **2013,** *221*, 247-251.

79. Zheng, Y.; Omasta, T. J.; Peng, X.; Wang, L.; Varcoe, J. R.; Pivovar, B. S.; Mustain, W. E., Quantifying and elucidating the effect of CO2 on the thermodynamics, kinetics and charge transport of AEMFCs. *Energy & Environmental Science* **2019,** *12* (9), 2806-2819.

80. Pandey, T. P.; Maes, A. M.; Sarode, H. N.; Peters, B. D.; Lavina, S.; Vezzù, K.; Yang, Y.; Poynton, S. D.; Varcoe, J. R.; Seifert, S.; Liberatore, M. W.; Di Noto, V.; Herring, A. M., Interplay between water uptake, ion interactions, and conductivity in an e-beam grafted poly(ethylene-co-tetrafluoroethylene) anion exchange membrane. *Physical Chemistry Chemical Physics* **2015,** *17* (6), 4367-4378.

81. Ziv, N.; Mustain, W. E.; Dekel, D. R., The Effect of Ambient Carbon Dioxide on Anion-Exchange Membrane Fuel Cells. *ChemSusChem* **2018,** *11* (7), 1136-1150.

82. Gu, S.; Cai, R.; Luo, T.; Chen, Z.; Sun, M.; Liu, Y.; He, G.; Yan, Y., A Soluble and Highly Conductive Ionomer for High-Performance Hydroxide Exchange Membrane Fuel Cells. *Angewandte Chemie International Edition* **2009,** *48* (35), 6499-6502.

83. Kim, D.-G.; Takigawa, T.; Kashino, T.; Burtovyy, O.; Bell, A.; Register, R. A., Hydroxyhexafluoroisopropylnorbornene Block and Random Copolymers via Vinyl Addition Polymerization and Their Application as Biobutanol Pervaporation Membranes. *Chemistry of Materials* **2015,** *27* (19), 6791-6801.

84. Kim, D. G.; Bell, A.; Register, R. A., Living Vinyl Addition Polymerization of Substituted Norbornenes by a t-Bu3P-Ligated Methylpalladium Complex. *ACS Macro Letters* **2015,** *4* (3), 327-330.

85. Wang, C.; Mo, B.; He, Z.; Shao, Q.; Pan, D.; Wujick, E.; Guo, J.; Xie, X.; Xie, X.; Guo, Z., Crosslinked norbornene copolymer anion exchange membrane for fuel cells. *Journal of Membrane Science* **2018,** *556*, 118-125.

86. He, X.; Liu, J.; Zhu, H.; Zheng, Y.; Chen, D., Novel quaternary ammonium functional addition-type norbornene copolymer as hydroxide-conductive and durable anion exchange membrane for direct methanol fuel cells. *RSC Advances* **2015,** *5* (78), 63215-63225.

87. Lue, S. J.; Shieh, S.-J., Water States in Perfluorosulfonic Acid Membranes Using Differential Scanning Calorimetry. *Journal of Macromolecular Science, Part B* **2009,** *48* (1), 114-127.

88. Mecheri, B.; Felice, V.; Zhang, Z.; D'Epifanio, A.; Licoccia, S.; Tavares, A. C., DSC and DVS Investigation of Water Mobility in Nafion/Zeolite Composite Membranes for Fuel Cell Applications. *The Journal of Physical Chemistry C* **2012,** *116* (39), 20820-20829.

89. Moster, A. L.; Mitchell, B. S., Hydration and proton conduction in Nafion/ceramic nanocomposite membranes produced by solid-state processing of powders from mechanical attrition. *Journal of Applied Polymer Science* **2009,** *113* (1), 243-250.

90. Grove, N. R.; Kohl, P. A.; Bidstrup Allen, S. A.; Jayaraman, S.; Shick, R., Functionalized polynorbornene dielectric polymers: Adhesion and mechanical properties. *Journal of Polymer Science Part B: Polymer Physics* **1999,** *37* (21), 3003-3010.

91. Shin, B.-G.; Cho, T.-Y.; Yoon, D. Y.; Liu, B., Structure and properties of polynorbornene derivatives: Poly(norbornene dicarboxylic acid dialkyl ester)s and poly(norbornene dimethyl dicarboxylate)s. *Macromolecular Research* **2007,** *15* (2), 185-190.

92. Tetsuka, H.; Isobe, K.; Hagiwara, M., Synthesis and Properties of Addition-Type Poly(norbornene)s with Siloxane Substituents. *Polymer Journal* **2009,** *41* (8), 643-649.

93. Dorkenoo, K. D.; Pfromm, P. H.; Rezac, M. E., Gas transport properties of a series of high Tg polynorbornenes with aliphatic pendant groups. *Journal of Polymer Science Part B: Polymer Physics* **1998,** *36* (5), 797-803.

94. Poynton, S. D.; Slade, R. C. T.; Omasta, T. J.; Mustain, W. E.; Escudero-Cid, R.; Ocón, P.; Varcoe, J. R., Preparation of radiation-grafted powders for use as anion exchange ionomers in alkaline polymer electrolyte fuel cells. *Journal of Materials Chemistry A* **2014,** *2* (14), 5124-5130.

95. Ferraz, C. P.; Fonseca, L. R.; Tomazetti, V.; Silva, F. C. S.; Lima-Neto, B. S.; Carvalho, V. P., Copolymers from norbornene and norbornadiene with organized morphologies and high Tg values obtained via ROMP with a highly reactive [RuCl3(PCy3)2] complex. *New Journal of Chemistry* **2016,** *40* (11), 9424-9431.

96. Lee, L.-B. W.; Register, R. A., Hydrogenated Ring-Opened Polynorbornene: A Highly Crystalline Atactic Polymer. *Macromolecules* **2005,** *38* (4), 1216-1222.

97. Liaw, D.-J.; Wang, K.-L.; Lee, K.-R.; Lai, J.-Y., Ring-opening metathesis polymerization of new norbornene-based monomers containing various chromophores. *Journal of Polymer Science Part A: Polymer Chemistry* **2007,** *45* (14), 3022-3031.

98. Ahlfield, J. M.; Liu, L.; Kohl, P. A., PEM/AEM Junction Design for Bipolar Membrane Fuel Cells. *Journal of The Electrochemical Society* **2017,** *164* (12), F1165-F1171.

99. Lin, B.; Qiu, L.; Lu, J.; Yan, F., Cross-Linked Alkaline Ionic Liquid-Based Polymer Electrolytes for Alkaline Fuel Cell Applications. *Chemistry of Materials* **2010,** *22* (24), 6718-6725.

100. Chen, D.; Hickner, M. A., Degradation of Imidazolium- and Quaternary Ammonium-Functionalized Poly(fluorenyl ether ketone sulfone) Anion Exchange Membranes. *ACS Applied Materials & Interfaces* **2012,** *4* (11), 5775-5781.

101. Hu, E. N.; Lin, C. X.; Liu, F. H.; Yang, Q.; Li, L.; Zhang, Q. G.; Zhu, A. M.; Liu, Q. L., Cross-Linked Poly(vinylbenzyl chloride) Anion Exchange Membranes with Long Flexible Multihead for Fuel Cells. *ACS Applied Energy Materials* **2018,** *1* (7), 3479-3487.

102. Dang, H.-S.; Jannasch, P., Exploring Different Cationic Alkyl Side Chain Designs for Enhanced Alkaline Stability and Hydroxide Ion Conductivity of Anion-Exchange Membranes. *Macromolecules* **2015,** *48* (16), 5742-5751.

103. Pan, J.; Lu, S.; Li, Y.; Huang, A.; Zhuang, L.; Lu, J., High-Performance Alkaline Polymer Electrolyte for Fuel Cell Applications. *Advanced Functional Materials* **2010,** *20* (2), 312-319.

104. Mahmoud, A. M. A.; Elsaghier, A. M. M.; Otsuji, K.; Miyatake, K., High Hydroxide Ion Conductivity with Enhanced Alkaline Stability of Partially Fluorinated and Quaternized Aromatic Copolymers as Anion Exchange Membranes. *Macromolecules* **2017,** *50* (11), 4256-4266.

105. Amel, A.; Yitzhack, N.; Beylin, A.; Pan, J.; Hickner, M. A.; Ein-Eli, Y., Chemical and Thermal Stability of Poly(phenylene oxide)-Based Anion Exchange Membranes Containing Alkyl Side Chains. *J Electrochem Soc* **2018,** *165* (14), F1133-F1138.

106. Chen, C.; Tse, Y.-L. S.; Lindberg, G. E.; Knight, C.; Voth, G. A., Hydroxide Solvation and Transport in Anion Exchange Membranes. *Journal of the American Chemical Society* **2016,** *138* (3), 991-1000.

107. Martínez-Arranz, S.; Albéniz, A. C.; Espinet, P., Versatile Route to Functionalized Vinylic Addition Polynorbornenes. *Macromolecules* **2010,** *43* (18), 7482-7487.

108. Wang, L.; Bellini, M.; Miller, H. A.; Varcoe, J. R., A high conductivity ultrathin anion-exchange membrane with 500+ h alkali stability for use in alkaline membrane fuel cells that can achieve 2 W cm−2 at 80 °C. *Journal of Materials Chemistry A* **2018,** *6* (31), 15404-15412.

109. Li, Q.; Peng, H.; Wang, Y.; Xiao, L.; Lu, J.; Zhuang, L., The Comparability of Pt to Pt-Ru in Catalyzing the Hydrogen Oxidation Reaction for Alkaline Polymer Electrolyte Fuel Cells Operated at 80 °C. *Angewandte Chemie International Edition* **2019,** *58* (5), 1442-1446.

110. Wang, L.; Peng, X.; Mustain, W. E.; Varcoe, J. R., Radiation-grafted anion-exchange membranes: the switch from low- to high-density polyethylene leads to remarkably enhanced fuel cell performance. *Energy & Environmental Science* **2019,** *12* (5), 1575-1579.

111. Ul Hassan, N.; Mandal, M.; Huang, G.; Firouzjaie, H. A.; Kohl, P. A.; Mustain, W. E., Achieving High-Performance and 2000 h Stability in Anion Exchange Membrane Fuel Cells by Manipulating Ionomer Properties and Electrode Optimization. *Advanced Energy Materials* **2020**, 2001986.

112. Zhu, L.; Yu, X.; Peng, X.; Zimudzi, T. J.; Saikia, N.; Kwasny, M. T.; Song, S.; Kushner, D. I.; Fu, Z.; Tew, G. N.; Mustain, W. E.; Yandrasits, M. A.; Hickner, M. A., Poly(olefin)-Based Anion Exchange Membranes Prepared Using Ziegler–Natta Polymerization. *Macromolecules* **2019,** *52* (11), 4030-4041.

113. Dang, H.-S.; Jannasch, P., High-Performing Hydroxide Exchange Membranes with Flexible Tetra-Piperidinium Side Chains Linked by Alkyl Spacers. *ACS Applied Energy Materials* **2018,** *1* (5), 2222-2231.

114. Ayers, K. E.; Anderson, E. B.; Capuano, C. B.; Niedzwiecki, M.; Hickner, M. A.; Wang, C.-Y.; Leng, Y.; Zhao, W., Characterization of Anion Exchange Membrane Technology for Low Cost Electrolysis. *ECS Transactions* **2013,** *45* (23), 121-130.

115. Vincent, I.; Kruger, A.; Bessarabov, D., Development of efficient membrane electrode assembly for low cost hydrogen production by anion exchange membrane electrolysis. *International Journal of Hydrogen Energy* **2017,** *42* (16), 10752-10761.

116. Pavel, C. C.; Cecconi, F.; Emiliani, C.; Santiccioli, S.; Scaffidi, A.; Catanorchi, S.; Comotti, M., Highly Efficient Platinum Group Metal Free Based Membrane-Electrode Assembly for Anion Exchange Membrane Water Electrolysis. *Angewandte Chemie International Edition* **2014,** *53* (5), 1378-1381.

117. Xiao, L.; Zhang, S.; Pan, J.; Yang, C.; He, M.; Zhuang, L.; Lu, J., First implementation of alkaline polymer electrolyte water electrolysis working only with pure water. *Energy & Environmental Science* **2012,** *5* (7), 7869-7871.

118. Mandal, M.; Huang, G.; Hassan, N. U.; Mustain, W. E.; Kohl, P. A., Poly(norbornene) anion conductive membranes: homopolymer, block copolymer and random copolymer properties and performance. *Journal of Materials Chemistry A* **2020,** *8* (34), 17568-17578.

119. Bessarabov, D.; Millet, P.; Pollet, B. G., *PEM Water Electrolysis*. Elsevier Science: 2018.

120. Wang, Z.; Mandal, M.; Sankarasubramanian, S.; Huang, G.; Kohl, P. A.; Ramani, V. K., Influence of Water Transport Across Microscale Bipolar Interfaces on the Performance of Direct Borohydride Fuel Cells. *ACS Applied Energy Materials* **2020,** *3* (5), 4449-4456.

121. Zhang, D.; Zeng, K., Evaluating the Behavior of Electrolytic Gas Bubbles and Their Effect on the Cell Voltage in Alkaline Water Electrolysis. *Industrial & Engineering Chemistry Research* **2012,** *51* (42), 13825-13832.

122. Zheng, Y.; Huang, G.; Wang, L.; Varcoe, J. R.; Kohl, P. A.; Mustain, W. E., Effect of reacting gas flowrates and hydration on the carbonation of anion exchange membrane fuel cells in the presence of CO2. *Journal of Power Sources* **2020,** *467*, 228350.

123. Dekel, D. R.; Rasin, I. G.; Page, M.; Brandon, S., Steady state and transient simulation of anion exchange membrane fuel cells. *Journal of Power Sources* **2018,** *375*, 191-204.

124. Yang, D.; Yu, H.; Li, G.; Zhao, Y.; Liu, Y.; Zhang, C.; Song, W.; Shao, Z., Fine microstructure of high performance electrode in alkaline anion exchange membrane fuel cells. *Journal of Power Sources* **2014,** *267*, 39-47.

125. Bernt, M.; Gasteiger, H. A., Influence of Ionomer Content in IrO2/TiO2Electrodes on PEM Water Electrolyzer Performance. *Journal of The Electrochemical Society* **2016,** *163* (11), F3179-F3189.

126. Weber, A. Z.; Borup, R. L.; Darling, R. M.; Das, P. K.; Dursch, T. J.; Gu, W. B.; Harvey, D.; Kusoglu, A.; Litster, S.; Mench, M. M.; Mukundan, R.; Owejan, J. P.; Pharoah, J. G.; Secanell, M.; Zenyuk, I. V., A Critical Review of Modeling Transport Phenomena in Polymer-Electrolyte Fuel Cells. *Journal of the Electrochemical Society* **2014,** *161* (12), F1254-F1299.

127. Henkensmeier, D.; Najibah, M.; Harms, C.; Žitka, J.; Hnát, J.; Bouzek, K., Overview: State-of-the Art Commercial Membranes for Anion Exchange Membrane Water Electrolysis. *Journal of Electrochemical Energy Conversion and Storage* **2020,** *18* (2).

128. Huang, G.; Mandal, M.; Ul Hassan, N.; Groenhout, K.; Dobbs, A.; Mustain, W. E.; Kohl, P. A., Ionomer Optimization for Water Uptake and Swelling in Anion Exchange Membrane Electrolyzer: Oxygen Evolution Electrode. *Journal of The Electrochemical Society* **2020**.

129. Huang, G.; Mandal, M.; Ul Hassan, N.; Groenhout, K.; Dobbs, A.; Mustain, W. E.; Kohl, P. A., Ionomer Optimization for Water Uptake and Swelling in Anion Exchange Membrane Electrolyzer: Hydrogen Evolution Electrode. *Journal of The Electrochemical Society* **2020**.

130. Bender, G.; Carmo, M.; Smolinka, T.; Gago, A.; Danilovic, N.; Mueller, M.; Ganci, F.; Fallisch, A.; Lettenmeier, P.; Friedrich, K. A.; Ayers, K.; Pivovar, B.; Mergel, J.; Stolten, D., Initial approaches in benchmarking and round robin testing for proton exchange membrane water electrolyzers. *International Journal of Hydrogen Energy* **2019,** *44* (18), 9174-9187.

131. Lipian, J.; Mimna, R. A.; Fondran, J. C.; Yandulov, D.; Shick, R. A.; Goodall, B. L.; Rhodes, L. F.; Huffman, J. C., Addition Polymerization of Norbornene-Type Monomers. High Activity Cationic Allyl Palladium Catalysts. *Macromolecules* **2002,** *35* (24), 8969-8977.